Department of Energy Technology - Pontoppidanstræde 101
Aalborg University, Denmark

Multilink DC Transmission for Offshore Wind Power Integration

Master thesis

-10th Semester, 2011-

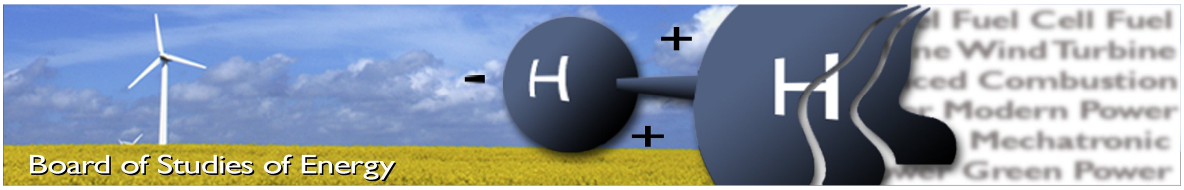

Title: Multilink DC Transmission for Offshore Wind Power Integration
Semester: 10^{th}
Semester theme: Master Thesis

Project period: 1^{th} of February– 30^{th} May 2010
ECTS: 30
Supervisors: Remus Teodorescu, Pedro Rodriguez, Rodrigo da Silva
Project group: PED4-1030

____
Bogdan-Ionuţ Crăciun

Copies: 3
Pages, total: 91
Appendix: 3
Supplements: 3 CDs

SYNOPSIS:

The wind energy industry has increased rapidly during the last decade as a result of constant improvement in terms of increased capacity of WTs and efficiency in energy extraction. This has made the manufacturers to go beyond their boundaries imposed by the onshore installation and tried the offshore challenges. In consequence, wind power became a serious competitor for the traditional energy sources.

The biggest challenge was the integration of such distributed power systems into the grid without affecting the stability and in the same time meeting TSO requirements. Another issue was the power transportation over long distances and the limitations that the HVAC faced in offshore installations.

The new concept of VSC-based HVDC enabled the possibility to go further into the sea and increase the power production. Using VSCs for interfacing the DC grid with the AC grid brought many advantages and also made possible to fulfill TSO requirements.

The HVDC system gains much more flexibility on a basis of multi terminal operation. Having extra converters brings also new ideas in sharing the active power and one of the solutions is the use of virtual impedance correlated with a droop controller.

This master thesis analysis the sharing of active power produced by the WF in a MTDC operation. The first objective was to model the system in PSCAD/EMTDC and than the control structure tested under different situations. The second objective was to validate the simulation on a laboratory platform using 15 kW VSCs.

By signing this document, each member of the group confirms that all participated in the project work and thereby that all members are collectively liable for the content of the report.

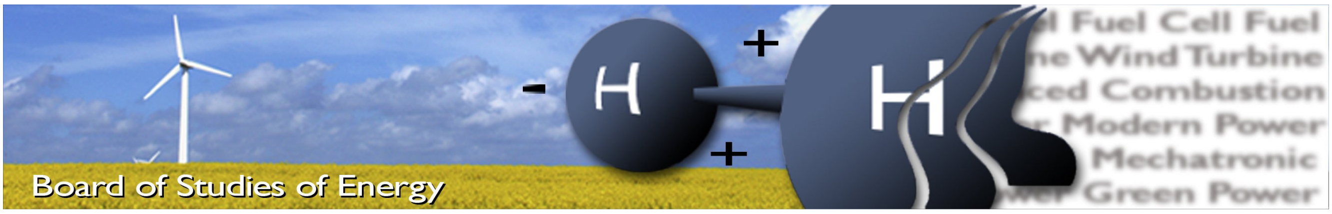

Preface

The present Master thesis entitled *Multilink DC Transmission for Offshore Wind Power Integration* was written by group PED4-1030 in 10th Semester formed by one degree student at the Department of Energy Technology, Aalborg University. This project has been carried out between 1th of February– 30th May 2010.

Reading Instructions

The references are shown in form of numbers put in square brackets. Detailed information about literature is presented in the References. While the format for equations is (X.Y) for figures and tables is X-Y, where X is the number of chapter and Y is the number of equation/figure/table.

In the thesis, the chapters are consecutive numbered and the appendixes are labeled with letters. The enclosed CD-ROM contains the thesis report written in Microsoft Word, Adobe PDF format, documents used throughout the thesis, PSCAD/EMTDC simulation files and the experimental results.

Acknowledgement

The author would like to express his gratitude to his supervisors Remus Teodorescu and Rodrigo da Silva for the support and ideas provided throughout the entire project period.

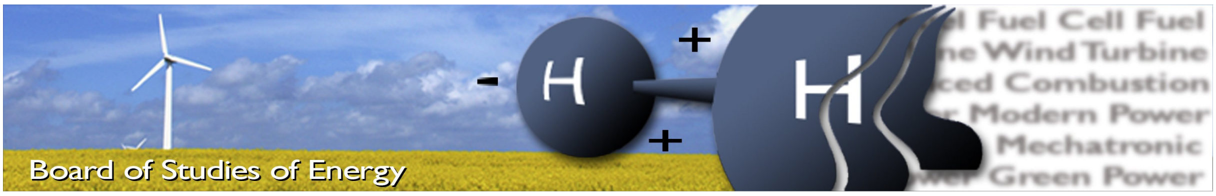

Table of contents

Nomenclature

List of abbreviations

AC	Alternative Current
CC	Cluster Coupled
CSC	Current Source Converter
DC	Direct Current
DFIG	Double Fed Induction Generator
FACTS	Flexible Alternative Current Transmission System
FRT	Fault Ride Through
HVAC	High Voltage Alternative Current
HVDC	High Voltage Direct Current
IGBT	Insulated Gate Bipolar Transistors
IGCT	Insulated Gate Commutated Thyristor
GE	General Electric
LCC	Line Commutated Converter
LVRT	Low Voltage Ride Through
MTDC	Multi Terminal Direct Current
PCC	Point of Common Coupling
PI	Proportional Integrator
PLL	Phase Lock Loop
PMSG	Permanent Magnet Synchronous Generator
PR	Proportional Resonant
PWM	Pulse Width Modulation
REC	Receiving End Converter
SEC	Sending End Converter
TSO	Transmission System Operator
VSC	Voltage Source Converter
WF	Wind Farm
WPP	Wind Power Plant
WT	Wind Turbine
WTG	Wind Turbine Generator

Chapter 1

Introduction

This chapter realizes a short presentation of the High Voltage Direct Current (HVDC) transmission system and MTDC interconnection. Various wind turbine (WT) trends are highlighted and different grid code requirement are presented with the purpose to underscore their importance in the integration of the wind energy. Later on the problem is defined, the objectives are listed, the project limitations are mentioned and finally the project outline summarizes the structure and content of the report.

1.1 Background

The utilization of wind energy has a tradition of about 3000 years. Until the early twentieth century wind power was used to provide mechanical power for water pumping or to grind grain. The first wind turbines for electricity generation had been developed at the beginning of the twentieth century. [1]

From the early 1970s the WT technology experienced a gradual increase in complexity, due to the developments in disciplines such as aerodynamics, structural dynamics, mechanics as well as power electronics. Over the last ten years, the global wind energy capacity has increased rapidly and proved to be the fastest developing renewable energy technology. [1]

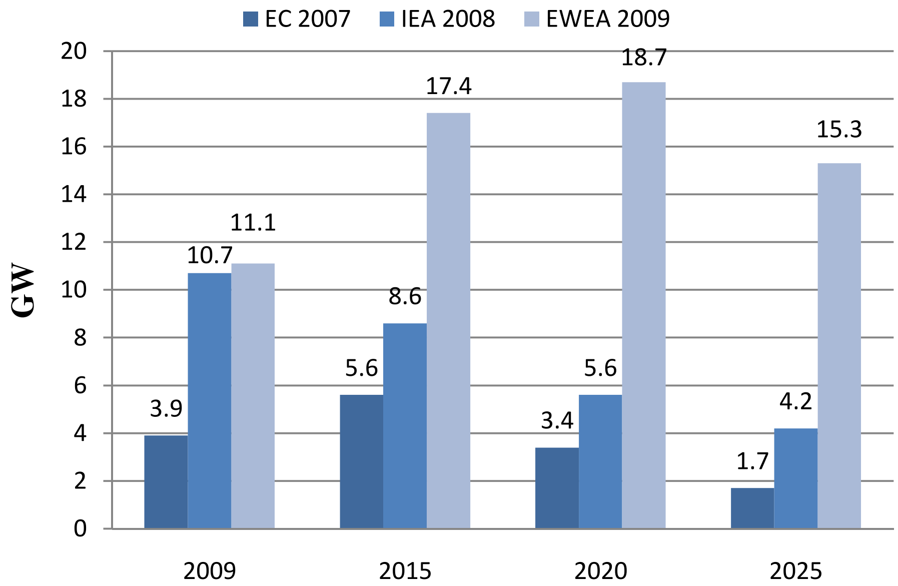

Figure 1-1 Average annual increases in wind energy capacity in the EU. The European commission IEA and EWEA compared[2]

The present wind power share of the world's electricity generation is of 1.92%, but a bigger share up to 9.1% in 2020 was indicated by the forecasts and the predictions presented in[3]. The European Wind Energy Association scenario shows that by 2030, wind power could be satisfying 22% of Europe's total electricity supply [1].

As a result of this scenario, high level of wind power (>30%) should be integrated into large inter-connected power systems and major issues can appear if the existing power systems are not properly redesign. In some regions of the world, for example in Northern Germany (31.45%), Denmark (18%) or on the Swedish Island of Gotland (22%), wind energy supplies a significant amount of the total energy demand. Currently China, USA, Germany, India and Spain concentrate more than 74% of worldwide wind energy capacity in their countries. A more optimistic strategy is adopted by Denmark which has a long term target that by year 2050, the country should be "fossil fuel free" [3]-[4].

From Figure 1-2 it can be observed that in future, many countries around the world are likely to experience similar penetration levels, as wind power is an interesting economic alternative in areas with appropriate wind speeds.

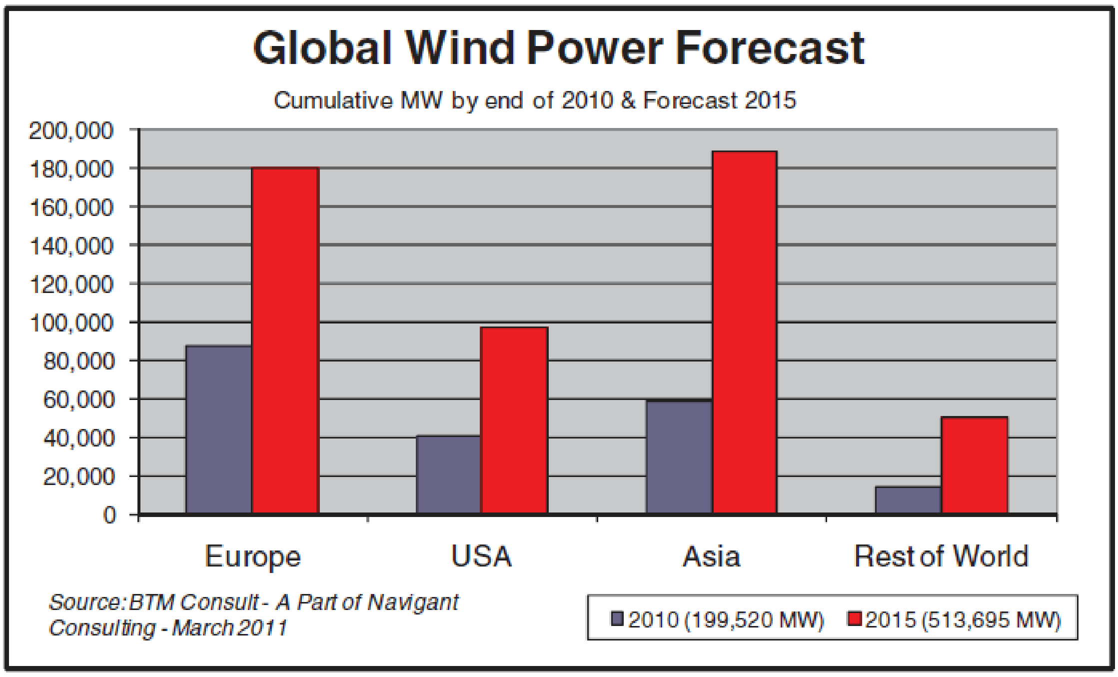

Figure 1-2 Global wind power projections [3]

1.1.1 WT trends

The past years shows that the wind power industry is a well defined and profitable business. That's why each year a lot of resources are involved in order to improve and extend the efficiency and the installed power of the wind turbines.

As showed in Figure 1-3 the wind turbine size is still increasing but in order to fulfill the environmental requirements an increasing trend is to remove dispersed single wind turbine in favor of concentrated wind turbines in large wind farms. Both onshore and offshore wind farms are quickly developing in a global scale.

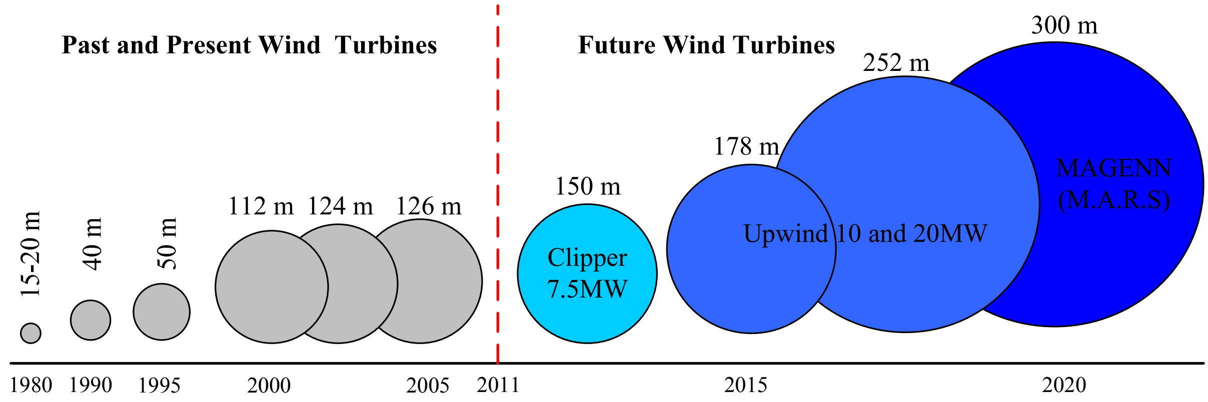

Figure 1-3 Trends in WT Rotor Diameter [5].

Offshore wind energy is more attractive, because of higher and constant wind speed and more space than onshore wind energy. Land structures and forests affect the wind flow. The strongest wind forces to drive the WT for maximal energy output are available over the sea. Offshore turbines thus produce more electricity per installed generation capacity than onshore wind power plants. However, the cost of offshore wind farms are about 30-60% higher than onshore wind farms of same capacity. In addition to the higher maintenance cost, the cost difference between onshore and offshore wind farm is due to the cost of foundations and the grid connection. Furthermore, site access is limited in time as it is highly dependent on weather conditions. These conditions require a high degree of technical robustness and reliability for offshore wind turbines. From an environmental point of view regarding noise emissions and visual impacts, the footprint of an offshore WF is smaller than an onshore WF[5]

As part of the new energy plan the Danish government illustrates a doubling of wind capacity by 2025, from the present 3100 MW to 6200 MW (see Figure 1-4). According to the new trends, offshore wind farms will provide a large part of this increase. At present, however, the market is dominated by onshore wind farms[2].

While the wind turbine market continues to be dominated by conventional gear-driven wind turbine systems, the direct drive or one-stage gear is more attractive due to higher overall efficiency and availability of omitting the gear-box.

The main trend of modern wind turbines design uses a pitch controlled machine with variable-speed. The concept was realized at the beginning with a Double Fed Induction Generator (DFIG) topology but in the early 2000s another topology was introduced by Enercon, using a full scale converter with a permanent magnet synchronous generator (PMSG)[6].

The DFIG topologies clearly are the most dominant concept but there is, however, an increasing trend for PMSG topologies. Lately, the leading wind turbine generator (WTG) suppliers such as GE Energy and MADE have switched to synchronous-type generators for the larger 2 MW+ turbine segment despite the increased system cost. This trend to adapt new grid stability requirements for WTs means that WTs topology must have built-in capacity to support the grids by remaining connected in case of a voltage dip.

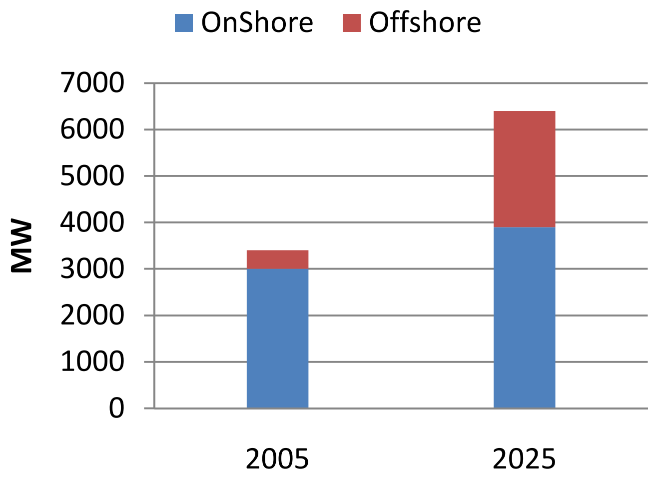

Figure 1-4 Objective of Danish wind generation capacity[7]

1.1.2 Grid code requirements

Wind generation has become a substantial share of the total power generation. As a result, WTs have started to affect the stability of electric power systems, by interacting with conventional power plants. Therefore, the WT has to meet special regulations imposed by the TSO in order to operate without affecting the system stability.

Grid codes are technical documents containing rules governing the operation, development and use of the power system. Taking into consideration the large number of requirements and the purpose of this section, only the most relevant are presented. These requirements are divided in two main categories: Normal operation and under grid disturbance.

a) Normal operation grid requirement

Frequency and Voltage deviations

A Wind Power Plant (WPP) should maintain its operating frequency and voltage, at the point of common coupling (PCC), within a range around the rated values. From Figure 1-5 it can be seen that this requirement specifies the amount of time in which the WPP should operate for certain deviations of the frequency or voltage[6].

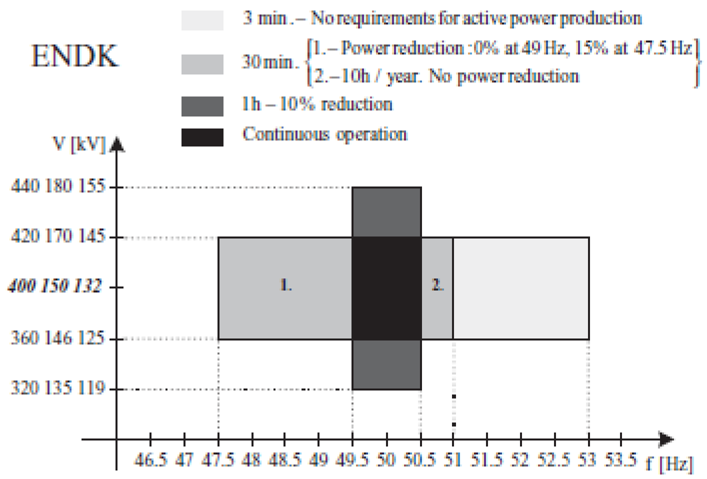

Figure 1-5 Voltage – Frequency operation window (Danish TSO) [6]

Active Power Control

Through this requirement the TSO imposes to the WF to behave as much as possible as a conventional power plant. This grid requirement can be divided in two, depending on the level of control in which the WPP is involved: the first case is when the WPP is in the secondary control and it has to provide only the amount of power requested by the TSO; the second case is when the WPP is in the primary control and it has to participate in frequency control[6].

When system frequency is above or below the nominal value it means there is too much or less generated power. The system operators prefers to have a plant capable of offering the so called "spinning reserve"; it means that the plant should be available and ready to respond to frequency change by reducing or increasing their output automatically. Wind cannot be boosted in the same way as the steam in the traditional plant. For some wind plant, the technical solution is to operate under the rated output power, so by adjusting the blade pitch a boost will be obtained, see Figure 1-6.

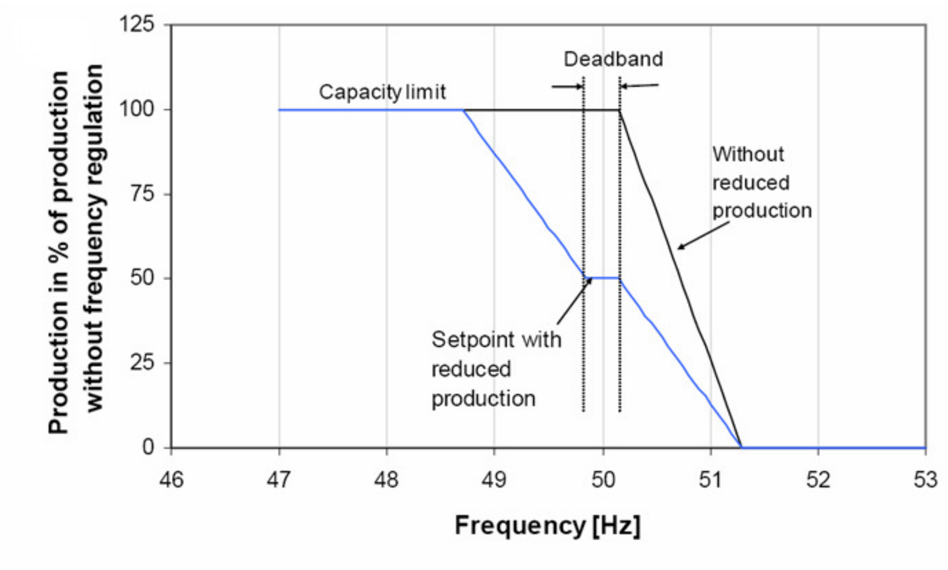

Figure 1-6 Active power and frequency control of a WT [5]

Reactive Power Control

According to this grid code, the WF has to provide reactive output regulation, often in response to power system voltage variations, same as the conventional power plants. (see Figure 1-7).

The reactive power control requirements are related to the characteristics of each network; since the influence of the reactive power injection to the voltage level is dependent on the network short-circuit capacity and impedance [6]

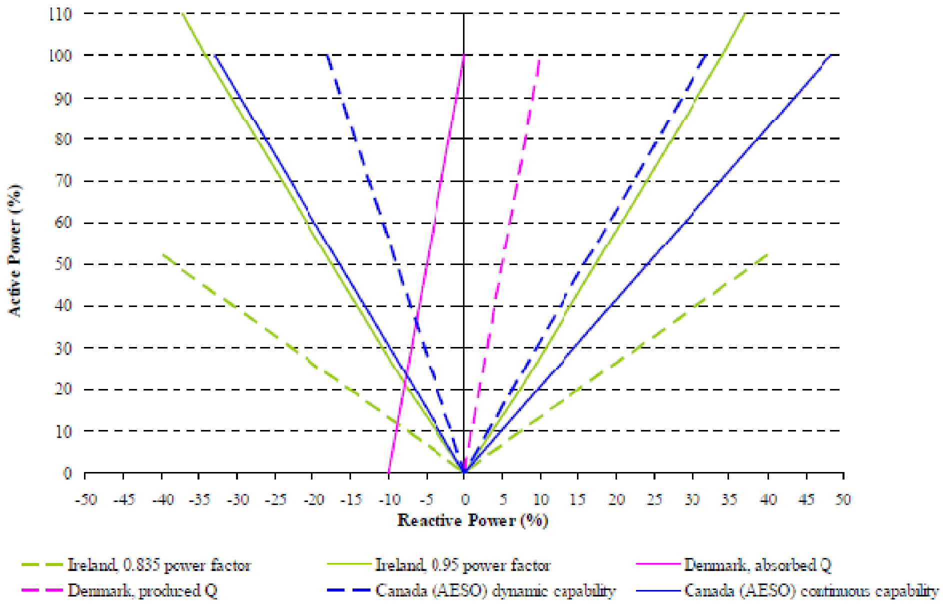

Figure 1-7 Reactive power grid code demands for WT[8]

b) Under grid disturbances requirements

All the grid codes share in common the relatively new requirements for WFs to contribute to grid stability. The main goals are to ride through momentary network faults and in the same time to provide grid support.

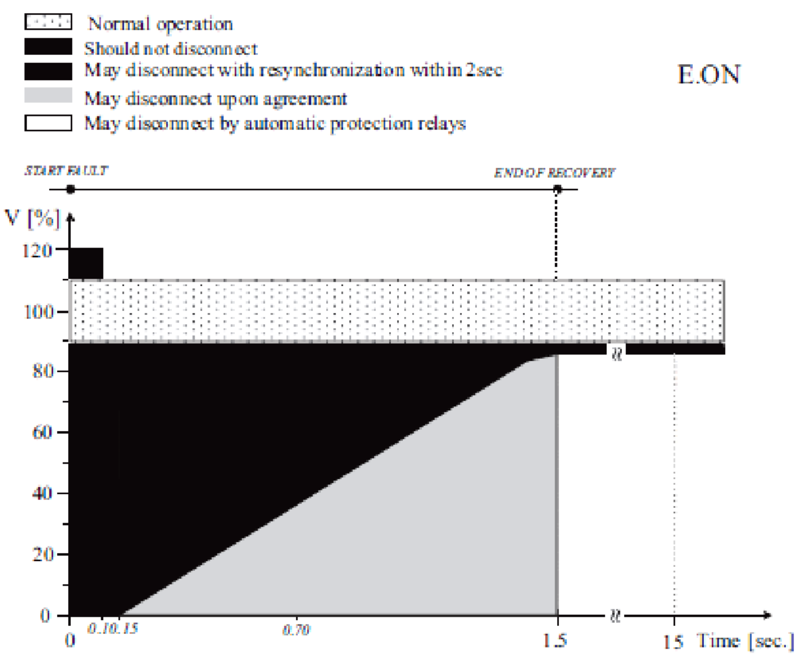

Figure 1-8 LVRT (German TSO E.ON)[6]

TSO are imposing the FRT capability of WTs due to the fact that when a disturbance appear if the WF is immediately disconnected, instead of helping the system to regain its stability will produce the increasing of the fault. Therefore, WFs must withstand voltage dips to a value of 0% of the nominal voltage for a specified duration. Such requirements are described by a voltage vs. time characteristic, denoting the minimum required immunity of the wind power plant as shown in Figure 1-8 [6].

1.1.3 Overview of HVDC transmission

1.1.3.1 HVAC or HVDC

The development of electrical power supplies began more than one hundred years ago. At the beginning, there were only small DC networks within narrow local boundaries, which were able to cover the direct needs of industrial plants by means of hydro energy. With an increasing demand on energy and the construction of large generation units, typically built at remote locations from the load centers, the technology changed from DC to AC, consequently the power transmitted, voltage levels and transmission distances increased[9]

HVDC transmission and HVAC have developed to a viable technique with high power ratings since the 60s. From the firsts small DC "mini networks", there are now systems transmitting 3 - 4 GW over large distances with only one bipolar DC transmission (1.000 - 2.000 km or more are feasible with overhead lines). With submarine cables, transmission levels up to 600 – 800 MW over distances of nearly 600 km have already been attained (NORNED project 2007), and cable transmission lengths up to 1.300 km are in the planning stage[9].

HVDC is the preferred method for transmitting large amounts of power over large distances, especially through submarine cables. This is because HVDC requires fewer cables to transfer the same amount of power compared to HVAC, has reduced power losses over long distances and requires no compensation equipment to maintain power transfer. The reasons behind these advantages are presented in the following section[10].

a) AC charging Current and effects on Power Transfer

A characteristic of AC cable is the charging current induced in the cable due to the capacitance between each phase conductor and earth. Figure 1-9 illustrates the reduction in effective power carrying capability of 132kV and 245kV AC cables as the lengths exceed 60km. This charging current can be minimized by connecting reactive compensators at regular intervals along the cable. However, as an offshore network requires very long submarine cable, providing the necessary reactive compensation would present an added technological and financial challenge.

In HVDC transmission a charging current only occurs during the instant of turning on or off and therefore has no effect on the DC current rating neither on the power transfer capability of the cable. Thus the HVDC transmission does not have the issues with length and voltage level limitations which are associated with AC transmission cables[10].

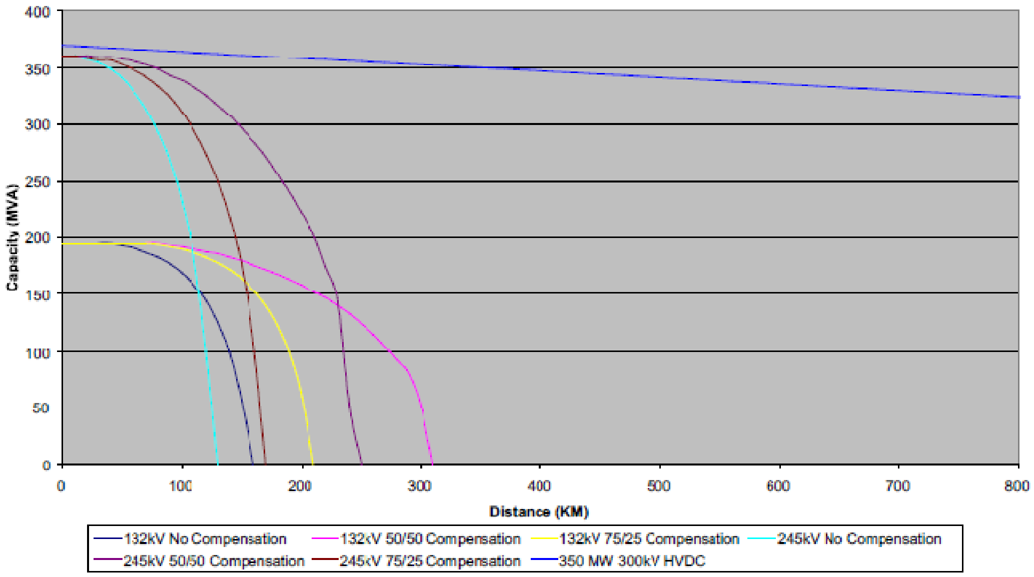

Figure 1-9 FACTS and HVDC cable power capacity comparison[10].

b) Conductor Size and AC Skin and Proximity Effects

In AC transmission the current flow concentrates in the peripheral surfaces of the conductors due to the “skin effect” or due to the “proximity effect”. Consequently, because the conductor cross sectional area is underutilized, AC transmission can require the use of very large conductors, or a large number of smaller conductors.

Since HVDC has the ability to use the full cross-sectional area of the conductors, a much smaller conductor can be used for the same level of power transfer (see Figure 1-10). Moreover, if the cables are placed close one to each other, the magnetic fields caused by the passage of current is canceled (e.g. ships navigational systems will be unaffected while passing over the DC link)[10].

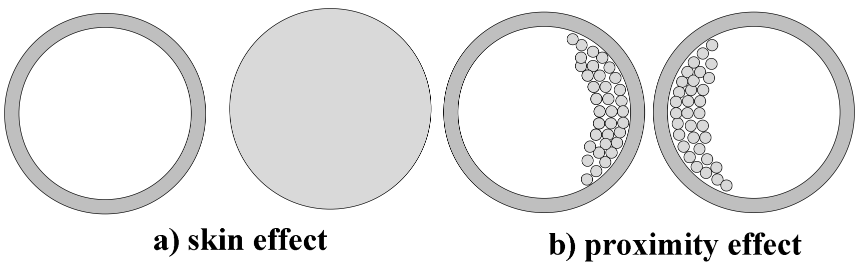

Figure 1-10 a) AC and DC cable usage b) proximity effect

1.1.3.2 HVDC application

In a HVDC system, electric power is taken from one point of a three-phase AC network, converted to DC in a rectifier station, transmitted to the receiving point by an overhead line or underground/subsea cable, then converted back to AC through an inverter station and injected into the receiving AC network, see Figure 1-11.

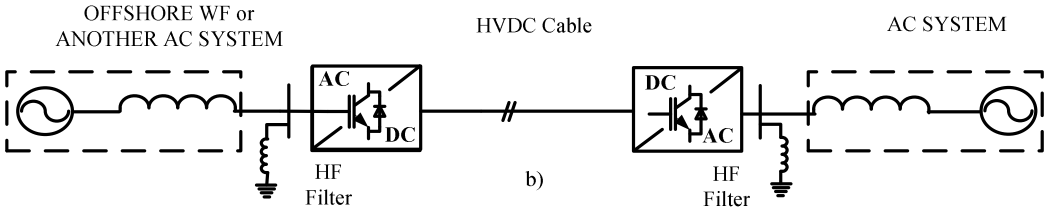

Figure 1-11 HVDC bipolar transmission

There are two main technologies used in HVDC transmission: the Current Source Converter (CSC) and the Voltage Source Converters (VSC). In the next section different applications of the VSC HVDC transmission are presented.

a) long distance bulk power transmissions using underground/submarine cable

In case of underground or submarine HVDC cables there is no physical restriction concerning the distance, the power level and also there are considerable savings in installed cable costs. The HVDC transmission systems provide an economical alternative to AC transmission systems regarding the bulk power delivery from remote locations such as hydroelectric developments or large scale wind farms whenever the breakeven distance is exceeded[11-12].

Some examples in this type of application are: Gotland Sweden (1999), Directlink connection Australia (2000), CrossSound USA (2002), Troll A Offshore Norway (2005) and more recent the Valhall Offshore Norway(2009)[13].

b) asynchronous connections of AC power systems

The HVDC transmissions systems offer a reliable and economical way of interconnection between two AC asynchronous networks, since it can provide control of the power flows and consequently assistance in management of the separated systems.

Some examples for this type of application are: Directlink connection Australia (2000), Estlink Estonia-Finland (2006) and NORD E.ON1 Germany (2009)[12-13].

c) stabilization of power flows in integrated power systems

The HVDC transmissions systems offer a reliable and economical way of interconnection between two AC asynchronous networks, since it can provide control of the power flows and consequently assistance in management of the separated systems.

Some examples for this type of application are: Directlink connection Australia (2000), Estlink Estonia-Finland (2006) and NORD E.ON1 Germany (2009)[9].

d) offshore transmission

Due to advantages, such as: self-commutation, black-start capability and dynamic voltage control, VSC-based HVDC transmissions can be used to serve isolated loads on islands or offshore platforms. Moreover, VSC-based HVDC transmission systems can provide reactive power support both to wind farms and to interconnection point[12].

It can be summarized that HVDC systems are mainly used for transmission of bulk power over long distances because the technology becomes economically attractive compared with conventional AC lines, see Figure 1-12 [10].

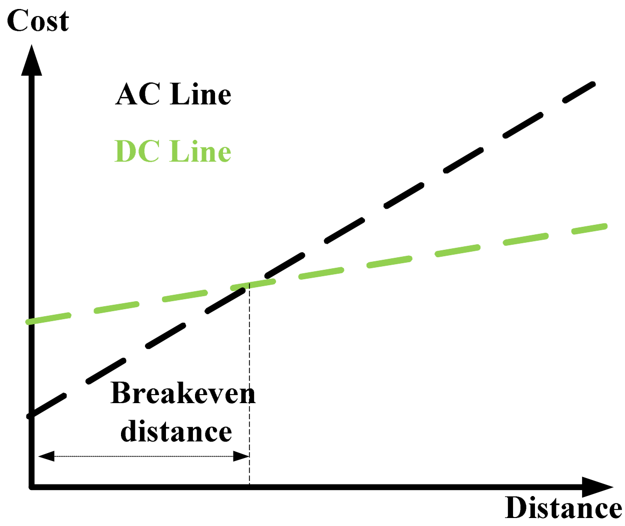

Figure 1-12 Cost as a function of distance for HVDC and HVAC systems[10].

1.1.3.3 HVDC topology

The original motivation for the development of DC technology was the transmission and distribution efficiency, as the power loss of a DC line is lower than a corresponding AC line. Other advantages like feasibility, fault ride through capability and the possibility of black start make this solution more and more attractive. Therefore the HVDC transmission systems are proved to be superior to AC transmission from an economical and technical point of view[14-15].

From Figure 1-13 it can be easily observed that the HVDC transmission uses only two cables instead of three, but it also can be observed that it needs two additional components (the Sending Station and the Receiving Station).

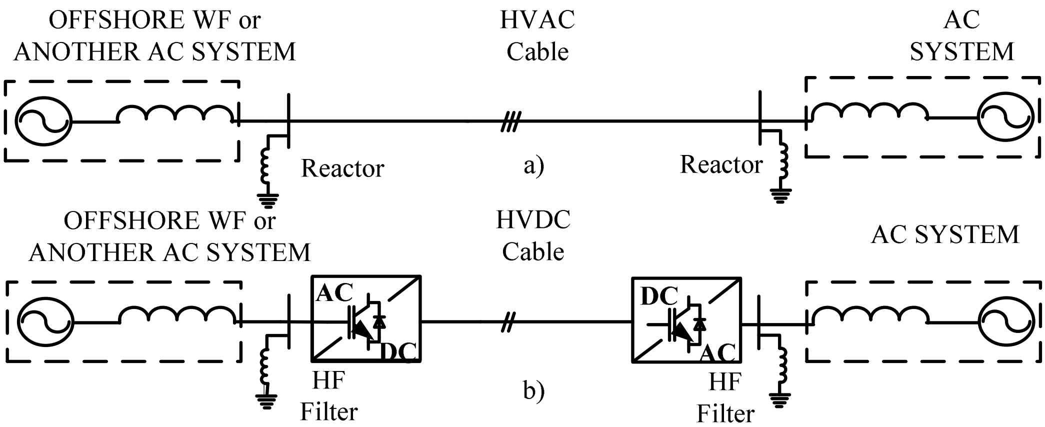

Figure 1-13 Interconnection of two AC systems a) HVAC option b) HVDC option

There are two different HVDC transmission technologies for power transmission: Voltage Source Converter (VSC) HVDC using insulated gate bipolar transistors (IGBT) or insulated gate commutated thyristor (IGCT) and Line Commutated Converter (LCC) HVDC using the classical thyristors.

The performance of HVDC technology was increased thanks to the substantial progress made in the ratings and reliability of thyristor valves. When the amount of energy that has to be transferred is large or long distances are involved, the HVDC transmission system proved to be an economically viable solution. The LCC HVDC technology has been operated with high reliability and little maintenance for more than 30 years[14].

The increasing penetration of the power electronics technologies into the power systems is mainly due to the continuous progress of the high-voltage high-power fully controlled semi conductors such as the IGBT and the IGCT. The VSC HVDC technology using IGBTs recently has gained growing interest due to its simplified modularity. However, the power handling capacity of a single IGBT semiconductor used in VSC HVDC is lower than the corresponding capability of a thyristor used in a LCC HVDC.

HVDC with VSC-based transmission has been greatly improved in flexibility due to the four-quadrant operation of the converter. One of the main advantages of VSC-based transmission is its ability to control reactive power in both directions, independently of the real power flow. Although this topology has superior advantages, the maximal rating of VSC HVDC is limited to around 500 MW, while single LCC HVDC link can possibly transmit more than one GW power[16].

a) Line Commuted Converter HVDC

LCC is the most widely used HVDC transmission alternative but it has very limited flexibility due to the use of thyristor switching and very large series impedance to support the rapid changes in the AC power supply. The lack of turn-off controllability of the conventional thyristor results in poor power factors and considerable waveform distortion. Thus, while the LCC configuration is very simple, the external plant required for reactive power compensation and filtering is elaborate and expensive.

In rectifying operation due to the firing delay and commutation angles the converter current always lags the voltage in each phase; therefore the converter consumes reactive power. On the other hand when it operates in inverter mode several conditions has to be fulfilled such as: the presence of an AC source to provide the commutating voltage; the presence of a DC power supply and the firing angle larger than 90 degrees.

An important drawback of the LCC is the commutation failures caused by voltage drop or phase angle change in the AC system, resulting from a switching event or system fault. Another cause for these commutation failures is the miscalculation of the firing angle which can conduct to a short circuit in the DC side and loss of power transmission. This kind of events are random and have a statistical nature, therefore one of the design objective of an LCC is to minimize them[14].

b) Voltage source converter HVDC

The VSC based HVDC installations has several advantages compared to conventional HVDC such as, independent control of active and reactive power, dynamic voltage support at the converter bus for enhancing stability possibility to feed to weak AC systems or even passive loads and reversal of power without changing the polarity of DC voltage (advantageous in multi-terminal DC systems)[17].

The VSC-based HVDC transmission system mainly consists of two converters controlled through PWM strategy which are operating at frequencies higher than the line frequency, one rectifier and one inverter stations connected in a back to back topology by a DC bus (see Figure 1-14).

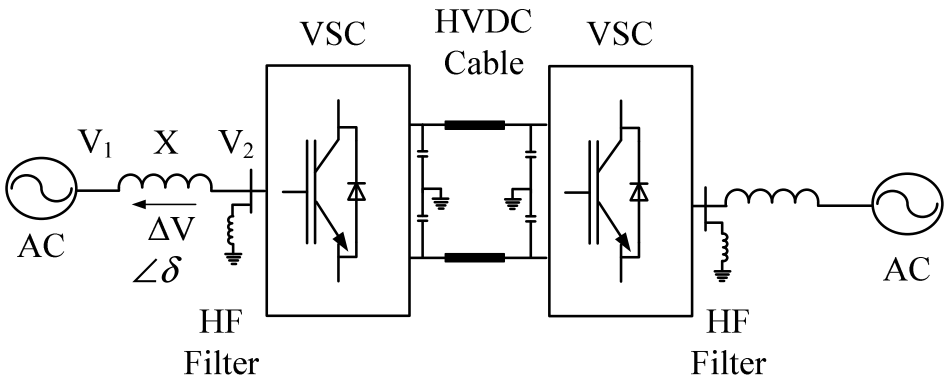

Figure 1-14 VSC interconnection

Using PWM, the AC output of the converter carries significant harmonics at frequencies close to switching frequencies or multiples. For that reason a high frequency filter is normally installed to prevent these harmonics from causing undesirable effects in the AC system.

VSC transmission allows only one polarity and thus the cable does not require to be designed for polarity reversals. The magnetic fields are almost completely eliminated by adopting the bipolar system and they do not produce ground currents. This simplifies the cable design, permitting the replacement of the conventional oil-impregnated paper insulation with the polymeric insulation. The polymeric insulation material can withstand high forces and repeated flexing and is thus more suited for deep-water installation. Moreover, the lifetime of the cable insulating materials is better for DC than AC[14].

Figure 1-15 shows the fundamental frequency phasor representation of the VSC operating as an inverter and supplying active and reactive power to the AC system. In this operating condition the diagram shows that the VSC output voltage V_2 has larger amplitude and leads the AC system voltage V_1 which means that power is injected [14].

Active and reactive power exchanged between these two sources is expressed as:

$$P = V_1 \cdot V_2 \cdot \frac{\sin\delta}{X} \tag{1.1}$$

$$Q = \frac{V_1}{X}(V_2 \cdot \cos\delta - V_1) \tag{1.2}$$

where δ is the phase angle difference and X the reactance between V_1 and V_2.

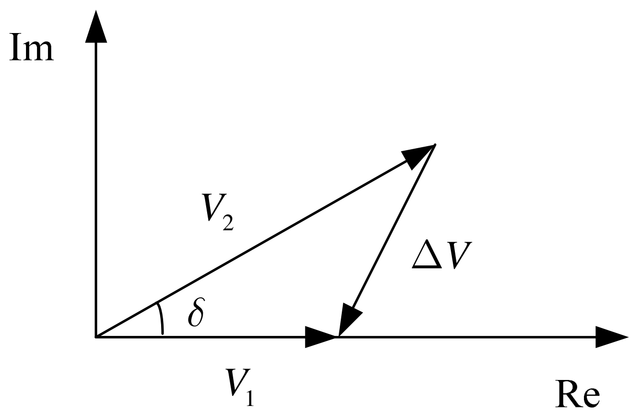

Figure 1-15 Phasor diagram between converter voltage and grid voltage

Figure 1-16 illustrates the case when the VSC operates purely as a reactive power compensator. When the converter voltage V_2 and the AC system voltage V_1 have the same magnitude (Figure 1-16 a) there is no exchange of reactive power between the converter and the system .While V_2 is larger than V_1 the current leads the voltage by 90 degrees (Figure 1-16 b), the converter behaves as a capacitor and, thus, generates reactive power. On the other hand, when V_2 is smaller than V_1 the current lags the voltage by 90 degrees and the converter behaves like an inductor and absorbs reactive power (Figure 1-16 c).

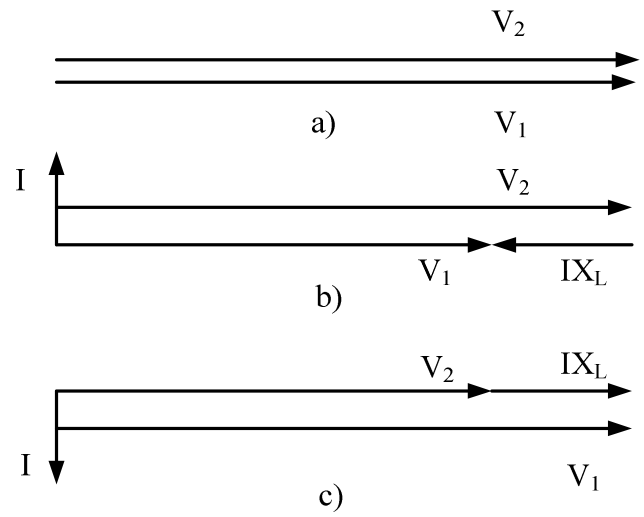

Figure 1-16 Purely inductive operation of the VSC

In this mode of operation the VSC is similar to a synchronous compensator but with the advantage of not having an inertia and practically instantaneous response (usually known as STATCOM). Thus the VSC acts as an AC voltage source, controlled to operate at the same frequency as the AC system to which it is connected[14].

Therefore by adjusting $V_2 \cdot \sin\delta$ and $V_2 \cdot \cos\delta$ a VSC can operate at any power factor as shown below.

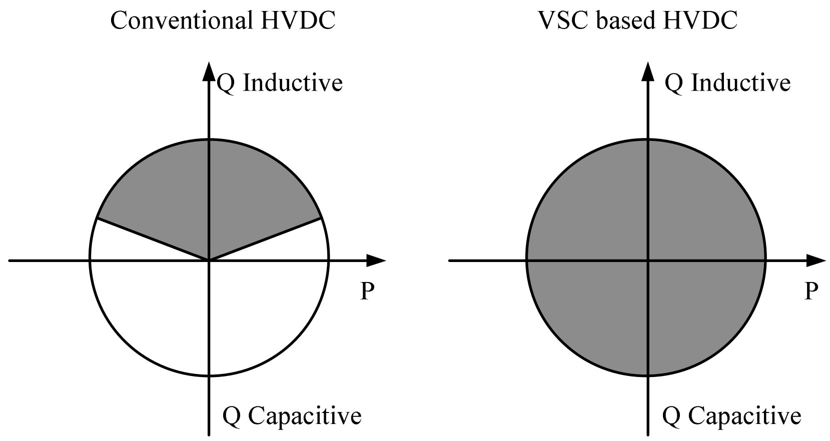

Figure 1-17 Four quadrant operation of the VSC

1.1.3.4 MTDC operation of the HVDC system

In addition to transmitting power over long distances, MTDC systems are also used to interface independent AC systems and to enable voltage and frequency support from one system to another. Due to its flexibility and fast control, it also has the potential to be utilized for the interconnection of WF.

Figure 1-18 show the topology of multi terminal VSC-HVDC systems for large-scale WFs, where a common DC-bus is shared by several VSCs. In this way, the system is more reliable because compared with the traditional point to point connection where all the energy produced by the WF was processed by only one converter; the multi-terminal topology allows the energy to be shared between the converters[18].

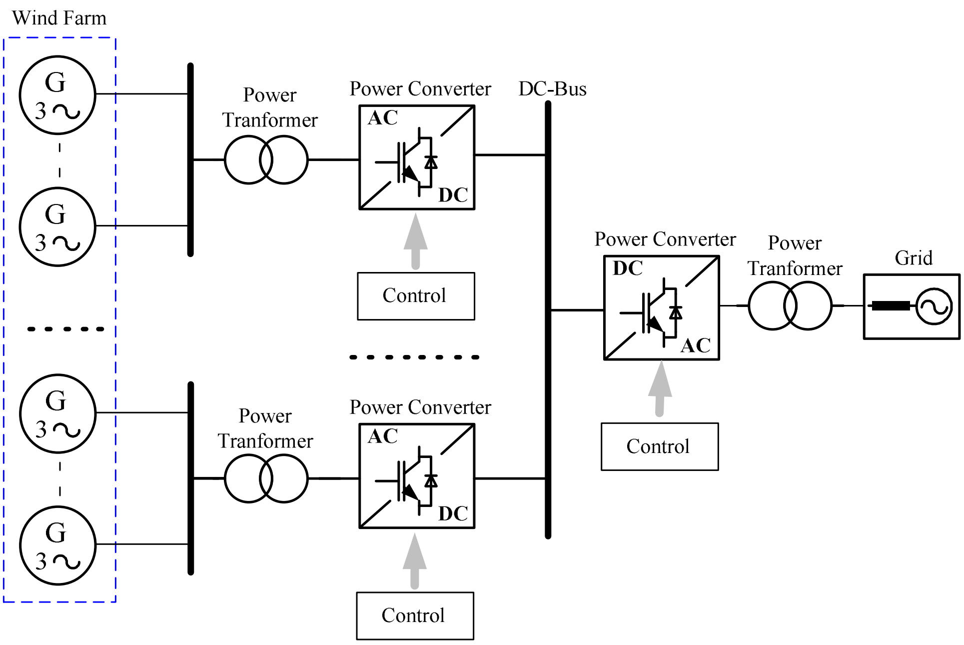

Figure 1-18 Multi-terminal WF connection

Another advantage which makes this topology more attractable is that only a small number of WTs are connected to one VSC. Connecting a small number of WTs from the WF to every converter means creating a cluster which has certain properties like different frequency in the AC collector depending on the wind speed present in the cluster and finally a better overall power extraction from the wind. This type of MTDC improves also the reliability and availability of the system because in case of a fault in the AC collector of the WF or due to maintenance only a small number of WTs are disconnected and stopped, while the rest still produce power.

A more general description of the multi-terminal HVDC system is presented in Figure 1-19 where the MTDC system connects different AC grids with distributed generation units (offshore WF or oil and gas platforms) or supplies passive load. Each converter is a VSC and the DC side of each converter is connected in parallel through the DC network [19-20].

There are potential economic and performance benefits associated with using MTDC for such power distribution applications. The MTDC system has the ability to balance the power and enhance the reliability of the system.

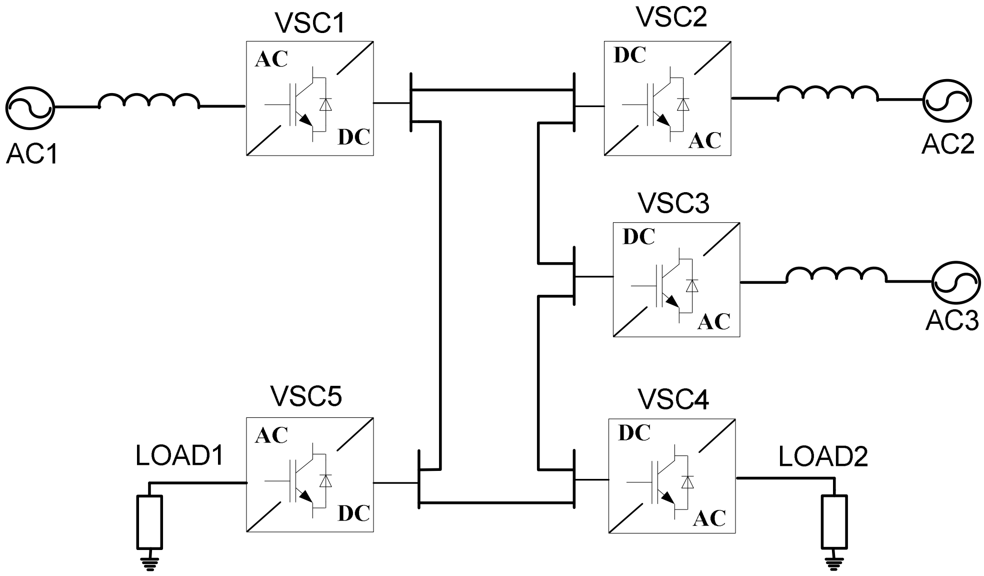

Figure 1-19 MTDC connection using VSCs [19].

In general, each converter is controlled by the local control and the whole system is coordinated by the master control. The local control transforms the setting values into the firing pulses and controls the related variables of the converters. The main objective of the MTDC system is to use a master control which can optimize the whole performances of the system both in normal operation but also in different operating conditions like grid faults or stability problems created by overloads.

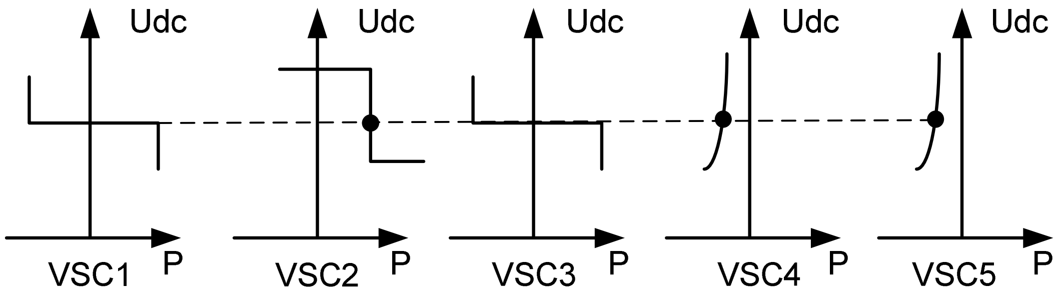

Figure 1-20 Control strategy of every VSC in the MTDC system [19]

From Figure 1-20 it can be observed that both VSC1 and VSC3 adopt the DC voltage control strategy and VSC2 operates at constant active power. VSC4 and VSC5, which act as inverter stations to supply passive networks, adopt the constant AC voltage controllers and ensure a fixed AC voltage and frequency on the AC side [19].

1.2 Problem formulation

With VSC-HVDC, the concept of super-grids, which aims to connect a wide area using long distance transmission lines in order to take advantage of renewable sources distantly located, became possible through Multi terminal VSC-HVDC (see Figure 1-21). A multi terminal HVDC system consists of more than two converters connected through DC line cables and sharing the same DC bus.

Multi terminal HVDC system has advantages over two-terminal HVDC one in many aspects such as:

- Control flexibility,
- Reliability and economy.

In this case, there are some benefits that can be listed:

- Bulk power transmission,
- AC network interconnection over a long or medium distance,
- Economical advantages such as total installed converter rating in an MTDC system is usually less than that of several equivalent two HVDC systems,
- MTDC systems offer low cost transmission lines and/or cables,
- The inherent overload capability of MTDC transmission lines can increase the capacity of transmission corridors.

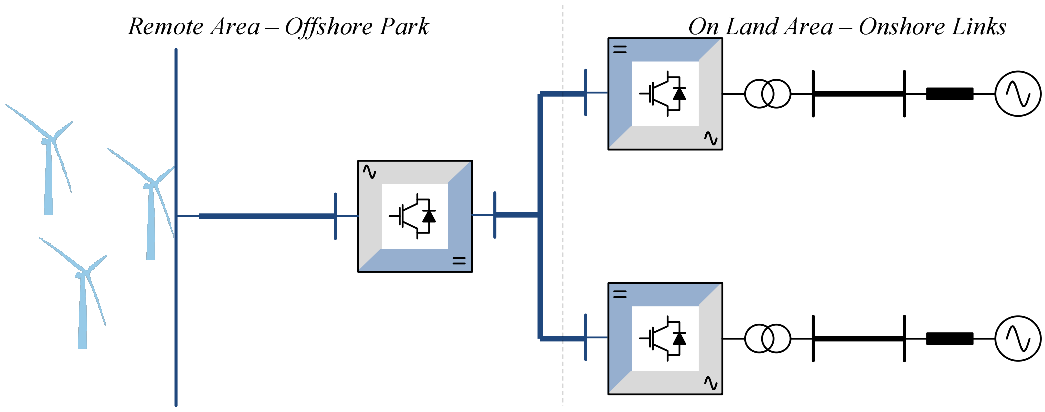

Figure 1-21VSC based MTDC

Examples for them are MTDC systems provide greater flexibility in dispatching transmitted power, in a larger interconnected power system, MTDC systems can provide a powerful control action to damp out troublesome electromechanical oscillations, in conjunction with phase shifting transformers and generation shifting, MTDC systems may be used to enforce desired power flow patterns in a large interconnected power system, the fundamental control principle for MTDC systems is a natural generalization of that for existing two HVDC systems.

When more than one receiving-end station is considered, the power flow needs to be controlled in order to achieve a determined power exchange among interested partners who divide the same DC link. Also, different AC grid requirements can be permitted where the onshore stations are connected. Due to that, the share of power can change and must be controlled.

1.3 Objectives

The main objectives of this project are the followings:

- Implement control strategies for DC voltage control and analyze the power sharing requirements for different conditions.
- Validate the control using PSCAD/EMTDC simulation software
- Build and implement the overall system on a dSPACE control platform in the laboratory
- Evaluation and validation of the results by scaling down the MTDC system to 15kW

1.4 Limitations

During the project development several limitations had to be considered. Thus, the most important limitations of this project were summed up and are presented as follows:

- The implementation in the laboratory had to be scaled down to 15 kW due to lack of high voltage, high power equipment
- The system is simulated without the offshore station
- For the HVDC cable only the resistive character was consider
- The value of the capacitor is different than the desired value due to construction constrains of the 15 kW converters.

1.5 Thesis outline

The first chapter realizes a short presentation of the High Voltage Direct Current (HVDC) transmission system and MTDC interconnection. Various wind turbine (WT) trends are highlighted and different grid code requirement are presented with the purpose to underscore their importance in the integration of the wind energy. Later on the problem is defined, the objectives are listed, the project limitations are mentioned and finally the project outline summarizes the structure and content of the report.

The second chapter gives an overview of the HVDC MTDC system. A brief description with the complete model of a multi-terminal system including an equivalent model for the wind farm, the HVDC cable, the power converters, the filters and the grid connection is presented in the first part. Moreover, a detailed analysis of each component is made in order to reproduce a proper system behavior.

In this third chapter, the control structure and design of a multi terminal HVDC system is illustrated. The chapter begins with a brief description of the overall system and the main objectives are highlighted, then the control strategies and design of the grid connected VSC including current control, DC voltage control, active power control, the design of the PLL are presented. Moreover, the grid connected VSC operation is presented in a point to point HVDC connection where the converters have different control strategies. Finally, the VSC operation is described in MTDC configuration and the DC bus sharing is emphasized.

In the fourth chapter, the performance of the multi terminal HVDC system is evaluated. In the first part, the PSCAD model is validated for different cases like steps in power production, different sharing factor in active power or different values for the virtual resistance. Moreover, the performance of the system is analyzed under special conditions such as abnormal functioning and parts of the MTDC system has to be stopped. Finally, the chapter ends with an analysis and the results are evaluated.

The fifth has the goal to validate the MTDC system on a real implementation. In the first part, the description of the laboratory setup is realized followed by the validation of the control under different situations. Moreover, the study cases proposed Chapter 4 are also analyzed and the results are compared.

In the last chapter the conclusions are presented and also the ideas for future work are summarized.

Chapter 2

MTDC modeling

This chapter gives an overview of the HVDC MTDC system. A brief description with the complete model of a multi-terminal system including an equivalent model for the wind farm, the HVDC cable, the power converters, the filters and the grid connection is presented in the first part. Moreover, a detailed analysis of each component is made in order to reproduce a proper system behavior.

2.1 MTDC system modeling

The complete model of the MTDC system including the WF, SEC station, DC cable, REC station, filter and the grid connection is presented in Figure 2-1

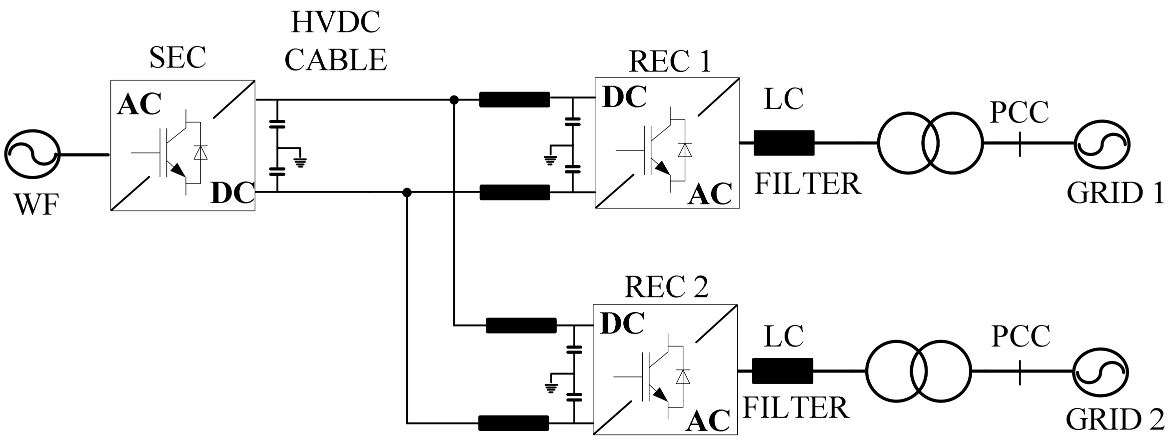

Figure 2-1 MTDC main parts

2.2 Presentation of MTDC system main parts

A description of each component of the MTDC system is presented further on. The order of the described components follows the order of the energy conversion process.

2.2.1 Equivalent model for WF

Increasing numbers of wind turbines are connected to electrical power systems, in order to reduce the adverse environmental impact of conventional electrical power generation. Compared to the large conventional power plants, which are characterized by a high rated power of installed generators and a relatively low number of units spread over a defined area, the wind turbines have a low rated power of individual units but their number is very high.

Moreover, the power produced by wind turbines has, in general, a non-controllable stochastic character since it depends on the weather conditions.

Considering an additional large number of wind turbines in the power system model would lead to long simulation times and, in some cases, to problems with the numerical stability of the simulation software. In order to avoid the necessity of developing a detailed model of a WF with tens or hundreds of WTs and their interconnections and to calculate the wind speed signal for each individual turbine, aggregated WF models are developed.

In the aggregation process, units with similar dynamic behavior were identify, which means units that are coherent (see Figure 2-2). The dynamic behavior of a wind farm depends strongly on the current point of operation of each wind turbine [21-22].

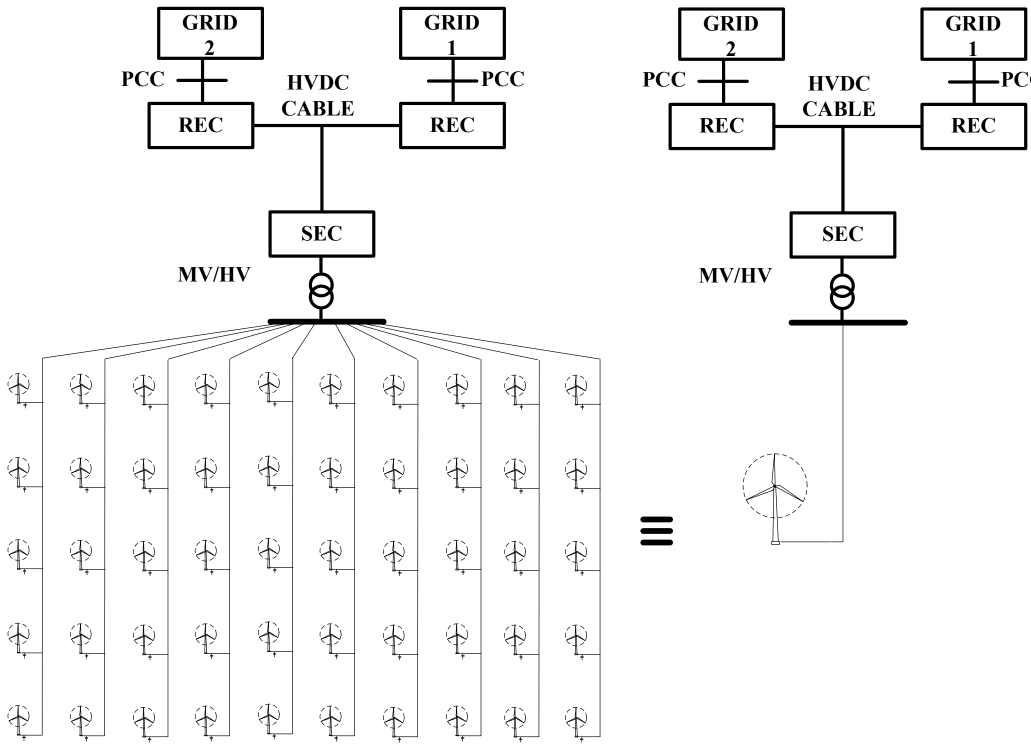

Figure 2-2 Aggregated WF model

In this project several assumptions were considered for the WF aggregation model because this was not the focus of the project and the purpose of the model was to consider the overall behavior:

- The whole WF was aggregated as a single WT consisting of all WT in the WF
- The wind direction is always the same, only the speed was varied
- The wake effect of each row of WT over the wind characteristics was neglected
- The type of generator used in the WTS is not a key factor since at high power ratings both types (induction generator and synchronous generator) have the same overall efficiency and the WTS efficiency was considered to be around 93% [23].
- Power losses in the sending end converter were considered to be 1-2% [24].

Taking into consideration the assumptions listed above, the total power produced by the wind farm is expressed as:

$$P_{WF} = P_{WT} \cdot n \cdot \eta_{WT} \cdot \eta_{SEC} \tag{2.1}$$

where,

P_{WT} - the power produced by one WT

n - the number of wind turbines

η_{WT} - the efficiency of a WT

η_{SEC} - the efficiency of the sending end converter

The power that the WT can absorb from the wind is proportional with the swept aria A the air density ρ at normal conditions, the power coefficient C_p and the cubic of the wind speed v^3 as described below:

$$P_{WT} = \frac{1}{2} \cdot \rho \cdot A \cdot C_p \cdot v^3 \tag{2.2}$$

2.2.2 HVDC cable

Polymeric cables are the preferred choice for HVDC mainly because of their mechanical strength, flexibility and low weight. The HVDC cable in PSCAD is modeled as a PI section (see Figure 2-3). In the single PI line model, R is the total line resistance, L is the total line inductance and C is the equivalent line capacitance at the beginning and at the end of the line.

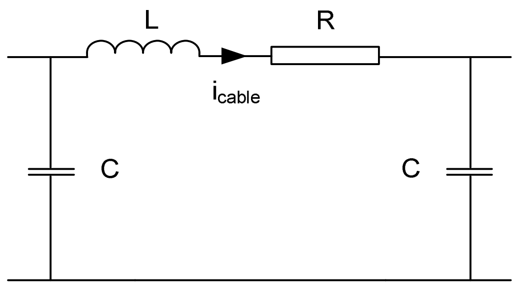

Figure 2-3 Standard PI model

In this project for the HVDC cable was simplified and it was modeled considering only the resistance and the inductance characteristics of the cable.

2.2.3 DC – capacitor

The DC capacitor is an important part of the HVDC system and the design of it has to satisfy certain requirements. Different actions like PWM switching and disturbances on the AC side will result in DC voltage ripple and oscillations. The aim of the capacitor is to limit the oscillations, provide a stable voltage and offer energy storage in order to control the power flow.

One aspect that characterizes the DC capacitor is the time constant, which is defined as the ratio between the energy stored at the rated DC voltage and the nominal apparent power of the converter (see Equation(2.3)). This time constant is the time needed to charge the capacitor from zero to rated DC voltage when is supplied with nominal power. Usually τ is chosen to be less than 5 $[ms]$ [25].

$$\tau = \frac{\frac{1}{2} \cdot C_{DC} \cdot V_{DC}^2}{S_N} \tag{2.3}$$

where,

C_{DC} - the DC capacitance in $[uF]$,

V_{DC} - the DC voltage in $[kV]$,

S_N - the rated apparent power in $[MVA]$.

2.2.4 Voltage source converter

The MTDC system consists of two PWM voltage source converters (VSC) as shown in Figure 2-4 . In a point to point HVDC configuration, one of the stations operates as an inverter while the other one functions as a rectifier. Using the voltage source converter in a MTDC system means adding flexibility to the system in such a way that both converters can operate either as inverters, either as rectifiers, either as in point to point HVDC configuration.

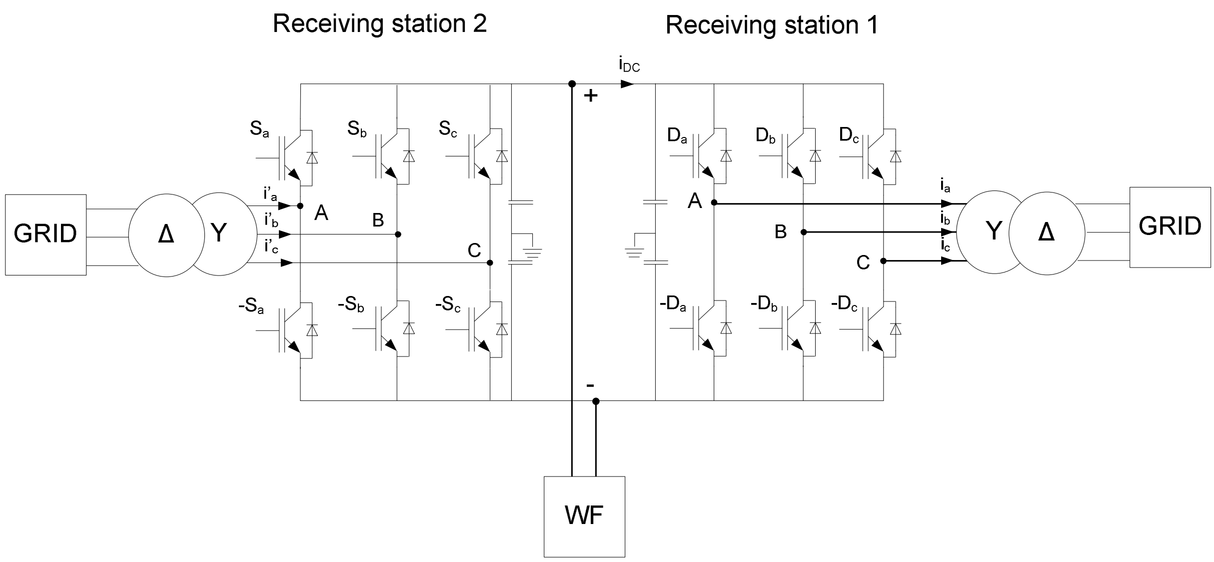

Figure 2-4 VSC in the MTDC system

In the circuit presented in Figure 2-4 there are two full-bridge converters having ideal IGBTs as switches. The status of the switch (S_x or D_x) can be either 1 or 0 which means that the device is on or off. Each of the legs has two switching devices which means that if both are conducting a short circuit will occur. In this case if one is turned ON, the other one has to be turned OFF.

Knowing the DC-link voltage and the switching states S_a, S_b, S_c from the converter in the receiving station 2 or the switching states D_a, D_b, D_c from the converter in the receiving station 1, every phase voltage can be expressed [26].

The phase voltages in a star connection are given in equation(2.4):

$$\begin{bmatrix} v_{AN} \\ v_{BN} \\ v_{CN} \end{bmatrix} = \frac{V_{DC}}{3} \begin{bmatrix} 2 & -1 & -1 \\ -1 & 2 & -1 \\ -1 & -1 & 2 \end{bmatrix} \begin{bmatrix} S_a \\ S_b \\ S_c \end{bmatrix} \tag{2.4}$$

Knowing the phase currents i_a, i_b, i_c and the switching variables, the DC-link current I_{DC} is calculated:

$$\mathrm{I}_{DC} = \begin{bmatrix} S_a & S_b & S_c \end{bmatrix} \begin{bmatrix} i_a \\ i_b \\ i_c \end{bmatrix} \tag{2.5}$$

2.2.5 Filter

The main goal of the filter is to reduce the high frequency harmonics around the switching frequency produced by the VSC.

The traditional way to solve the problem is to use an L filter which is easy to be implemented but it is useless for high power, due the fact that its inductance should be very high and will reduce the system dynamics. Adding a parallel capacitance (LC filter), the inductance value can be reduced. Still other problems might appear, like high inrush currents, high capacitance current at the fundamental frequency, or dependence of the filter on the grid impedance for overall harmonic attenuation[27].

Therefore a third order LCL filter (see Figure 2-5) can be used due to the good performances in current ripple attenuation even for small inductances and due to small size, which is very important for the MTDC system.

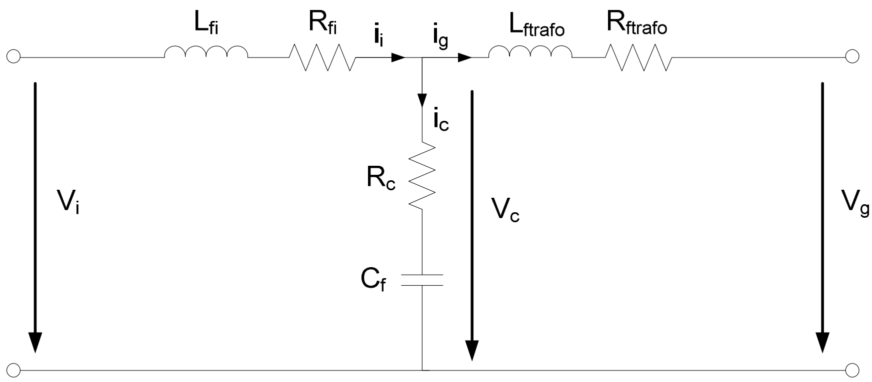

Figure 2-5 LCL filter single phase diagram

However, this filter configuration brings an undesired resonance frequency that may in fact increase the ripple. The resonance frequency can be calculated with following equation:

$$\omega_{res} = \sqrt{\frac{L_{fi} + L_{fg}}{L_{fi} L_{fg} C_f}} \tag{2.6}$$

One way to attenuate a part of the ripple of the switching frequency is to add a resistance added in series with the capacitor. The value of this resistor should be one third of the impedance of the filter capacitor at the resonant frequency. Another way to solve this problem is to apply an active filter which is a notch filter tuned at the resonance frequency of the LCL filter. Both of this methods have significant advantages like ripple attenuation, they avoid the resonance and reliability, they also have some drawback like increased power losses through heat dissipation, which leads to further costs for designing and building a cooling system[28].

2.2.6 Transformer

In order to connect the HVDC system to the grid a transformer is used at the PCC to increase the voltage level. Moreover, the transformer is also used for connecting the offshore AC grid of the WF with the VSC SEC.

In all situations, the main function of the transformer is voltage level conditioning and galvanic insulation of the two connected circuits.

2.2.7 The electrical grid

The proposed model of the grid is based on the Thevenin equivalent circuit. The equivalent circuit is shown in Figure 2-6.

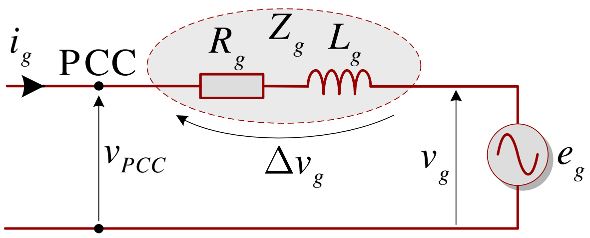

Figure 2-6 The equivalent Thevenin circuit of the grid

In the equation (2.7) is described the relation between the voltage at point of common coupling v_{PCC} and the grid voltage v_g.

$$v_{PCC} = v_g + \Delta v_g = v_g + i_g \cdot Z_g \tag{2.7}$$

Usually, the grid impedance is mainly inductive therefore the grid impedance is mostly considered as:

$$Z_g = R_g + j \cdot \omega \cdot L_g \tag{2.8}$$

Depending on the value of the grid impedance, the grid can be stiff (low grid impedance) or weak (high grid impedance).

Chapter 3

Control structure of the MTDC system

In this chapter the control structure of a multi terminal HVDC system is illustrated. The chapter begins with a brief description of the overall system and the main objectives are highlighted, then the control strategies and design of the grid connected VSC including current control , DC voltage control, active power control, the design of the PLL are presented. Moreover, the grid connected VSC operation is presented in a point to point HVDC connection where the converters have different control strategies. Finally, the VSC operation is described in MTDC configuration and the DC bus sharing is emphasized.

3.1 Control objectives

Wind farms with large number of WT are installed all around the world and the integration of such units especially the offshore ones are facing great challenges for the developers and also for the system operators when comes to connect them to the grid. Thus, the VSC based MTDC system is one feasible solution for delivering the power produced by the WF into the grid.

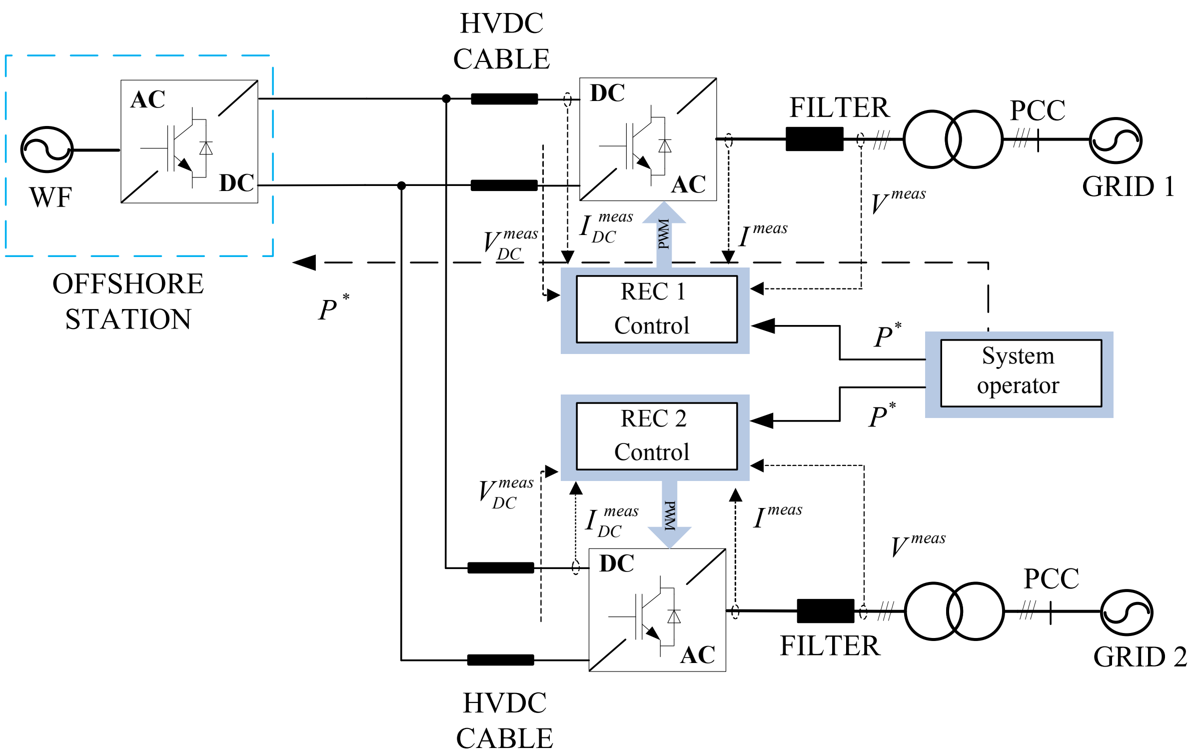

Figure 3-1 Overall control structure of the MTDC system

The control structure of the MTDC system which interfaces large wind power plants to the grid, presented in Figure 3-1, has to accomplish two main objectives: one of the objectives is to optimize the process in order to have satisfactory results and the second one is to provide protection for the equipment used in the system.

The control of the MTDC systems has to ensure that all the power produced by the WF is injected first into the DC link by means of the offshore station and then transferred into the grid by means of receiving stations. In this way the MTDC system acts like an energy buffer if no storage devices are present in the DC connection.

Power converters (see Figure 3-1) play an essential role in the safe operation of the system. The common point of the MTDC is the DC voltage which has to be kept at a constant value in all conditions. Disturbances in the DC link voltage can cause the system to trip and may disrupt the normal operation. This operation has to be accomplished furthermore when the system consists of multiple power generation units and multiple loads.

3.2 Control of the grid connected VSC

The receiving station consists of a voltage source converter which represents the key element in the MTDC system because makes the connection between the HVDC system and the AC grid. Its main contribution to the system is to keep the active power balance between generation and consumption and to supply the grid with reactive power when requested by TSO, especially during grid faults.

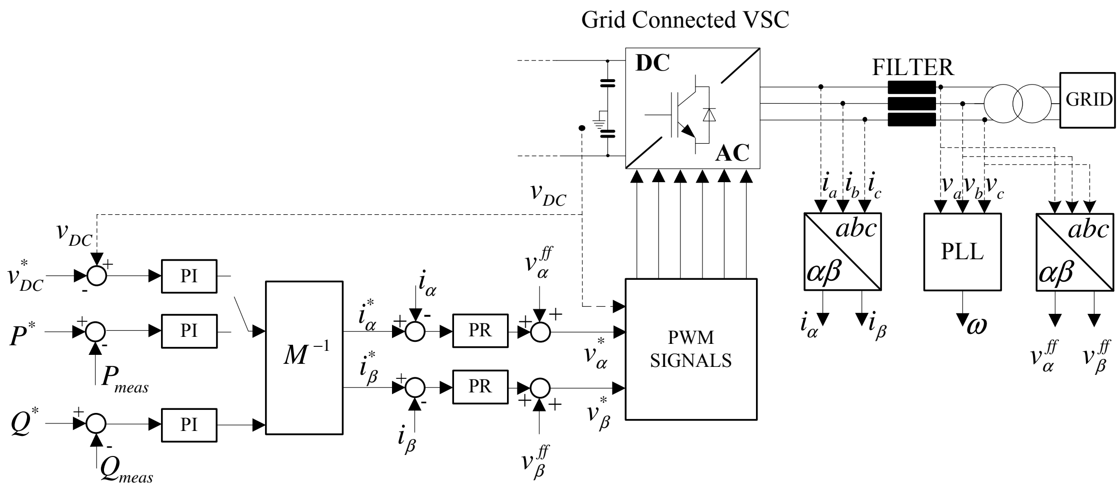

Figure 3-2 Control of the grid connected VSC

The control strategy applied to the grid connected converter consists mainly of two cascaded loops. While the inner loop realized in stationary reference frame is responsible with current control and power quality, the outer loop regulates the DC voltage or active power and reactive power imposed by the TSO.

To have a constant DC voltage, the measured DC voltage is compared with a reference and fed up into a PI controller. The output of the controller is cascaded by the inverse matrix used in the instantaneous power theory which acts as a gain in the system, in order to obtain the reference in α – axis current and β – axis current.

The AC voltage level can be controlled by the amount of reactive power injected into the grid. The difference between the measured and the reference in reactive power is also controlled by a PI controller and then multiplied by the inverse matrix used in the instantaneous power theory.

Even though in this case it seems that the PLL has no use, still it is used for synchronization with the grid and for determining the frequency because that is the resonant frequency of the resonant controller and the system will have a better performance during changes in the grid voltage.

3.2.1 Current loop

One way to structure the control loops is to use the implementation in stationary reference frame, as showed in Figure 3-2.

The grid currents are transformed into stationary reference frame using the *abc to αβ* transformation. Because the control variables are sinusoidal in the *αβ* reference frame and due to the fact that a PI controller is not capable to remove the steady-state error when controlling sinusoidal references, utilization of a different controller type is necessary[29].

The resonant controller has gained a large popularity in the last decade in current regulation of grid-connected applications. The controller is expressed as:

$$G_c(s) = K_P + K_I \cdot \frac{s}{s^2 + \omega^2} \tag{3.1}$$

As it can be seen in Figure 3-3, the controller has an infinite gain around the resonant frequency ω. The width of this frequency band depends of the integral term K_I. A low K_I leads to a very narrow band while a high K_I leads to a wider band. Thus, the difference between a PR controller and a PI controller is the way the integration action takes part.

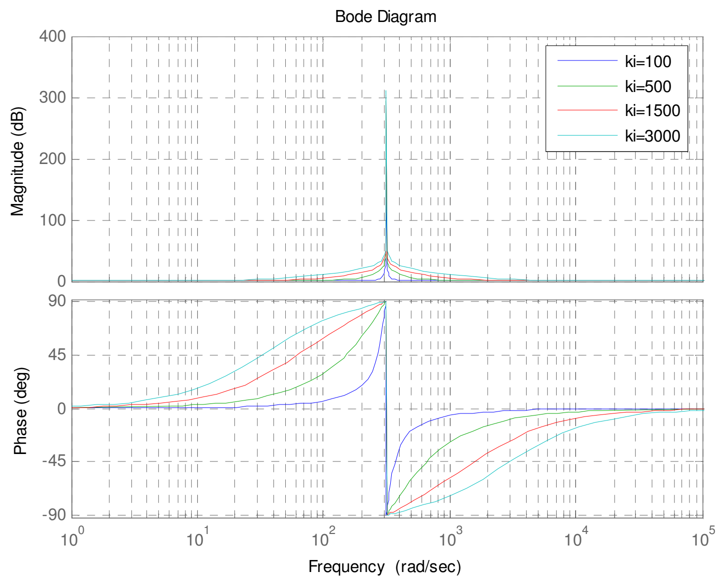

Figure 3-3 Bode diagram of a resonant controller

The integrator will only integrate frequencies very close to the resonance frequency and will not introduce stationary error or phase shift. The proportional term K_P it determines the bandwidth and the stability margins, in the same way as the PI controller[30].

The structure of the inner loop is implemented in the stationary reference frame and is presented in the figure below:

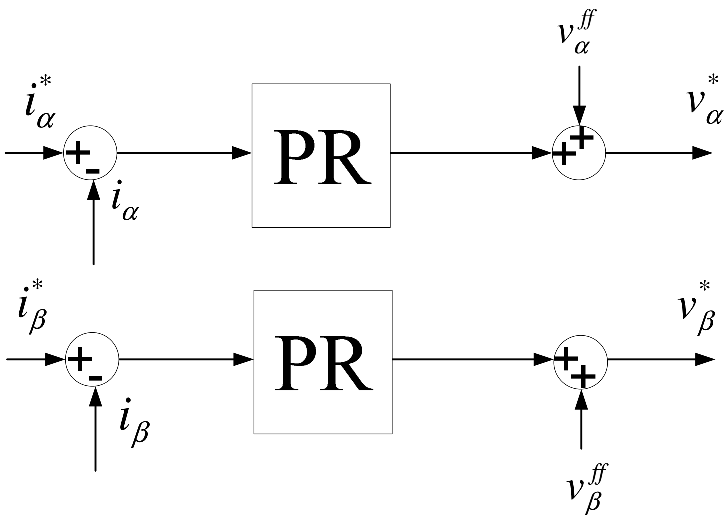

Figure 3-4 Control structure for the current controller

For a good performance of the current loop, the tuning of the resonant controller had to be made. In balanced grid situation, the current loop in α – axis and β – axis have the same performance and the same dynamic response, so in this way by tuning one of the controller in one axis the values obtained are considered also for the other axis. As it can be noticed in Figure 3-4, one benefit of using the resonant controller is that the axes are not coupled between each other and the control is simplified.

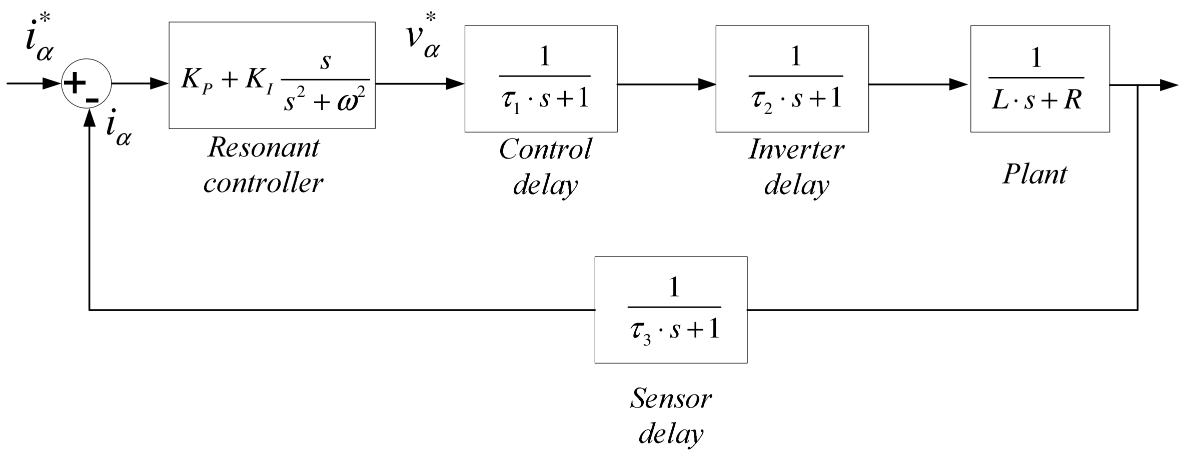

Figure 3-5 Block diagram for inner loop

The control diagram for α – axis is presented in Figure 3-5. Furthermore, some considerations were considered in order to simplify the control structure. Taking into account that the control should have a fast response in any situation, the delay introduced by it and the delay introduced by the converters should be disconsidered because is too small and insignificant for the system.

The simplified structure of the inner loop is presented below:

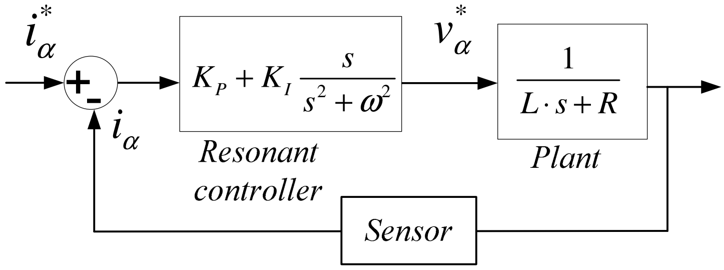

Figure 3-6 Simplified structure of the inner loop

In the simplified structure of the current loop the plant equation in the continuous domain is given by:

$$G_P = \frac{1}{L \cdot s + R} \tag{3.2}$$

where,

L - is the inductance of the filter $[mH]$

R - is the parasitic resistance of the filter $[\Omega]$

If the parasite resistance is mistreated, the plant equation is:

$$G_P = \frac{1}{L \cdot s} \tag{3.3}$$

One goal of the current controller is to have good performance but also to offer protection. In this way, the tuning process of the resonant controller had to be investigated and several steps were made. At the begging the resonant controller components K_p and K_I were obtained using the root locus method and after that the controller response was analyzed using MATLAB SISOTool and the parameters were adjusted.

Using the root locus method, the resonant controller had to meet some requirements in terms of damping factor and bandwidth and they are given as:

- The system should have a damping factor ζ of:

$$\zeta = 0.707$$

- The bandwidth of the controller is :

$$\omega_n = \frac{2 \cdot \pi \cdot f_s}{10}$$

where,

f_s - is the switching frequency $[\mathrm{Hz}]$

For the given requirements the values of K_P = 14.26 and K_I= 201.56 are found. Furthermore, SISOTool is used to verify the performance of the controller with the parameters obtained from the root locus criterion.

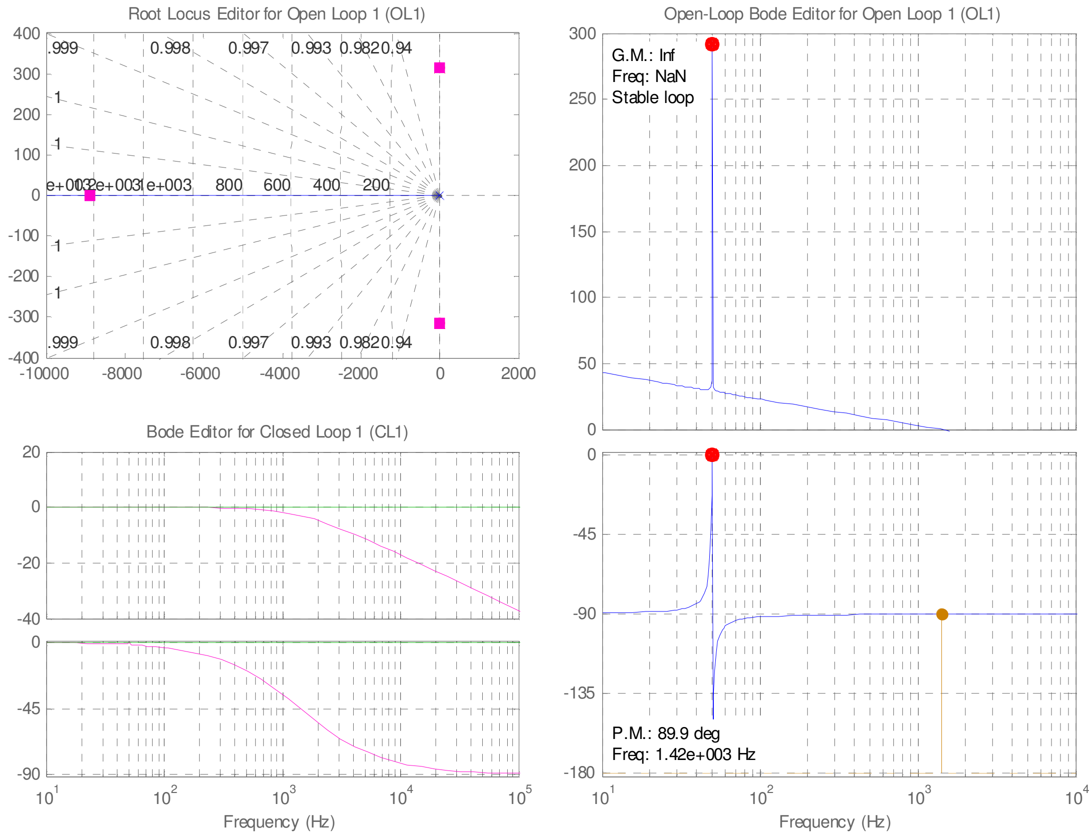

Figure 3-7 Root locus and Bode diagram for the inner loop

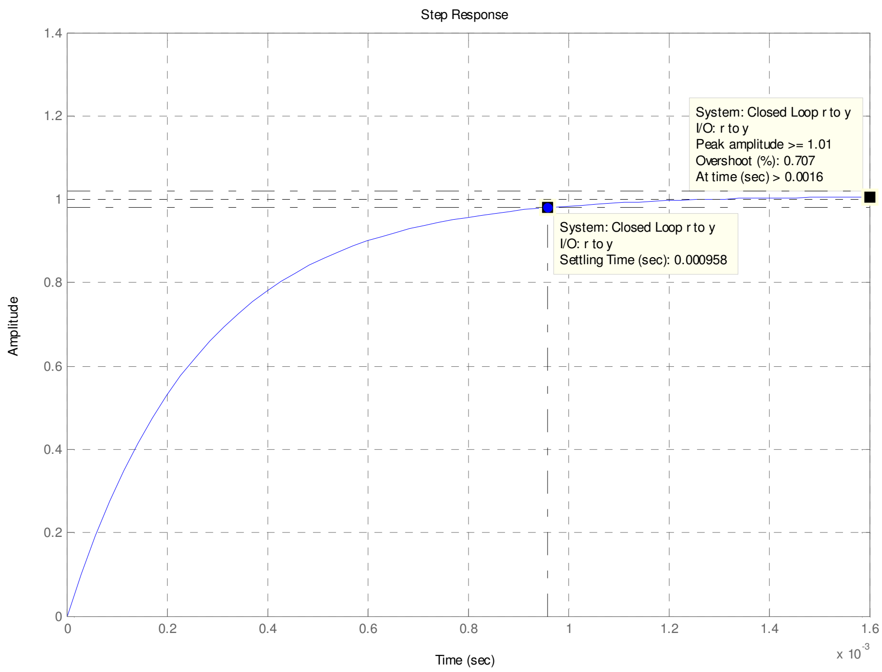

Figure 3-8 The step response of the current loop

In Figure 3-7 the Root locus and Bode diagram of the designed α-axis current loop are presented. It can be easily noticed that all the poles are in the left side of the complex plane, thus indicating that the system is stable and fulfills the requirements.

The step response is presented in Figure 3-8. The figure points out the following: a zero error in steady state, an overshoot of 0.7% and a settling time of $0.9[ms]$. The same values for K_P and K_I were used for β-axis resonant controller because the plant equation for the current remains the same.

3.2.2 DC voltage control

The outer loops presented in Figure 3-2 used in the control of the grid connected VSC have the purpose of controlling the DC voltage and the reactive power which the converters can inject or absorb from the grid. By controlling the DC voltage, the converter is ensuring that the active power on the DC side is transferred into the AC grid. In this way without any storage devices, the converter acts like an energy buffer and only the transmission losses and the switching losses are encountered taking into consideration that in the HVDC application the level of voltage and power is much bigger than in the case of low voltage application where the switching losses can be neglected.

As mentioned in the Section 3.2.1, all the delays produced by the control, the inverter, the analog to digital conversion and the sensor are also neglected for the outer loop.

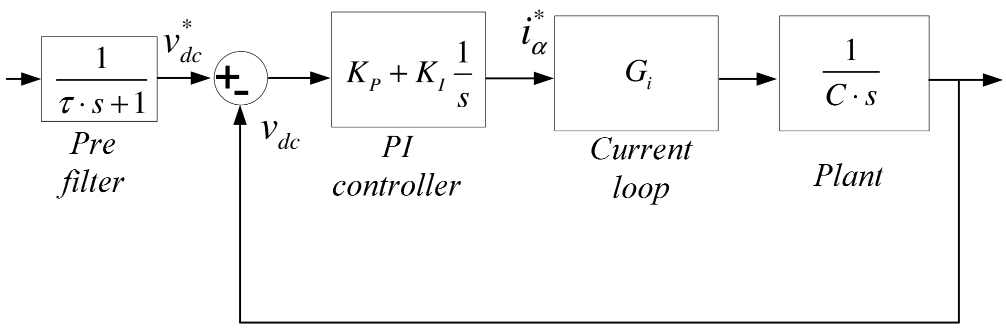

Figure 3-9 Block diagram of the outer loop

Any unbalance in the active power transferred through the converter will be the cause of DC voltage fluctuations. Since the value in the outer loop is DC value, the controller used in this case is a PI controller. The bandwidth of the controller is decided by Kp, while Ki is removing the steady state error. The output of the controller is then multiplied by a gain and will determine the reference in α – axis current β – axis current.

To control the DC voltage means to control the DC voltage across the capacitor on the DC side, therefore the plant equation for the outer loop is given by:

$$G_P = \frac{1}{C \cdot s} \tag{3.4}$$

where,

C - is the DC capacitance $[uF]$

Using the root locus method, the PI controller had to meet some requirements in terms of damping factor and bandwidth and they are given as:

- The system should have a damping factor ζ of :

$$\zeta = 0.707$$

- The bandwidth of the controller is :

$$\omega_n = \frac{2 \cdot \pi \cdot f_s}{100}$$

where,

f_s - is the switching frequency $[\mathrm{Hz}]$

As it can be noticed above the bandwidth of the outer loop controller has been selected to be 10 times smaller than the bandwidth of the inner loop. This means also that the current loop is 10 times faster than the DC voltage loop and the system performs in a stable region.

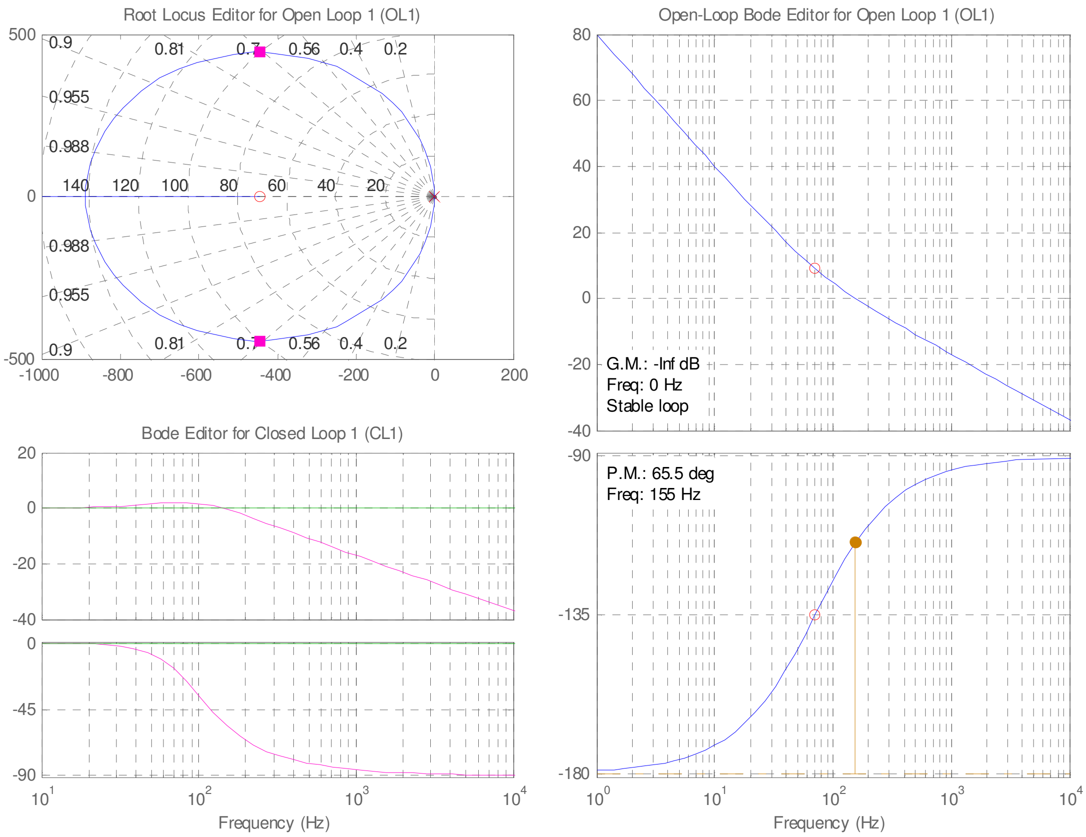

Figure 3-10 Root locus and bode diagram of the outer loop

For the given requirements, the values of K_P = 0.97 and K_I= 434.26 are found. Furthermore, SISOTool is used to verify the performance of the controller with the parameters obtained from root locus criterion and the results are presented in Figure 3-10.

The step response for the DC voltage loop is presented in Figure 3-11 and it can be observed that the settling time is 7.7 $[ms]$ which is approximately ten times larger than the settling time for the inner.

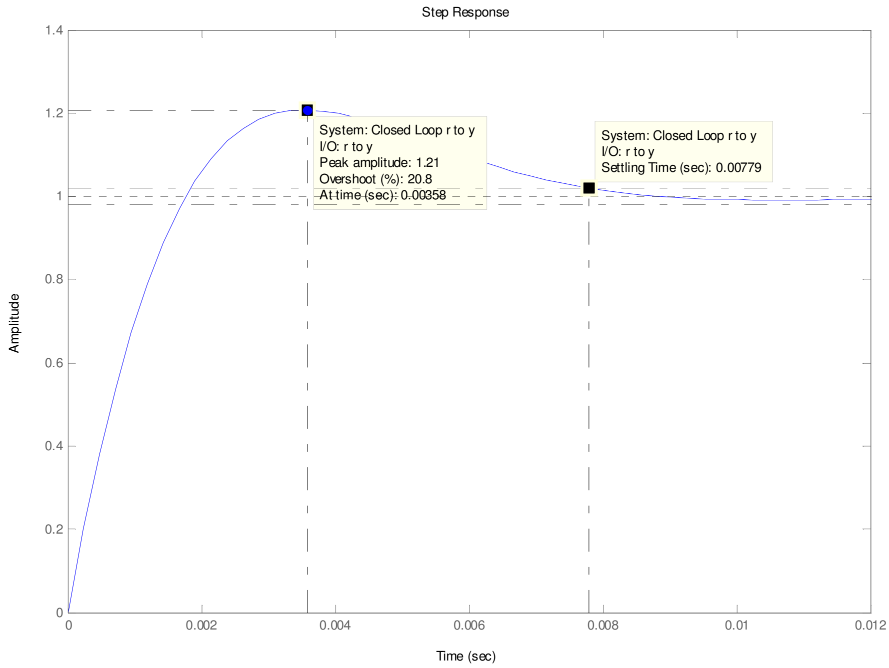

Figure 3-11 The step response for the outer loop

Using the root locus method only the placement of the poles is adjusted and as it can be seen from Figure 3-11 the overshoot is higher than admitted in MTDC systems where it should be around 5% considering the voltage level the system works[31].

In this case a tradeoff between system stability and performance has to be made. The use of a pre-filter is essential for the control architecture because it introduces a pole in the system in order to cancel the effect of the zero introduced by the controller and in this way it reduced the overshoot (see Figure 3-12). Usually a low pass filter is used tuned at the frequency of the zero (see Figure 3-10). The pre-filter transfer function is expressed as low pass filter and presented below:

$$G_{pf} = \frac{1}{\tau \cdot s + 1} \tag{3.5}$$

where,

$\tau = \dfrac{1}{\omega_{zeroPI}}$ - The time delay introduced by the pre-filter

ω_{zeroPI} - The frequency of the zero introduced by the PI controller.

The use of the pre-filter acts on the system as a compensator and brings the response of the system in the desired requirements.

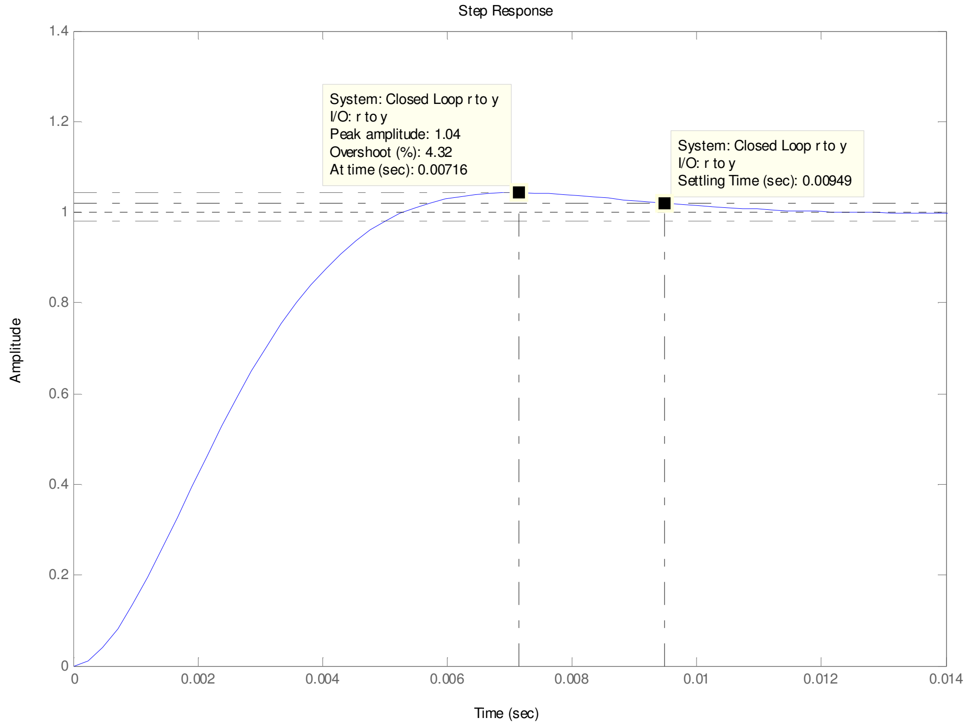

Figure 3-12 Step response of the outer loop with pre-filter

3.2.3 Active power control

The development of power electronics in power system has enabled new ways for transporting the power from one point to another. The HVDC solution brought a lot of flexibility in power transportation and distribution but also has brought new boundaries to the energy flow. The reason is that the converters are seen as nonlinear elements different from the traditional linear loads.

In case of the grid connected VSC used in the MTDC system, the problem of active and reactive power is raised and the *p-q theory* is analyzed.

Using the instantaneous values of voltage and current presented in Equations (3.6) and(3.7), the instantaneous complex power presented in Equation (3.8) is defined as the product of the voltage vector v and the conjugate vector i^* [32].

$$v = v_\alpha + jv_\beta \tag{3.6}$$

$$i = i_\alpha + ji_\beta \tag{3.7}$$

$$s = v \cdot i^* = (v_\alpha + jv_\beta)\cdot(i_\alpha - ji_\beta) = (v_\alpha \cdot i_\alpha + v_\beta \cdot i_\beta) + j\left(v_\beta \cdot i_\alpha - v_\alpha \cdot i_\beta\right) \tag{3.8}$$

Equation (3.9) defines p and q but also considers q as a product between voltage vector and lagging (inductive) current vector.

$$\begin{bmatrix} p \\ q \end{bmatrix} = \begin{bmatrix} v_\alpha & v_\beta \\ v_\beta & -v_\alpha \end{bmatrix} \begin{bmatrix} i_\alpha \\ i_\beta \end{bmatrix} \tag{3.9}$$

Taking into consideration the graphical approach presented in Figure 3-13 p can be defined as the dot product between the voltage and current vectors. This means the magnitude of the voltage vector is multiplied by the projection of the current vector. On the other hand q can be expressed as the cross product of the two vectors which indicates that q is the area of the parallelogram between them.

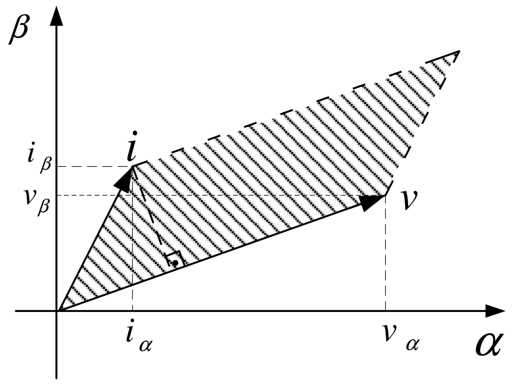

Figure 3-13 Vector representation of voltage and current in stationary reference frame

The control of the grid connected VSC is realized in stationary reference frame as presented in Figure 3-2 which indicates that the currents in α - axis and β - axis have to be controlled. Equation (3.10) calculates the references for i_α and i_β as it follows:

$$\begin{bmatrix} i_\alpha \\ i_\beta \end{bmatrix} = \frac{1}{v^2_\alpha + v^2_\beta} \begin{bmatrix} v_\alpha & v_\beta \\ v_\beta & -v_\alpha \end{bmatrix} \begin{bmatrix} p \\ q \end{bmatrix} \tag{3.10}$$

Expanding Equation (3.10) the current can be expressed as:

$$\begin{bmatrix} i_\alpha \\ i_\beta \end{bmatrix} = \frac{1}{v^2_\alpha + v^2_\beta} \begin{bmatrix} v_\alpha & v_\beta \\ v_\beta & -v_\alpha \end{bmatrix} \begin{bmatrix} p \\ 0 \end{bmatrix} + \frac{1}{v^2_\alpha + v^2_\beta} \begin{bmatrix} v_\alpha & v_\beta \\ v_\beta & -v_\alpha \end{bmatrix} \begin{bmatrix} 0 \\ q \end{bmatrix} \triangleq \begin{bmatrix} i_{\alpha p} \\ i_{\beta p} \end{bmatrix} + \begin{bmatrix} i_{\alpha q} \\ i_{\beta q} \end{bmatrix} \tag{3.11}$$

where,

$$i_{\alpha p} = \frac{v_\alpha}{v^2_\alpha + v^2_\beta} p$$

- is the instantaneous active current on α- axis

$$i_{\alpha q} = \frac{v_\beta}{v^2_\alpha + v^2_\beta} q$$

- is the instantaneous active current on α- axis

$$i_{\beta p} = \frac{v_\beta}{v^2_\alpha + v^2_\beta} p$$

- is the instantaneous active current on β - axis

$$i_{\beta q} = \frac{-v_\alpha}{v^2{}_\alpha + v^2{}_\beta} q$$

- is the instantaneous reactive current on β - axis

The instantaneous power on α and β axis is calculated as showed in Equation (3.12) and the total power is obtained using Equation(3.13).

$$\begin{bmatrix} p_\alpha \\ p_\beta \end{bmatrix} = \begin{bmatrix} v_\alpha i_\alpha \\ v_\beta i_\beta \end{bmatrix} = \begin{bmatrix} v_\alpha i_{\alpha p} \\ v_\beta i_{\beta p} \end{bmatrix} + \begin{bmatrix} v_\alpha i_{\alpha q} \\ v_\beta i_{\beta q} \end{bmatrix} \tag{3.12}$$

$$p = p_\alpha + p_\beta = v_\alpha i_{\alpha p} + v_\beta i_{\beta p} + v_\alpha i_{\alpha q} + v_\beta i_{\beta q} \tag{3.13}$$

The above equation can be dived in terms dependent producing active power (see Equation(3.14)) and terms which do not contribute to active power injection (see Equation(3.15))

$$p = v_\alpha i_{\alpha p} + v_\beta i_{\beta p} \tag{3.14}$$

$$0 = v_\alpha i_{\alpha q} + v_\beta i_{\beta q} \tag{3.15}$$

If the $\alpha\beta$ variables are transformed into abc variables the imaginary reactive power is expressed as:

$$q = v_\beta i_\alpha - v_\alpha i_\beta = \frac{1}{\sqrt{3}}(v_{ab} i_c + v_{bc} i_a + v_{ca} i_b) \tag{3.16}$$

It can be concluded that i_α and i_β both have active and reactive components, the sum of active power on α- axis and β - axis corresponds with the total instantaneous real power. The imaginary power q (see Figure 3-14) is proportional with the quantity of energy exchanged between the phases of the system and doesn't contributes to the power transfer[32].

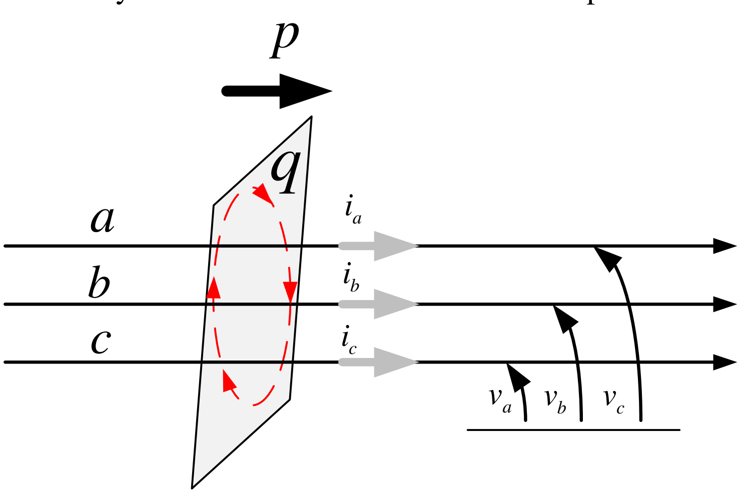

Figure 3-14 p and q representation in three wire system[32].

Taking into account the above mentioned, the control strategy for the grid connected VSC can be illustrated:

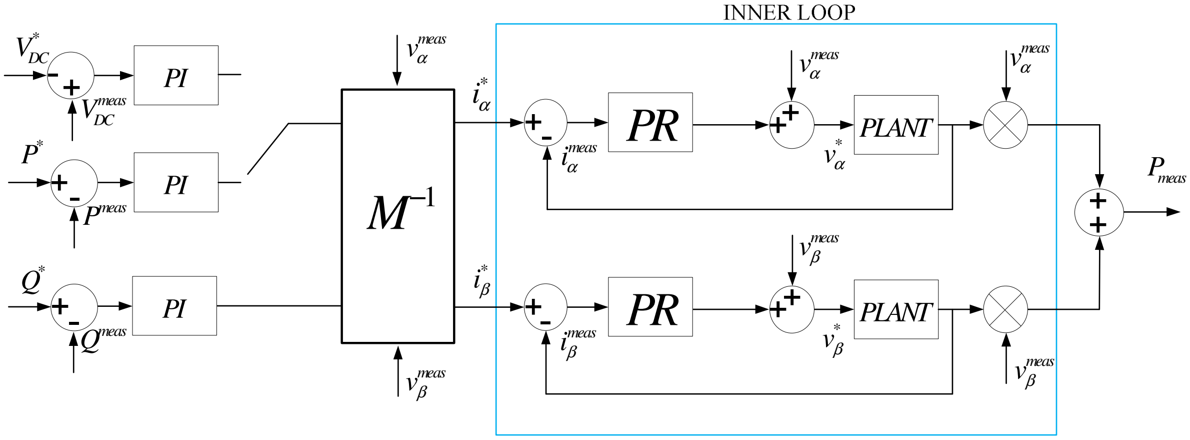

Figure 3-15 Block diagram of the active power control

In Figure 3-15 the outer loop controls either the DC voltage either the active power or reactive power. Both strategies are used in MTDC application. After the active power or DC voltage is measured and compared, depending on the control strategy, the error is regulated by a PI controller. The output of the controller is then fed up in a gain calculated using Equation(3.10) and the references in i_α and i_β current are obtained.

The current is than regulated using the resonant controller and injected into the grid. The injected current multiplied by the grid voltage will result in injection of active power.

3.2.4 Phase lock loop (PLL)

An important issue of the grid connected VSC control is the synchronization with the grid voltage at the PCC. The synchronization algorithm mainly outputs the phase of the grid voltage vector. The phase angle of the utility voltage is a critical piece of information for grid connected systems.

The PLL can be defined as a device which causes one signal to track another. It keeps an output signal synchronizing with a reference input signal in frequency as well as in phase. One of the structures used for grid synchronization, is the PLL and its schematic is illustrated in the figure below:

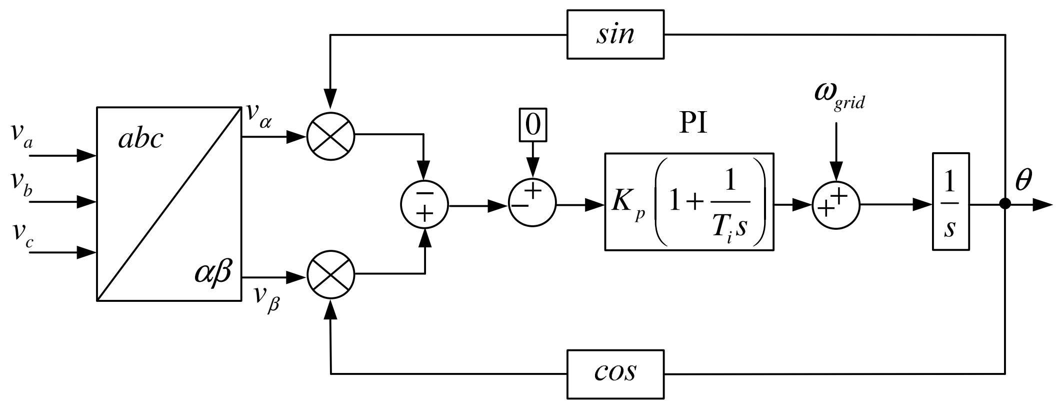

Figure 3-16 Block diagram of the PLL

In this system, the three phase utility voltages can be expressed as:

$$\begin{cases} v_a = V \cdot \sin(\theta) \\ v_b = V \cdot \sin\left(\theta - \dfrac{2\cdot\pi}{3}\right) \\ v_c = V \cdot \sin\left(\theta + \dfrac{2\cdot\pi}{3}\right) \end{cases} \tag{3.17}$$

Under the assumption that the utility voltage is balanced, equation (3.17) can be expressed in the stationary reference frame as:

$$\begin{cases} v_\alpha = \dfrac{2}{3}\cdot v_a - \dfrac{1}{3}\cdot v_b - \dfrac{1}{3}\cdot v_c \\ v_\beta = \dfrac{1}{\sqrt{3}}\cdot v_b - \dfrac{1}{\sqrt{3}}\cdot v_c \end{cases} \tag{3.18}$$

Using the PLL output $\hat{\theta}$ a, the above equation can be rewritten as:

$$V_q = -V_\alpha \cdot \sin\hat{\theta} + V_\beta \cdot \cos\hat{\theta} \tag{3.19}$$

Furthermore V_q has to be locked by setting it 0. Taking into consideration the new values, equation (3.19) can be represented as:

$$V_q = -\cos\theta \cdot \sin\hat{\theta} + \sin\theta \cdot \cos\hat{\theta} = \sin\theta \cdot \cos\hat{\theta} - \cos\theta \cdot \sin\hat{\theta} = \sin(\theta - \hat{\theta}) \tag{3.20}$$

Since the values of $\theta - \hat{\theta}$ are very small, equation (3.20) is approximated to:

$$V_q \simeq \theta - \hat{\theta} \simeq 0 \tag{3.21}$$

Therefore the magnitude of the controlled variable V_q determines the phase difference between the grid voltage and the inverter voltage. Moreover, a regulator, usually PI, can be used to control this variable and the output of this regulator is the grid frequency. An initial frequency value ω_{igrid} is then added to the output of the PI controller resulting in the estimated frequency of the grid voltage. The advantage of adding ω_{igrid} to the output of the PI controller is a better dynamic performance every time the PLL is reset. By integrating the grid frequency, the grid angle is obtained and is fed up into the transformation[30].

When is used for grid connected applications, the PLL can be influenced by the distortions taking place in the utility network. As a consequence, a low dynamic PLL will produce a filtered and stable output but with a longer synchronization time. On the other hand, a design for fast dynamics will produce an output which is able to synchronize rapidly to the input but distortions in the input signal will pass through and become part of the output signal. Therefore, designing a synchronization system is a tradeoff between the filtering performance and the time response.

In grid connected application the PLL has to operate with a lot of faults and distortions which occur in the utility grid due to different reasons. In this case the entity which decides the performance and the dynamics of the PLL is the filter. If the filter has a low dynamics the output will be stable but with longer synchronization time and if the filter is well tuned and has fast dynamics, the output will synchronize fast but distortions in the input will pass the filter and became part of the output.

Depending on the type of the application where the PLL is used, the user can decide if the performance has to be fast or low. If the PLL is used for synchronization with the voltages of the utility grid then the performance can be low. On the other hand if it is used in grid monitoring to detect faults, the performance has to be high.

One way of tuning PLL's filter, in this case a PI controller, is by having access on the settling time T_s and damping ratio ζ. Adjusting this two variables the dynamics can be changed according to the application.

The time domain transfer function of the PI controller in the PLL is given in equation (3.22) and has a similar form like the standard second order transfer function (see equation(3.23))[29].

$$H(s) = \frac{K_p \cdot s + \frac{K_p}{T_i}}{s^2 + K_p \cdot s + \frac{K_p}{T_i}} \tag{3.22}$$

$$G(s) = \frac{2 \cdot \zeta \omega_n \cdot s + \omega_n^2}{s^2 + 2 \cdot \zeta \cdot \omega_n \cdot s + \omega_n^2} \tag{3.23}$$

Therefore the controller parameters can be calculated with the following equations:

$$K_p = \frac{9.2}{T_s} \tag{3.24}$$

$$T_i = \frac{T_s \cdot \zeta^2}{2.3} \tag{3.25}$$

where,

$$\omega_n = \frac{4.6}{\zeta \cdot T_s} \tag{3.26}$$

The PLL's filter which is the PI controller had to meet some requirements in terms of damping factor and settling time and they are given as[29]:

- The filter should have a damping factor ζ of :

$$\zeta = 0.707$$

- The settling time T_s of the filter is :

$$T_s = 0.04\ [ms]$$

The step response of the PLL in case of a frequency boost of 1 Hz and 10 Hz is presented in Figure 3-17:

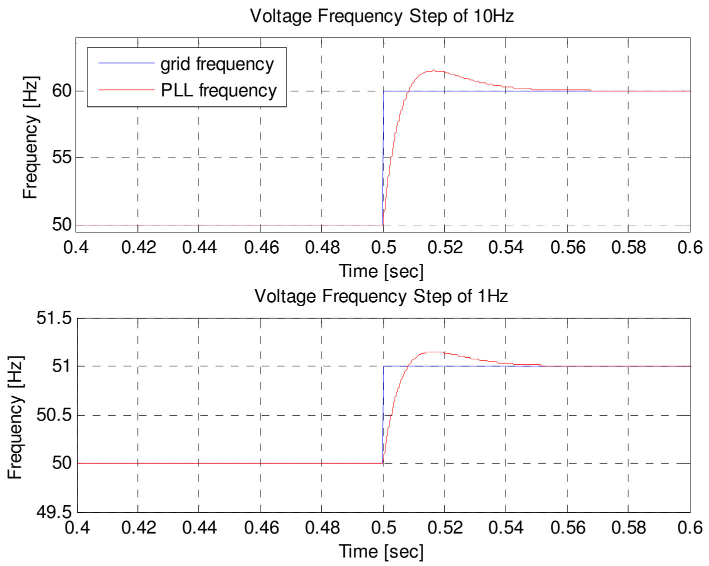

Figure 3-17 Frequency response of the PLL

The step is applied at 0.5 seconds and it can be observed from Figure 3-18, that the phase is changing accordingly.

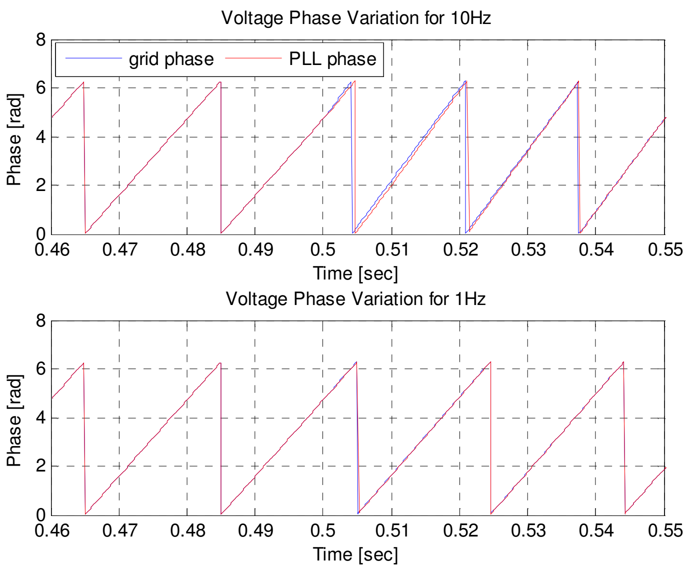

Figure 3-18 Phase response of the PLL

3.3 Control of VSC in MTDC operation

The control of the VSC in MTDC operation of the HVDC systems has to accomplish the same two goals in matters of protection and optimal operation. In a point to point HVDC application, the control of the system has to manage a bidirectional active power flow between the AC grids involved in the application but also to regulate the reactive power demand at the PCC in case TSO requires it.

Another challenge in power transition using the HVDC solution is when the system is used for connecting large wind farms because in this case the power flow should be from the wind farm to the grid and not the other way around. The use of the PWM VSC has the benefit of solving these problems and also brings much more stability to the system.

The use of the VSC in HVDC transition system has the advantage of decoupling one AC system from another and has the ability to independently control the active and reactive power as shown in Figure 3-19.

In terms of active power exchange between one system and another, the converters have different functions. While one of the VSC is used to keep constant the power reference, the other one regulates the DC voltage. In this manner the power flows from one grid to another and the system acts like an energy buffer if the DC losses and switching losses are neglected.

The reactive power is separately controlled at the both sides of the HVDC transition system. The amount of reactive power demanded by the AC system can also be controlled in case the voltage level is kept in the desired limits.

Offshore wind farms connected to the grid through HVDC can be controlled by it. The offshore station of the HVDC system can regulate the voltage level in the wind farm AC grid and can impose the frequency and all the active power produced by the wind farm is injected into the DC link.

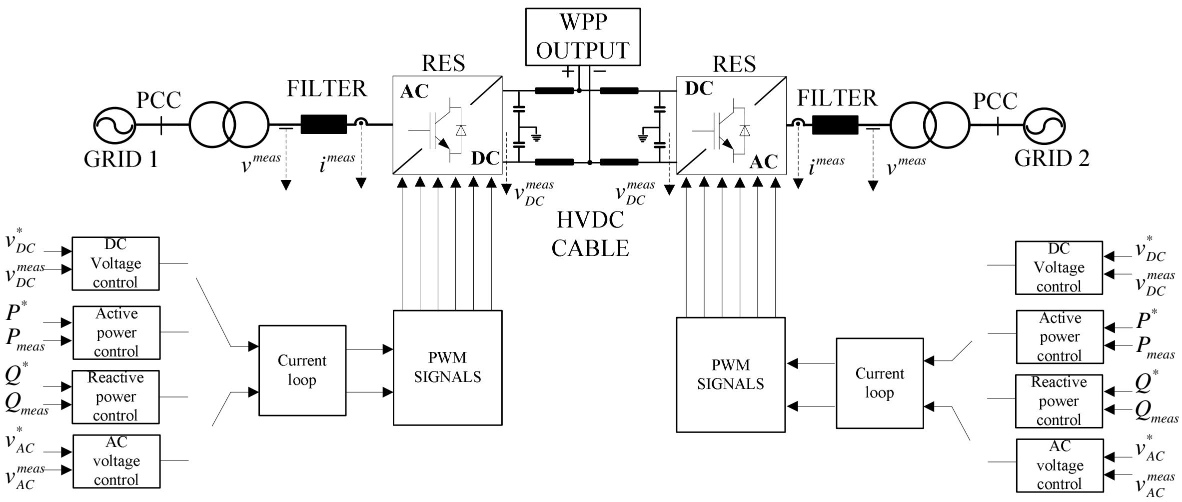

Figure 3-19 Control diagram of the HVDC system

The MTDC structure is more complex than the point to point HVDC configuration because more than two converters are connected in the DC bus. Adding extra converters into the system means new challenges in the control structure. For the safe operation of the MTDC system the DC voltage has to be kept at the set point with small variations. The constant DC voltage indicates a balanced active power flow among the VSCs in the system.

Figure 3-20 presents the simplified model of the MTDC system, where the power is injected into the DC link by one VSC and shared between two receiving stations[33].

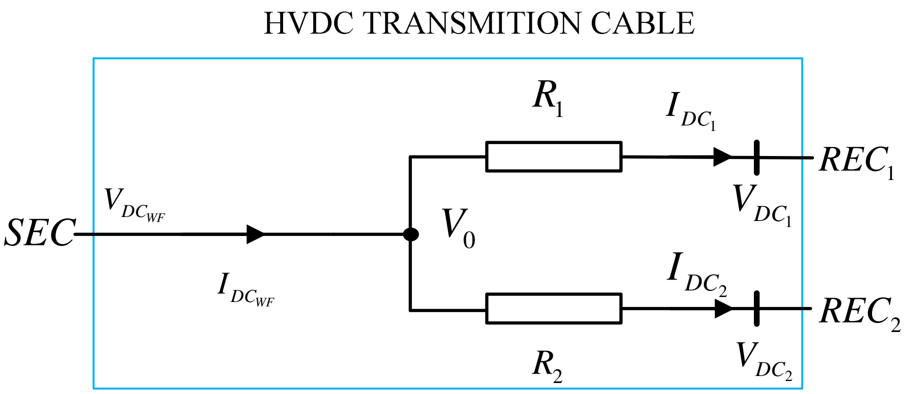

Figure 3-20 Simplified structure of the MTDC

The voltages at the receiving stations can be expressed as:

$$V_{DC_1} = V_0 - R_1 \cdot I_{DC_1} \tag{3.27}$$

$$V_{DC_2} = V_0 - R_2 \cdot I_{DC_2} \tag{3.28}$$

where,

V_{DC_1} - is the DC voltage of REC 1;

V_{DC_2} - is the DC voltage of REC 2;

V_0 - is the DC voltage in the common DC connection;

I_{DC_1} - is the DC current of REC 1;

I_{DC_2} - is the DC voltage of REC 2;

Both voltages at the receiving stations input have the same V_0 and is the voltage at the common connection. By substituting Equation(3.27) in Equation(3.28), the voltage at the second receiving station can be calculated knowing the DC voltage from the other station:

$$V_{DC_2} = V_{DC_1} + R_1 \cdot I_{DC_1} - R_2 \cdot I_{DC_2} \tag{3.29}$$

Knowing the DC voltages V_{DC_1} and V_{DC_2} and the DC currents I_{DC_1} and I_{DC_2} the DC powers are calculated:

$$P_{DC_1} = V_{DC_1} \cdot I_{DC_1} \tag{3.30}$$

$$P_{DC_2} = V_{DC_2} \cdot I_{DC_2} \tag{3.31}$$

The information given by the DC voltages and currents enables the possibility of sharing the power injected by the sending station. As mentioned above the DC voltage level has to be kept at the desired level but in the MTDC operation a droop control ensures a safe and stable performance of the entire system[33].

Figure 3-21 presents an equivalent model of the MTDC were the grid connected converters are considered as ideal voltage sources and the wind farm injects all the time current in the DC link.

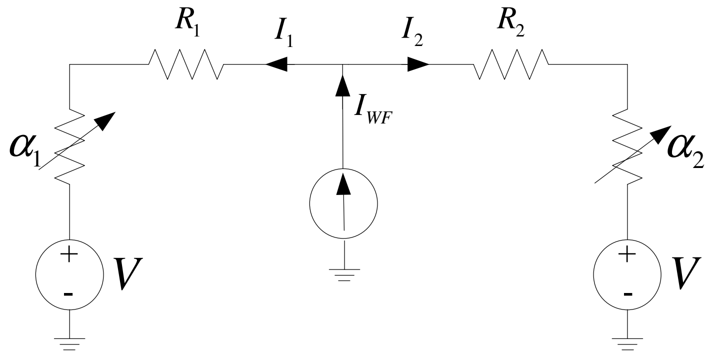

Figure 3-21 Equivalent model of the multi terminal system

In the droop algorithm the relationship between the powers shared by the converters is based on:

$$(R_1+\alpha_1)=k\cdot(R_2+\alpha_2) \tag{3.32}$$

where,

k - is the sharing factor

R_1 - is the resistance of HVDC line 1

R_2 - is the resistance of HVDC line 2

α_1 - is the virtual resistance for VSC 1

α_2 - is the virtual resistance for VSC 2

The sharing factor k is the decisive element in the droop controller structure because it determines the distribution of the DC current in the system (see Equation(3.33))[34].

$$k=\frac{I_1}{I_2} \tag{3.33}$$

where,

I_1 - is the DC current VSC1;

I_2 - is the DC current VSC2;

Another important aspect of the droop algorithm presented in Equation (3.32) is the use of the virtual resistance in the DC link. The purpose of this resistance is to ensure different references for the DC voltages at the input of each receiving station (see Figure 3-22). To avoid power variation on the DC side a low pass filter is introduced in the measured DC currents. This low pass filter is tuned at a frequency lower than the bandwidth of the DC voltage controller in order to keep the system stable.

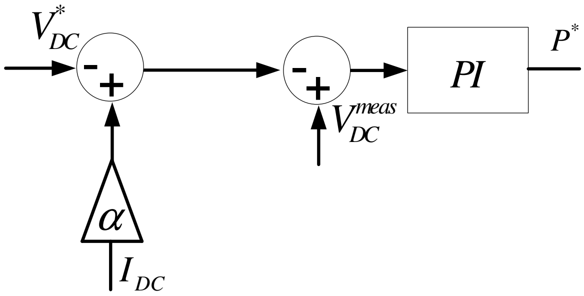

Figure 3-22 DC voltage reference generation

The ratio between the DC currents determines also the how much power is evacuated into the AC system by each converter:

$k < 1$ - the power sharing is $P_{AC_1} < P_{AC_2}$;

$k = 1$ - the power sharing is $P_{AC_1} = P_{AC_2}$;

$k > 1$ - the power sharing is $P_{AC_1} > P_{AC_2}$;

As showed in Equation(3.32), the droop control depends on the value of the sharing factor k and on the value of the virtual resistance α_1. Knowing these two values the virtual resistance for the other branch of the MTDC system is calculated. A positive value of α_1 produces a voltage rise in the DC link, while the negative reduces the voltage.

The droop equation reveals the linear dependency between the virtual resistances α_1 and α_2. This reliance is also affected by the sharing factor which in this case represents the slope of the characteristic (see Figure 3-23).

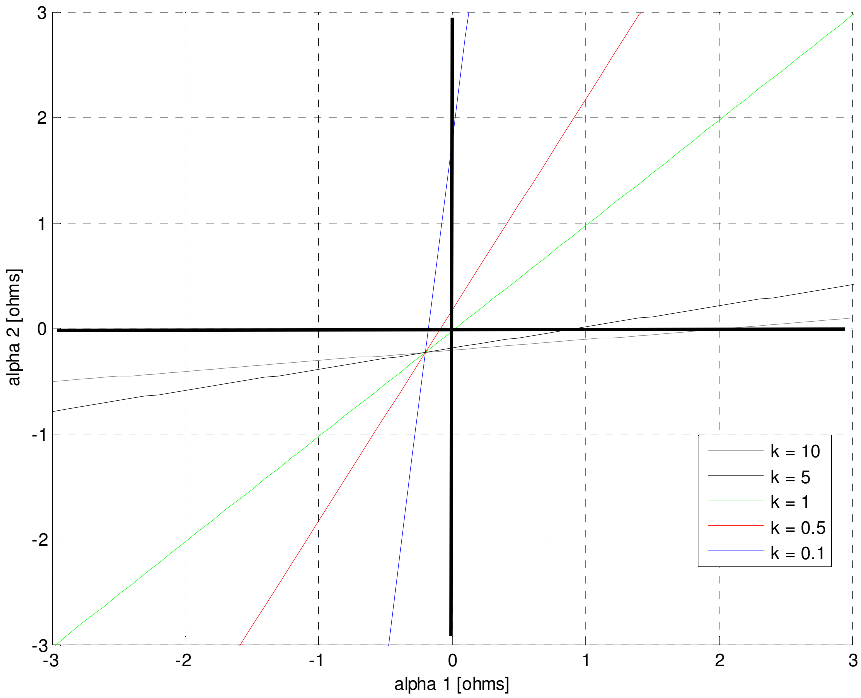

Figure 3-23 Graphical representation of the droop control

As it can be seen in Figure 3-23, there is a strong dependency between the sharing factor k and the virtual resistances. In case the sharing factor has values different than one, the changes in resistance are significant. These big changes are than reflected in generating the DC voltage references considering the fact that the virtual resistance produces a voltage drop which directly influences the level of voltage at the input of the converter.

Another important remark which can be presented from Figure 3-22 is that all the characteristics having different slopes in terms of sharing factor k intersect in the same point and that point is the approximated values of the HVDC lines resistances.

Chapter 4

Simulation of the MTDC system

In this chapter, the performance of the multi terminal HVDC system is evaluated. In the first part, the PSCAD model is validated for different cases like steps in power production, different sharing factor in active power or different values for the virtual resistance. Moreover, the performance of the system is analyzed under special conditions such as abnormal functioning and parts of the MTDC system has to be stopped. Finally, the chapter ends with an analysis and the results are evaluated.

The advantages presented by the HVDC system in matters in power transport and flexibility makes this solution a feasible option for future concepts in distribution and power transportation.

The multi terminal HVDC connection brings more flexibility to the point to point layout but also more challenges in the control structure. To investigate the behavior of the MTDC system some simplifications were maid and in consequence some aspects were ignored.

In order to validate the control and have a better understanding of the entire system and due to lack of high power high voltage equipment, the system modeled in PSCAD was considered to be the downscale system having 15 kW VSCs.

Wind farm and offshore station

A detailed model of the wind farm was not considered in this project or the topology of wind turbine. The purpose of the WF is to capture the maximum wind energy available and fed it up into the DC link by means of the offshore station. Also the control of the offshore station was not investigated and the entire offshore platform was approximated as a current source. Fluctuations in wind should be approximated as fluctuations in DC power this means fluctuations in DC current.

HVDC cable

Usually the model for the HVDC line is considered as a PI model. In this project the capacitance of the line was neglected and only the resistance and inductance were considered. The purpose for this simplification was to simulate the line as a simple delay in the system.

DC capacitor

The value of the DC capacitor was calculated using Equation(2.3). In the simulation the DC capacitance was considered to be the capacitance of the downscale model and it was $1100[uF]$.

VSC

For the grid connected VSC a two-level switching model was realized but the delay introduced by the converter was neglected in the control structure.

Filter

The filter considered is a LC filter with an inductance of $1.6[mH]$ and a capacitance of $10[\mu F]$

Electrical Grid

The electrical grid model is taken from PSCAD Library and is based on the Thevenin equivalent circuit. The values for the grid resistance and inductance are small in order to have a stiff grid.

4.1 Validation of the PSCAD model

In this section the response of the MTDC system will be analyzed and for this purpose different study cases have been performed.

The study cases of this section will mainly focus on the active power sharing produced by the wind farm. The power is shared between the receiving stations using the droop algorithm and the effect of the virtual resistance is emphasized.

4.1.1 DC power variation (steps)

The simulation for this study case was performed in order to present the effect of power sharing for different levels of power produced by the wind farm. The simulation time was considered to be 4 s and at the beginning the produced power was considered to be 0.5 p.u.. Gradually several steps were applied until 1 p.u. and after that the production was reduced to 0.2 p.u.. Figure 4-1 points out the DC current sharing between the receiving stations.

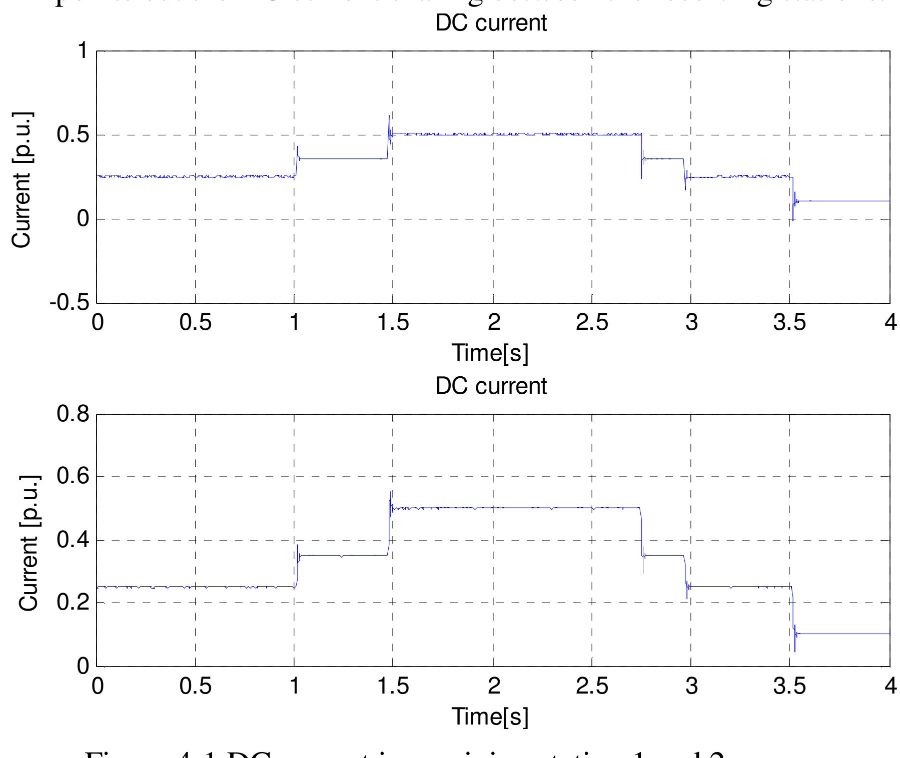

Figure 4-1 DC current in receiving station 1 and 2

The sharing of DC current reflects on the sharing of power on the AC side also. Figure 4-2 presents the current injected into the grid and as it can be seen follows the pattern of the input DC current. In a normal operation of the grid were the voltage has no fluctuations also the power injected is proportional with the current injected into the grid (see Figure 4-3)

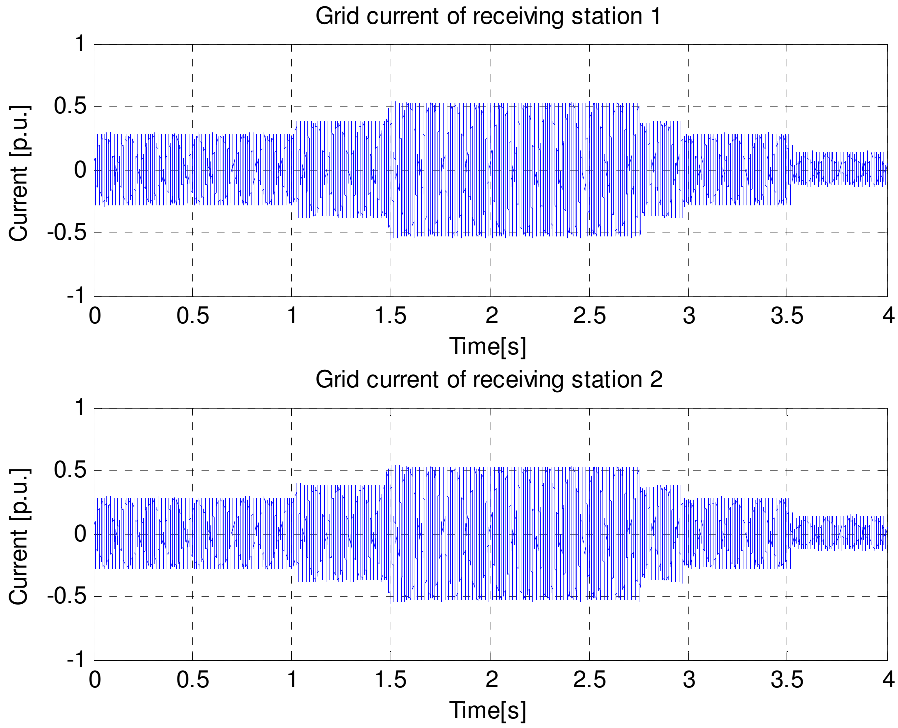

Figure 4-2 AC current of both receiving stations

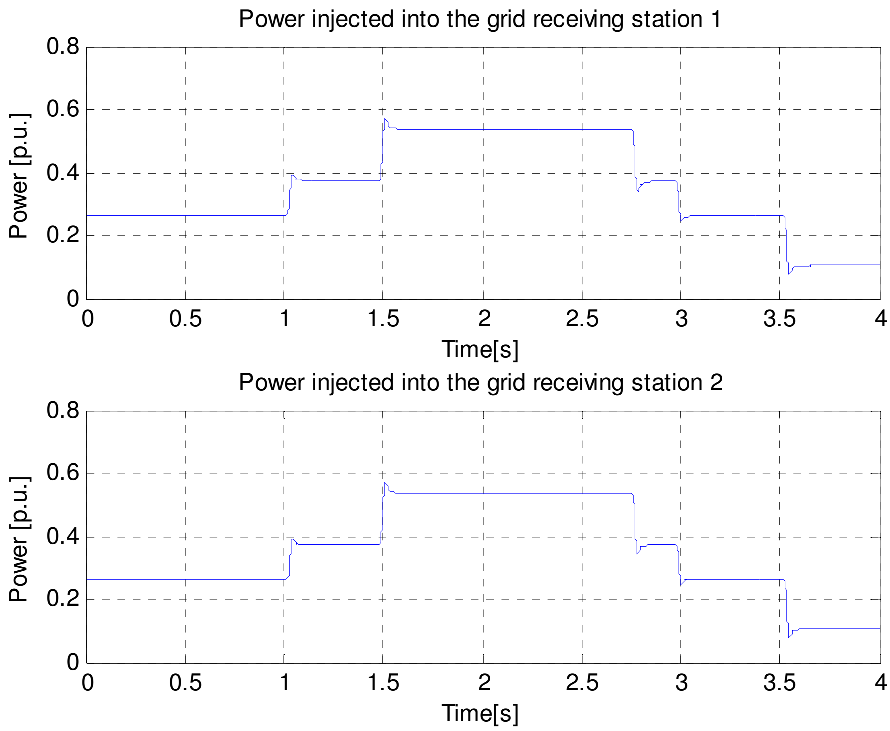

Figure 4-3 AC power injected into the grid

During all this steps, the control in both receiving stations has the goal to keep the DC voltage level at a desired level. This voltage level is based mainly on one set value and it's the same for both converters and then the difference is added accordantly to the droop algorithm and the set value of the virtual resistance. As it can be observed in Figure 4-4, steps in current produces steps in DC voltage and in any condition the voltage does not exceed the voltage limit of 5%, the level at which the controller was designed.

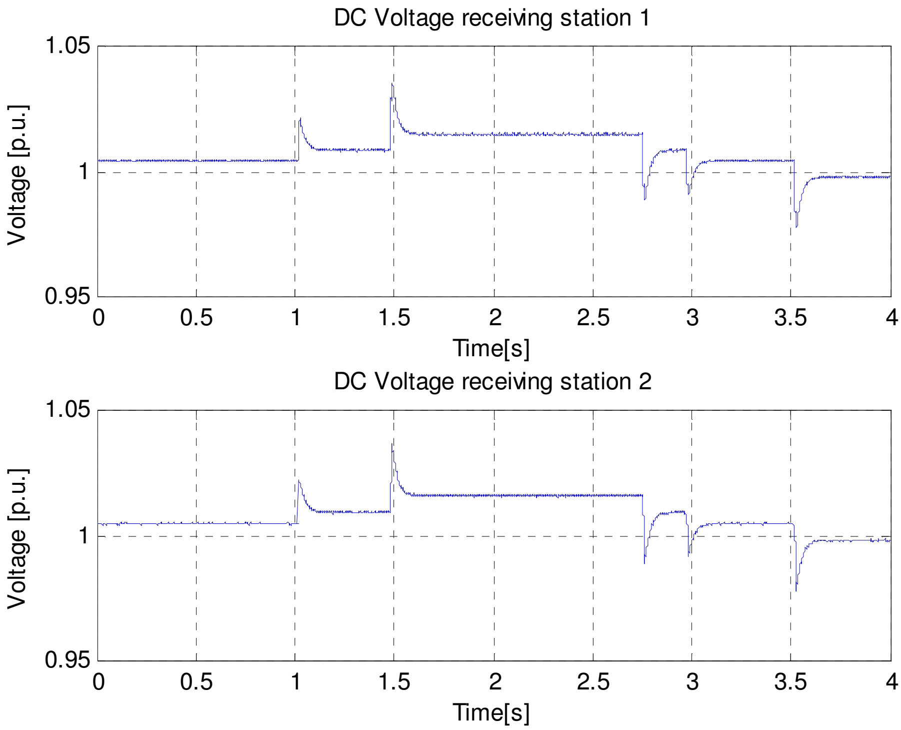

Figure 4-4 DC voltage level during steps in DC power

4.1.2 Effect of the sharing factor over the system

In this case the sharing factor k has values different than one as presented in the case above where power is shared equally between the converters.

Figure 4-5 shows the results where k has values smaller than one. In this sharing situation more current will flow through receiving station 1 than through receiving station 2. As it can be observed, until 1 [sec] the sharing of current is equal and after that values of 0.5, 0.2 and 0.1 were introduced as a sharing factor. This means I_1 is 2, 5 and respectively 10 times higher than the value of the DC current flowing in the second converter.

For this case the power produced by the wind farm was constant all the time and the virtual resistance was selected to be $1\,[\Omega]$. The value of the virtual resistance was decided on the fact that the voltage rise produced by it should not have a significant importance.

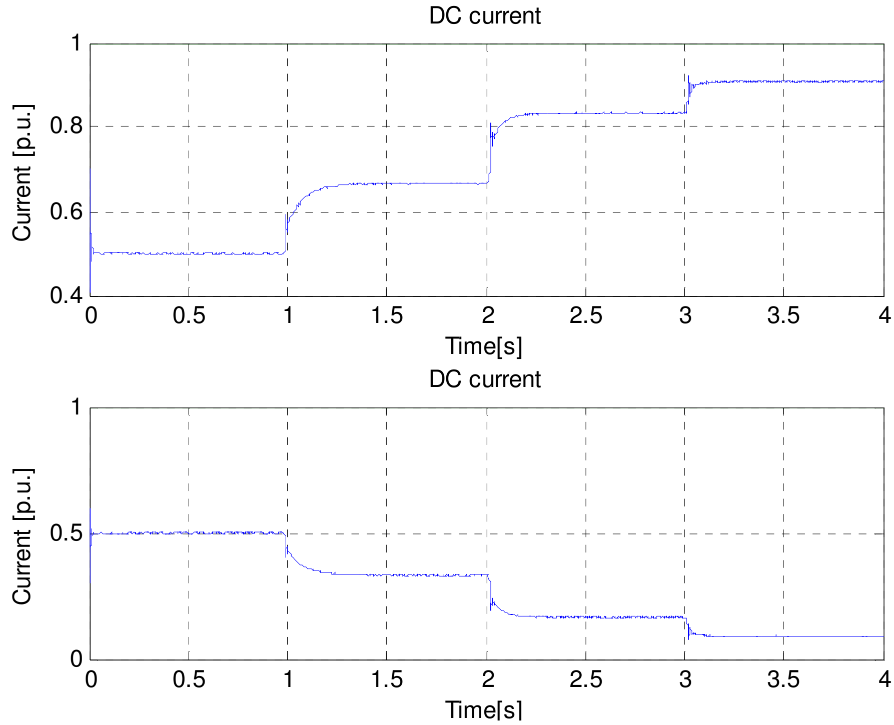

Figure 4-5 DC current sharing between the receiving stations (k < 1)

As expected, the consequence of DC current sharing reveals also in the AC current injected into the grid and the results are showed in Figure 4-6.

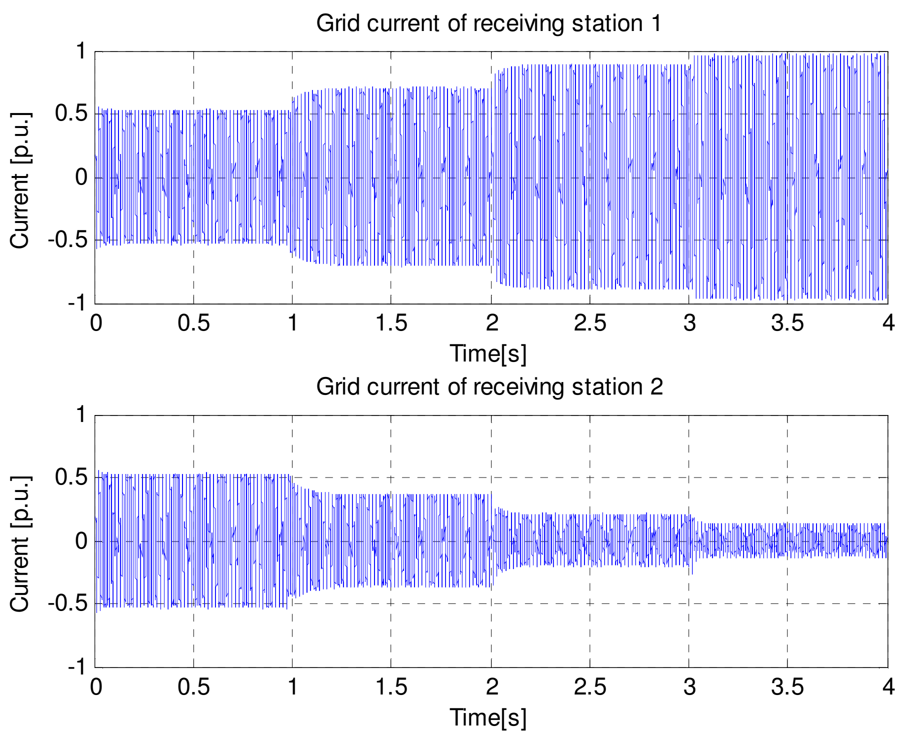

Figure 4-6 AC current injected into the grid (k < 1)

From Figure 4-7 it can be remarked that the power variations are dependent on the current transferred from the DC side into the grid and from Figure 4-8 it can be observed the voltage variation for different sharing factor.

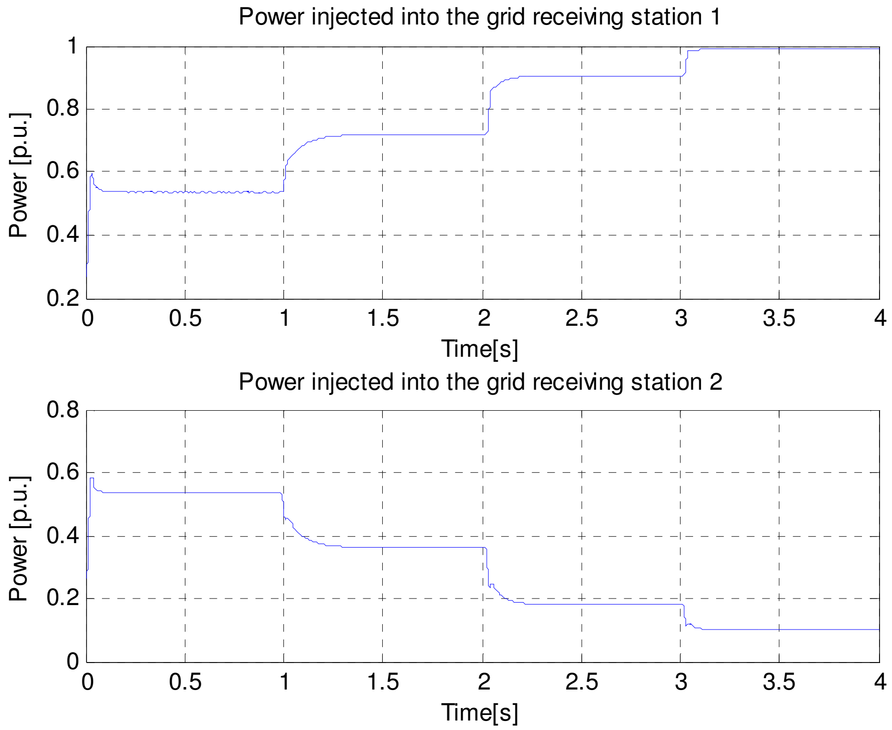

Figure 4-7 AC powers injected into the grid (k < 1)

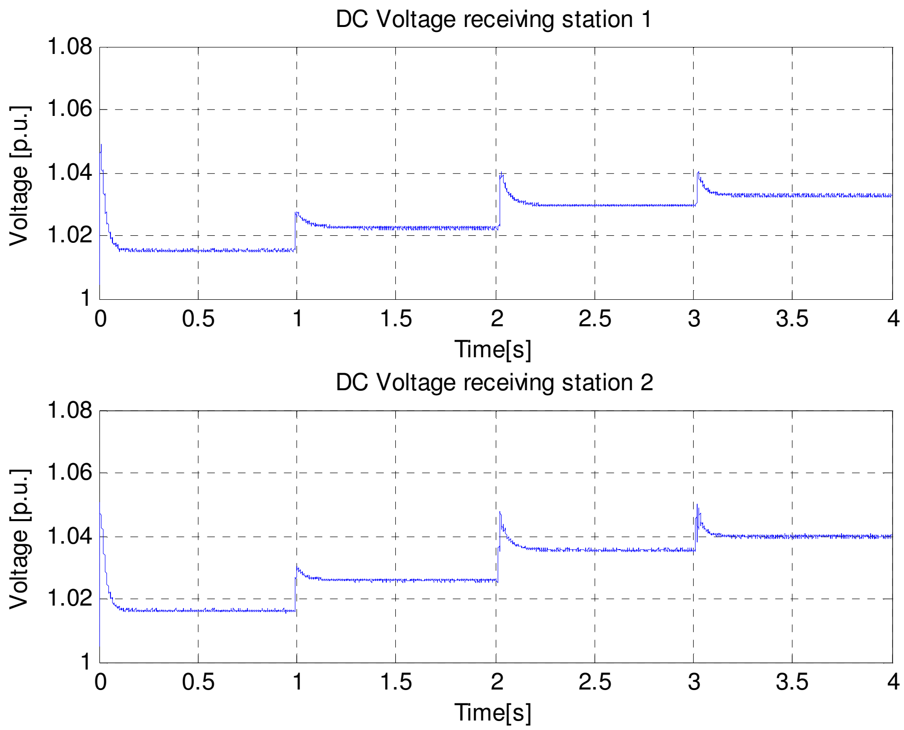

Figure 4-8 DC voltage variation (k < 1)

Another situation considered for the case of different sharing factor is when k is bigger than one. This means the opposite situation and now the ratio between the DC currents is reversed. The sharing factor was 1 until 1 sec and then increased to 2, 4 and 8(see Figure 4-9). The effect on the AC grid can be observed in Figure 4-10 and Figure 4-11 and the DC voltage variation in Figure 4-12.

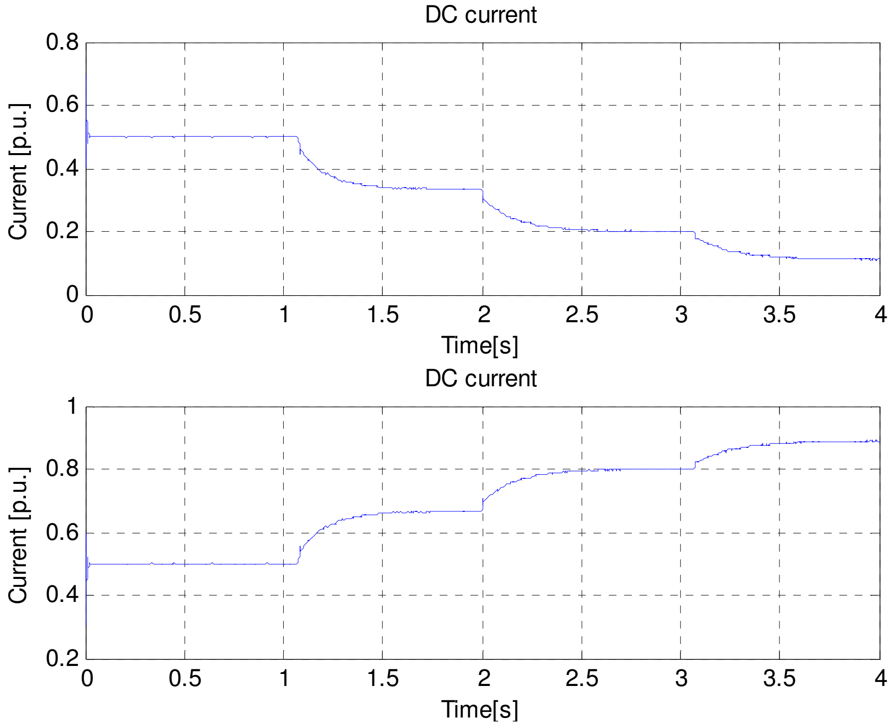

Figure 4-9 DC current sharing between the receiving stations (k > 1)

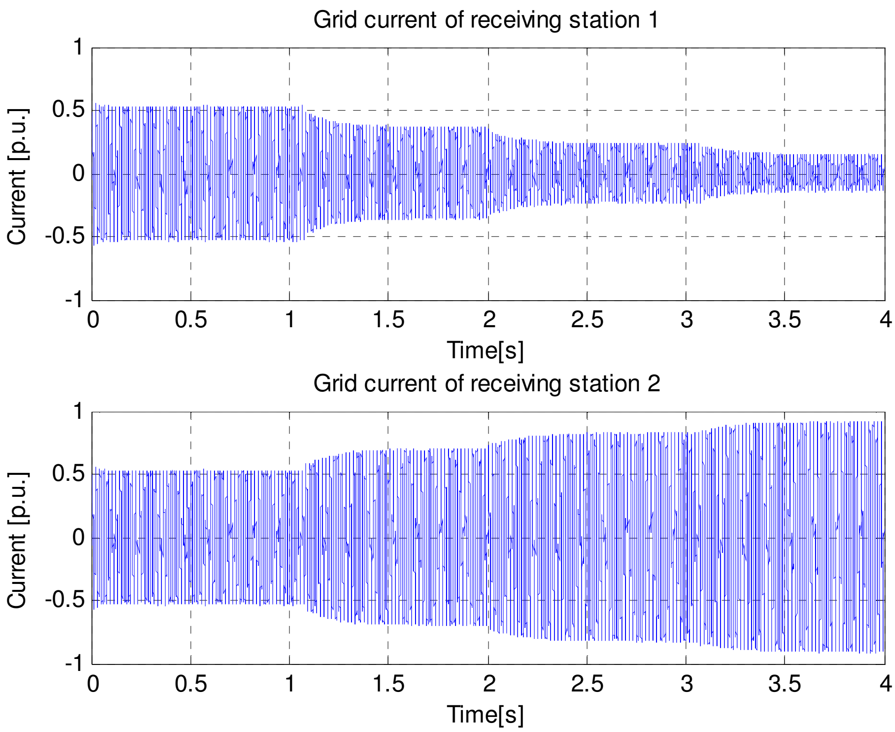

Figure 4-10 AC current injected into the grid (k > 1)

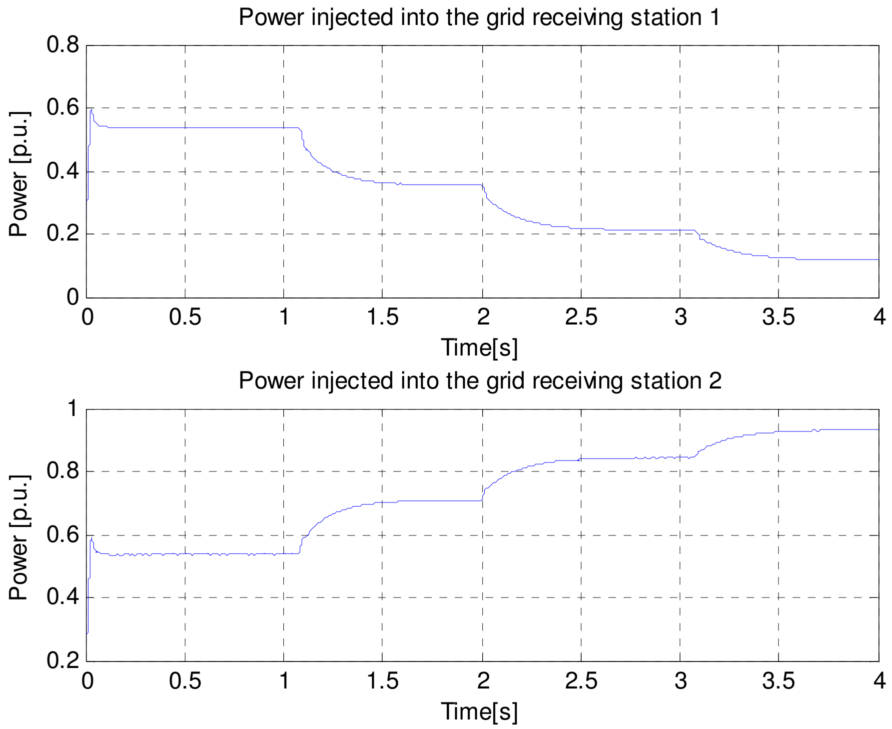

Figure 4-11 AC power injected into the grid (k > 1)

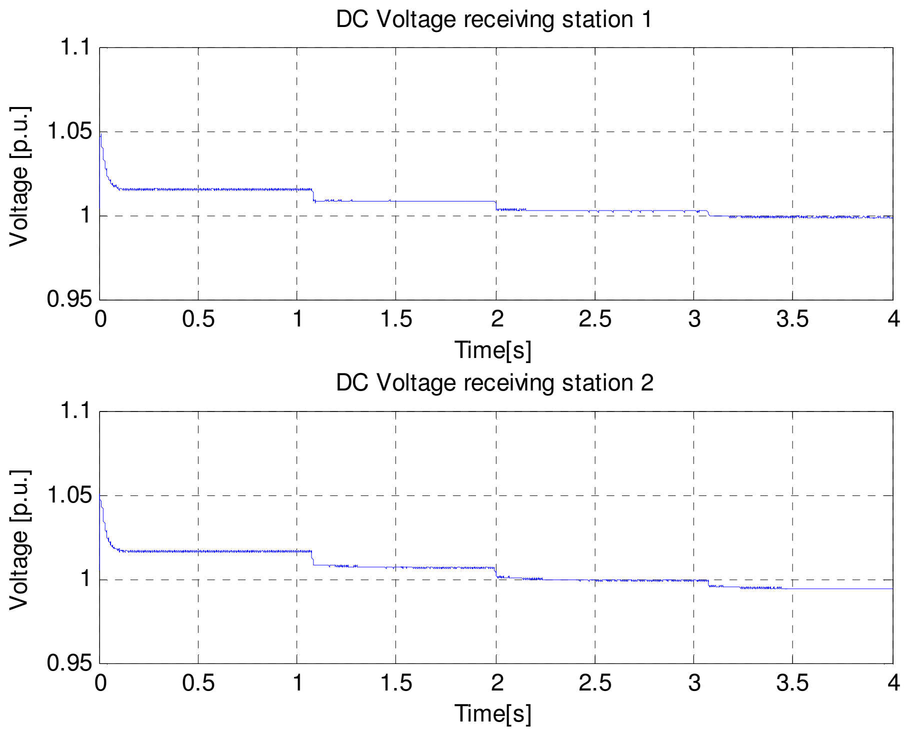

Figure 4-12 DC voltage variation (k > 1)

4.1.3 Effect of the virtual resistance in the system

In the MTDC control structure the sharing of power between the converters is realized by keeping the voltage level different at each converter. The references which these levels of voltage are calculated relates with the droop algorithm presented in Equation(3.32) and showed in Figure 3-22.

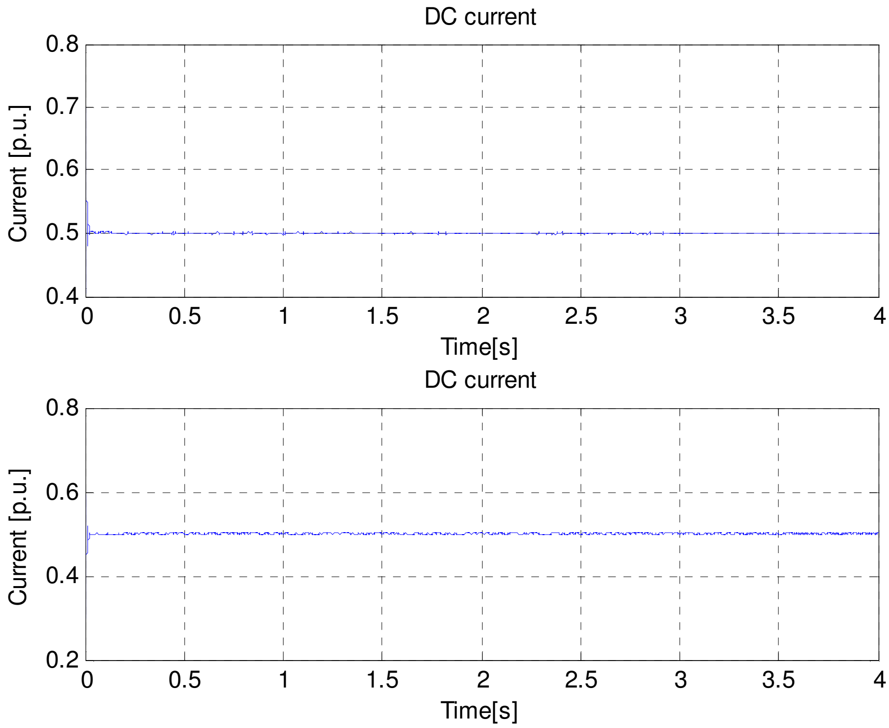

Figure 4-13 Current distribution for different value of the virtual resistance and the same sharing factor

To study the effect of the virtual resistance in the system, the sharing factor was considered to be unitary so the DC current is spited equally, the power production of the wind farm was supposed to be 1 p.u. and only the value of the virtual resistance was the one who was modified during the simulation.

At first, the value of the virtual resistance α_1 was chosen to be 1 ohm and during the simulation the value it was changed to -0.2 ohms and at the end the effect of a higher value of 10 ohms was analyzed. Knowing the value of α_1 and having all the time a constant value in the sharing factor, the droop algorithm automatically calculates the value of the other virtual resistance in the system α_2 .

Figure 4-13 shows the current sharing between the converters and it can be remarked that all the time it remains the same because the sharing factor has the same value for all the simulation period and it is independently of the value of the virtual resistance.

Changes in matters of virtual resistance has a direct influence over the voltage as is can be examined in Figure 4-14, where positive values of the virtual resistance produces a voltage rise while the negative values produces a voltage drop.

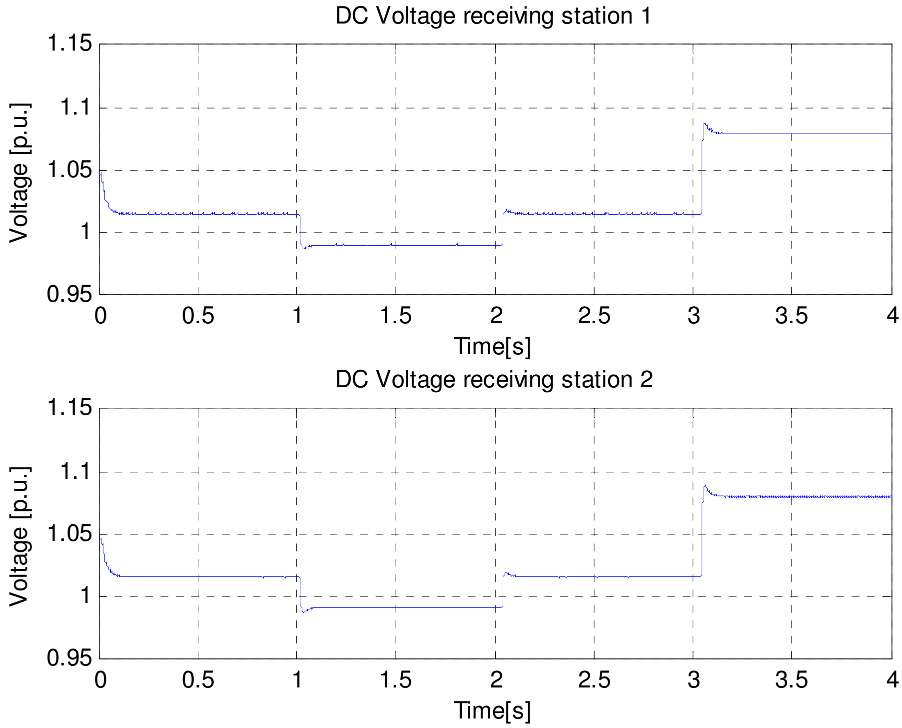

Figure 4-14 Effect of virtual resistance over the DC voltage

Bearing in mind the fact that the control structure of the MTDC manages the level of the DC voltage, in this way controls the flow of energy from the DC side to the AC side. Every change in the DC voltage is seen as a disturbance in the system and has a direct influence in the evacuated power as showed in Figure 4-15 and Figure 4-16.

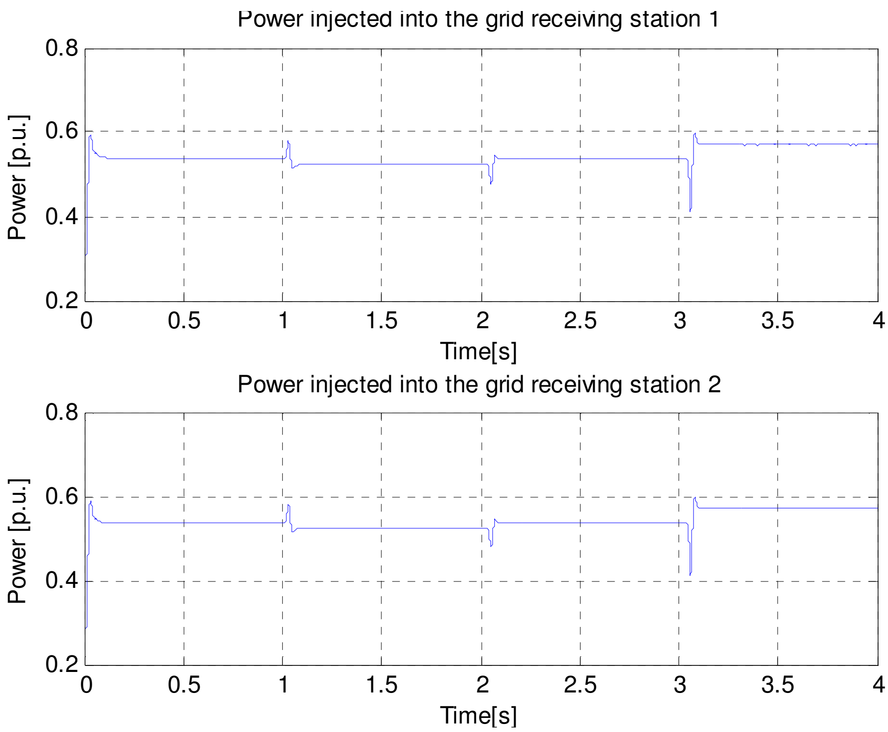

Figure 4-15 Effect of the virtual resistance over the AC power

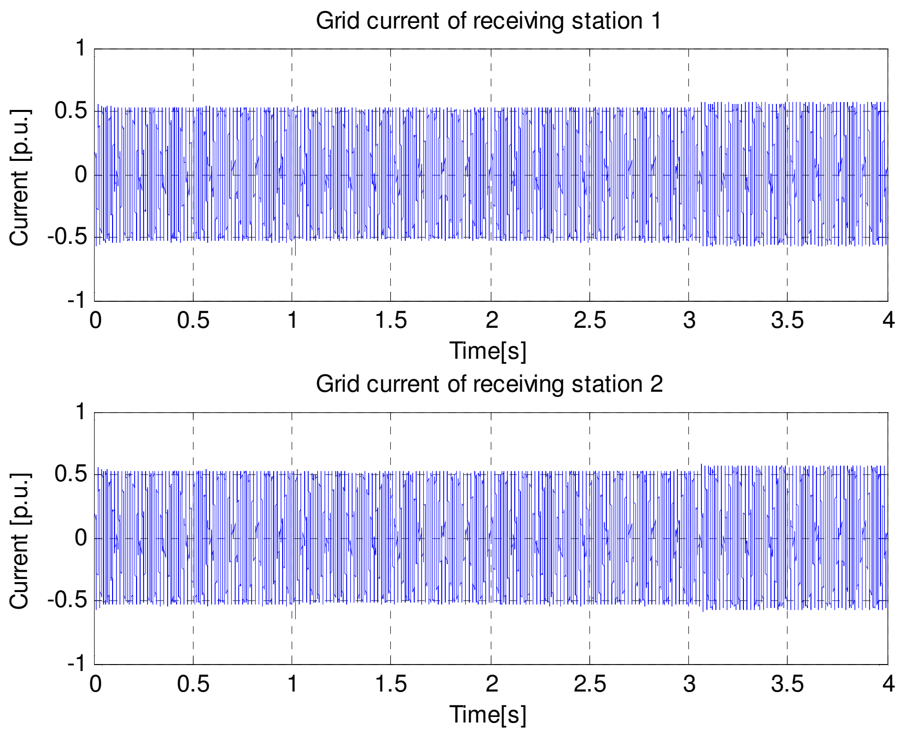

Figure 4-16 Changes in AC current due to the virtual resistance

4.2 Study cases

In the first part of the chapter, the MTDC system was validated and the control was proven. In the second part several scenarios were brought into discussion with the purpose of testing the stability of the whole system. Due to the fact that for this type of system boundaries for the DC voltage are not yet defined by the system operator, the limits were considered to be $\pm10\%$ of the rated DC voltage.

4.2.1 Wind farm trip

The multi terminal system divides the power produced by the wind farm among the receiving stations and for this study case, the situation considered was when the total wind power production is stopped. Even in this circumstance, the system has to keep constant the level of DC voltage imposed by the system operator.

For this study case, the system operates at the beginning with a unitary sharing factor and then the power was shared depending on the sharing factor imposed. When the wind farm is stopped as it can be seen in Figure 4-17, the active power injected into the DC link falls to zero and still the converters are controlling the voltage level between the imposed limits. Without any source of active power on the DC side, the amount of energy to keep the voltage level at the set point is taken from the grid and only when the wind farm is producing again, the normal operation is restored.

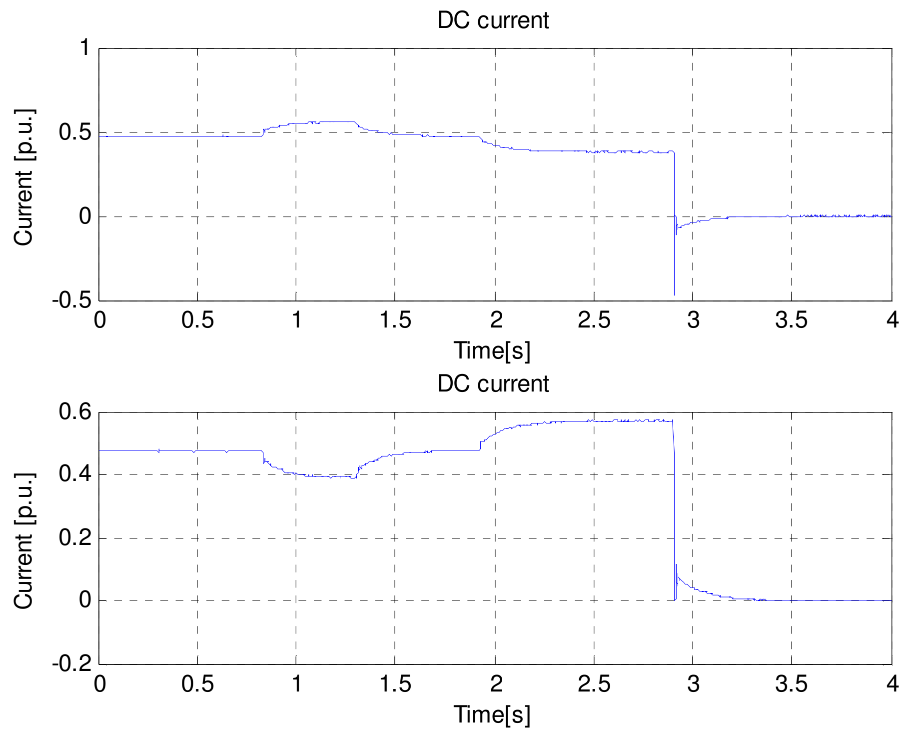

Figure 4-17 DC curent of each receiving station

Figure 4-18 shows the changes in voltage and during the trip of the wind farm the voltage level is restore to 1 p.u. due to the fact that no current is flowing into the DC circuit.

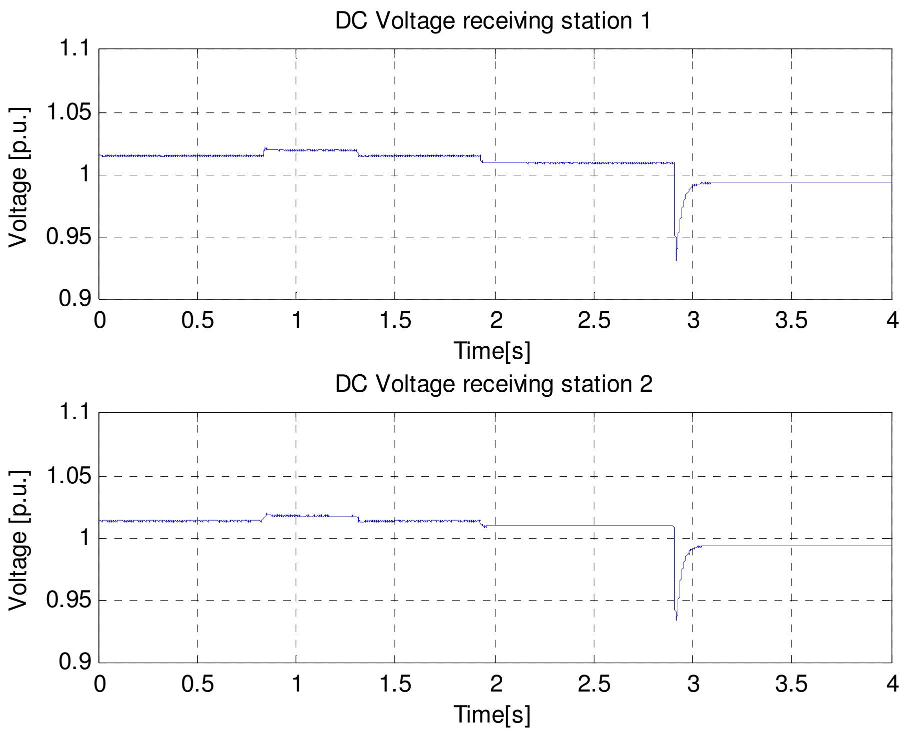

Figure 4-18 DC voltage

During the normal operation, the DC power at the input of each converter is transferred into the grid depending on the sharing factor imposed by the system operator, but during abnormal operation like in case when the wind power production is stopped the flow of power changes the sign and active power from the AC grid is used to keep the system running (see Figure 4-19 and Figure 4-20).

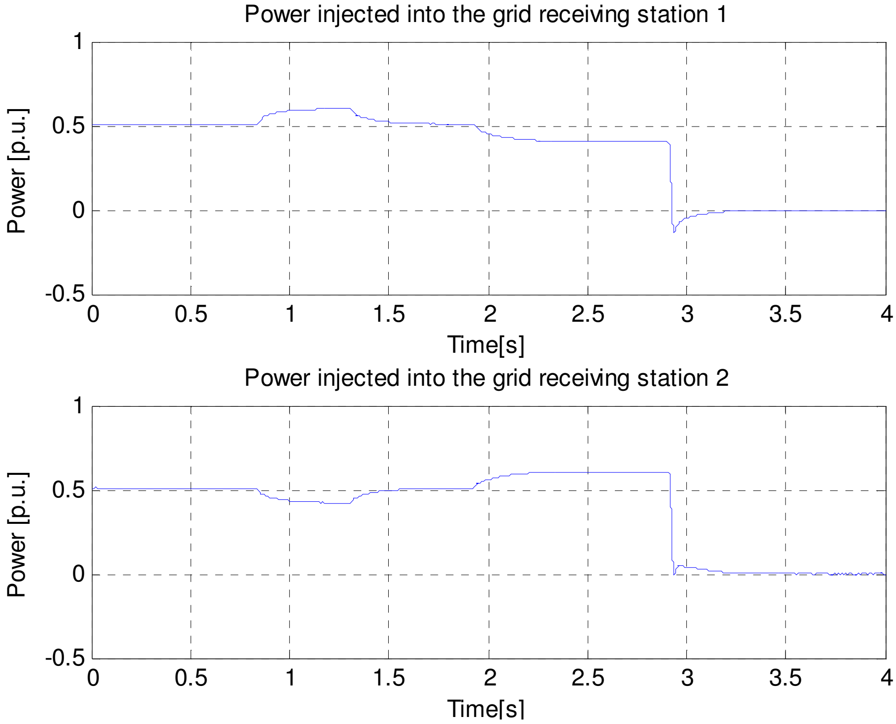

Figure 4-19 AC power during WF trip

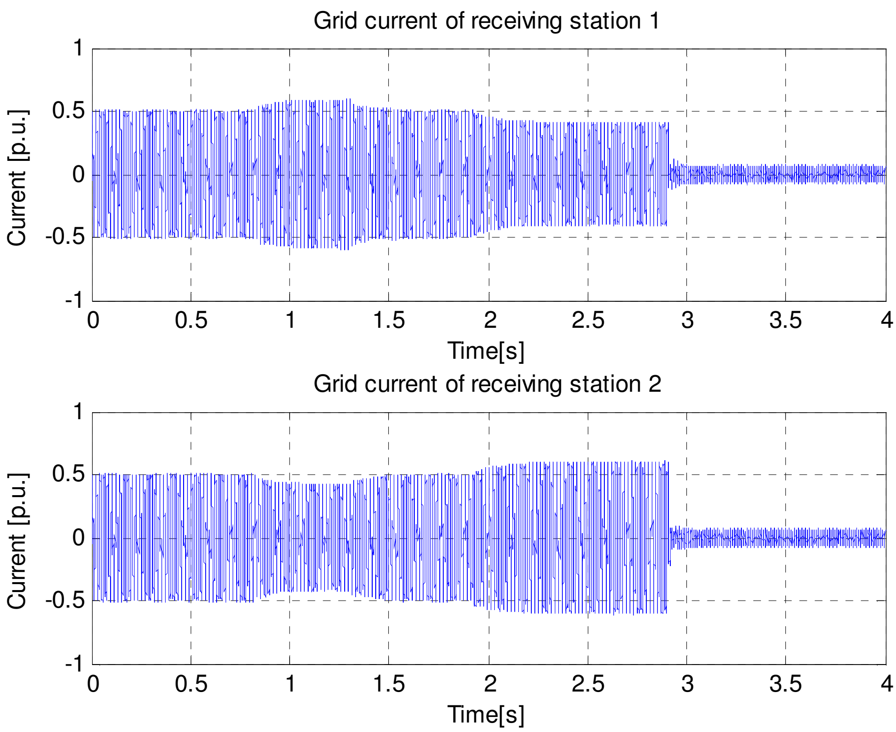

Figure 4-20 AC current during WF trip

One advantage using the MTDC system is that it has the characteristics of any point to point HVDC system and this is the decoupling effect of the AC systems. Due to the use of the VSC, the control architecture separates the WF AC grid from the normal grid and the consequence can be remarked in Figure 4-21, where the grid voltage remains unaffected by the trip of the WF.

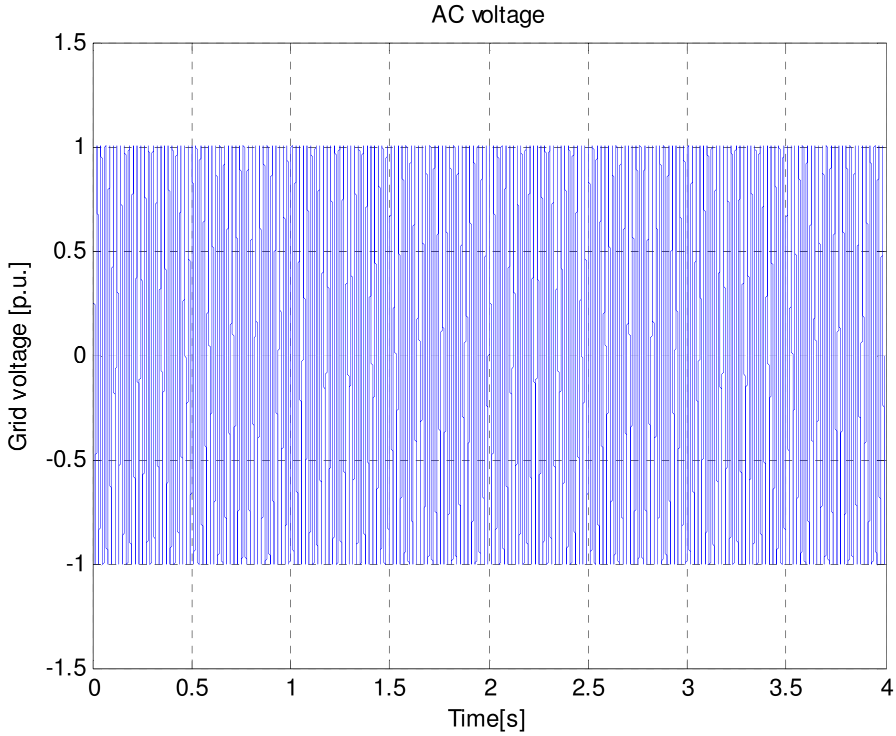

Figure 4-21 Grid voltage during WF trip

4.2.2 Receiving station trip

Another case considered for testing the MTDC system was the situation when one of the receiving stations suffers from inappropriate behavior and has to be shutdown. In this case the active power produced by the WF has to be evacuated and the only way to evacuate is either by means of the other receiving station, either inserting a chopper in the DC circuit in order to burn it .As a consequence, having too much active power in the DC side of the system means that the DC voltage will increase unless it is controlled.

In this study case it was taken into account the fact that the wind farm produces 1 pu of power and the sharing factor imposed is unitary which indicates that the converters are sharing the power equally. The trip of one receiving station occurs at 1.5 seconds and as presented in Figure 4-22, the DC current falls to 0 while the other receiving station ensures that the extra energy is pushed into the other AC grid.

During this transient period, the sharing factor remains the same and when the normal operation is restored and the receiving station is reconnected into the system, the sharing of power remains the same.

As presented in Figure 4-23 when one of the receiving stations in off, the voltage at the input of the other one will rise due to the droop controller which is active all the period. The rise of voltage occurs in this situation as a result of the DC current flowing through the converter as showed in Figure 3-22.

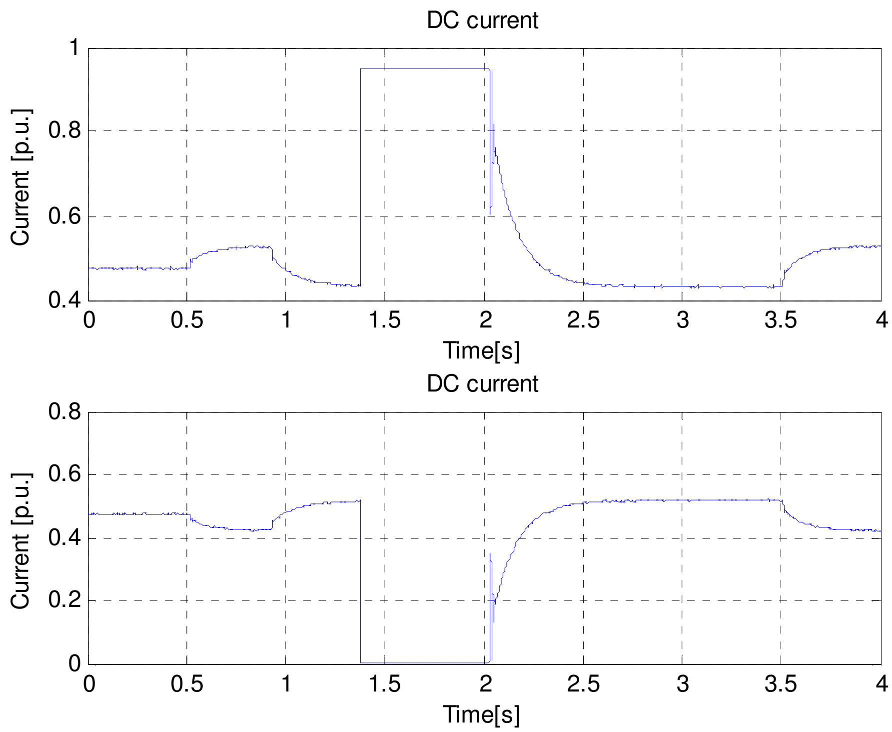

Figure 4-22 DC currents during receiving station trip

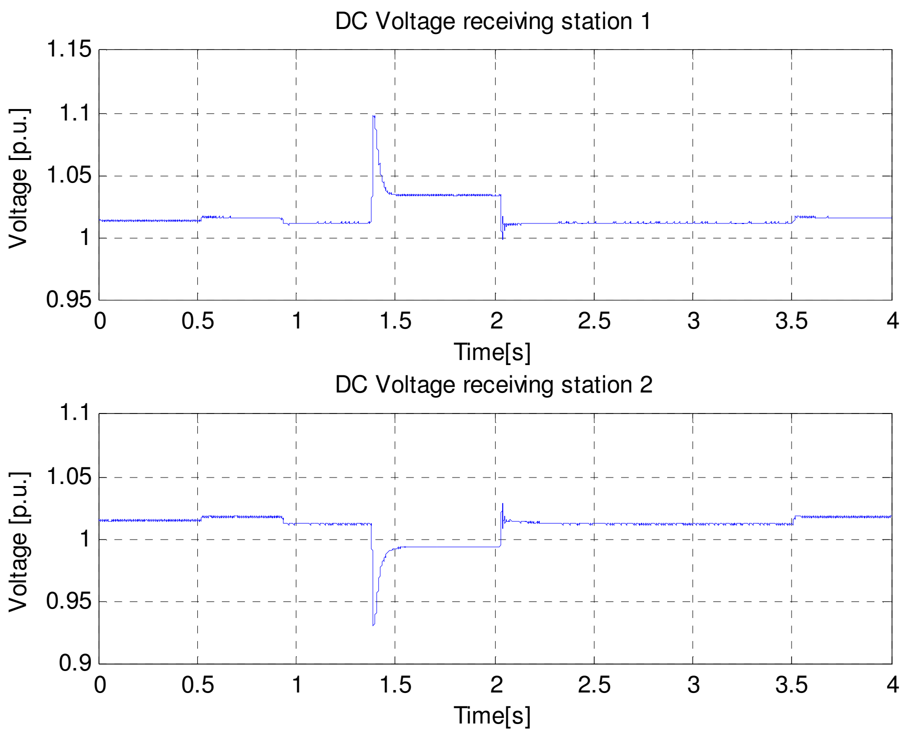

Figure 4-23 DC voltage during receiving station trip

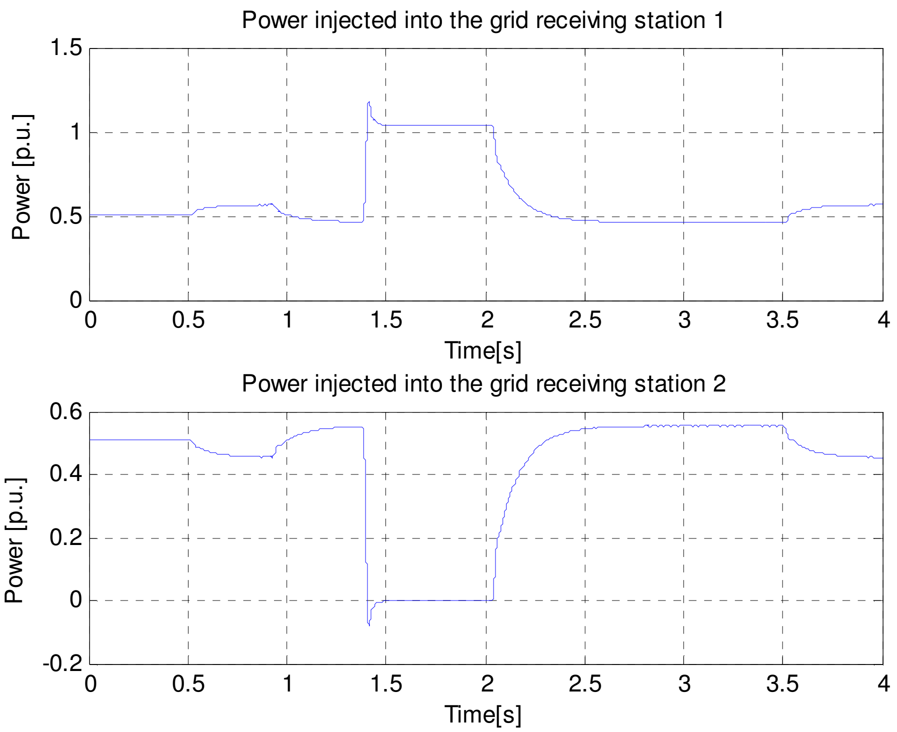

Figure 4-24 AC powers during receiving station trip

The AC powers and the grid current are presented in Figure 4-24 and Figure 4-25. As expected while one of the receiving stations is off, the whole produced power is processed by the other station.

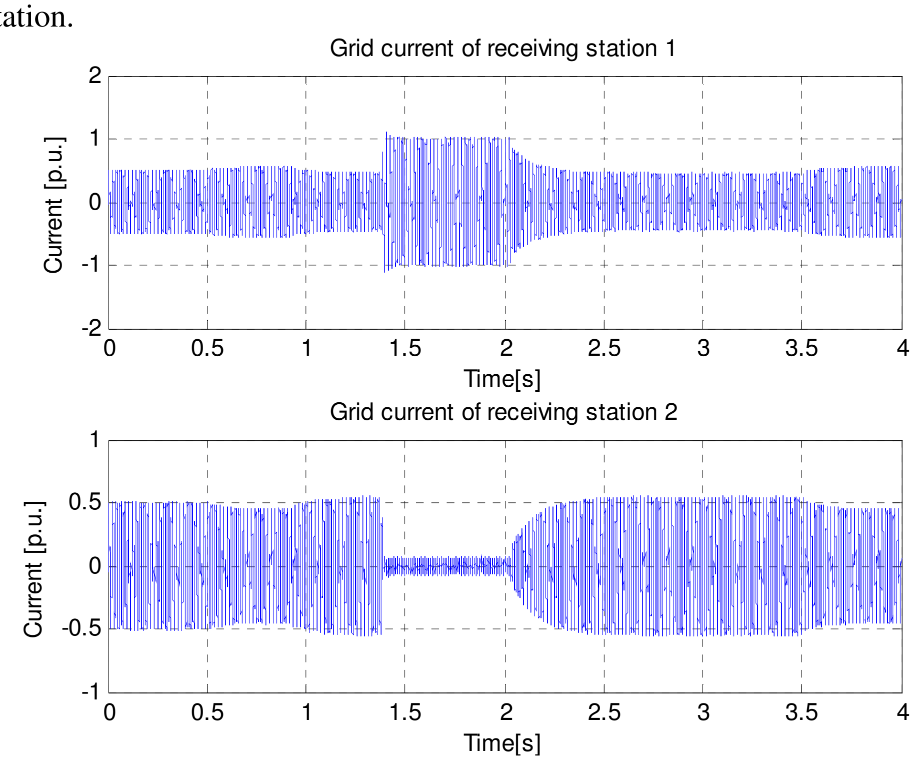

Figure 4-25 Grid current during receiving station trip

The same effect of decoupling can be observed also in Figure 4-26.This time the fault condition is at the connection of the other grid but still the disturbance in the MTDC system is not reflected into the AC grid on which all the power produced by the wind farm is injected.

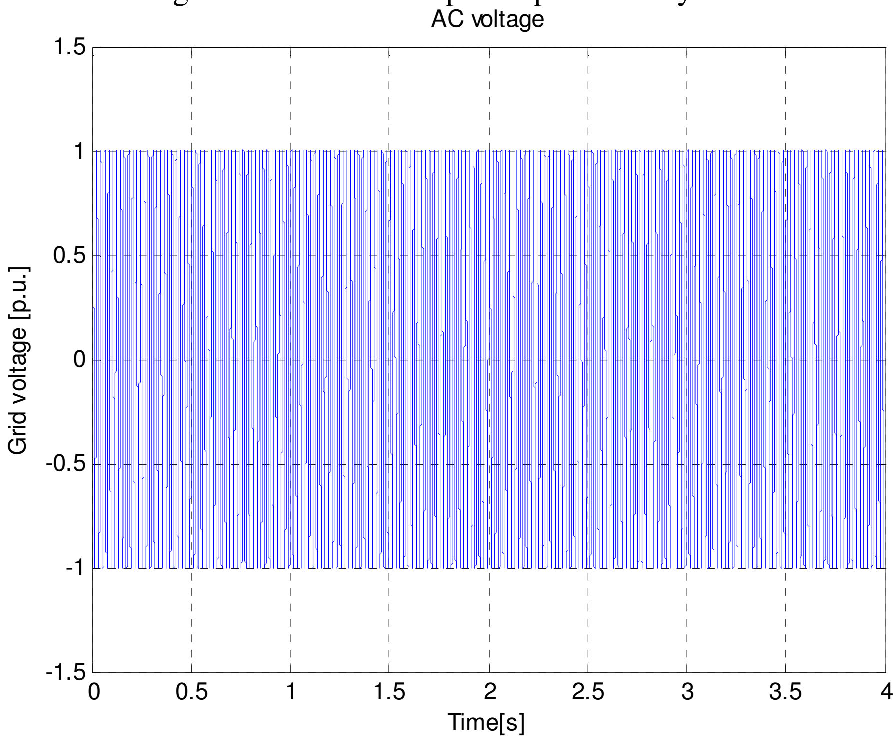

Figure 4-26 Grid voltage of the working station

4.2.3 Effect of mismatch between real and estimated line parameters

The droop algorithm presented in Equation(3.32) involves the sharing factor k , the virtual resistances α_1 and α_2 , but also it is dependent on the HVDC line parameters R_1 and R_2. If the line parameters are estimated correctly as showed in Figure 4-27, until at the half of the simulation, the sharing of power is kept according to the algorithm. This cannot be said in the case when the line parameters changes and in the droop controller the value of the line remains the same.

In order to prove the effect of the estimated line parameters over the power sharing the wind farm production was considered 1 p.u. and the sharing factor k was unitary all the time. The estimated line parameters were considered to be 0.15 ohms and then modified to 0.2 ohms. As it can be observed from Figure 4-27 and small changes in the line parameters produces significant changes in the sharing of DC current. Different power at the input of each converter means also different power injected into the grid (see Figure 4-28).

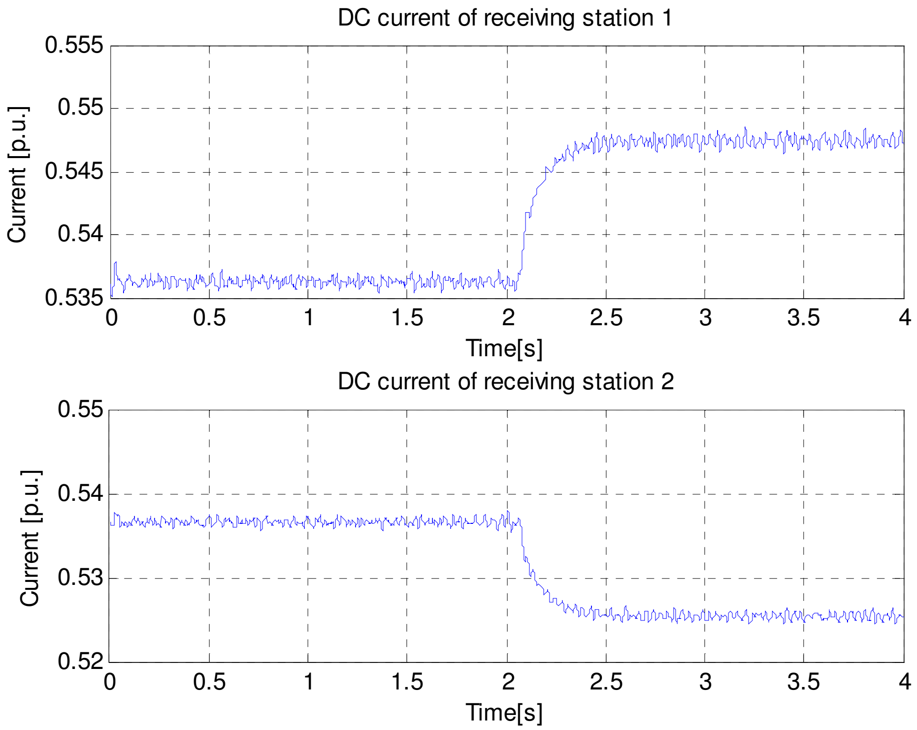

Figure 4-27 Effect of the mismatch in line parameters over the DC current sharing

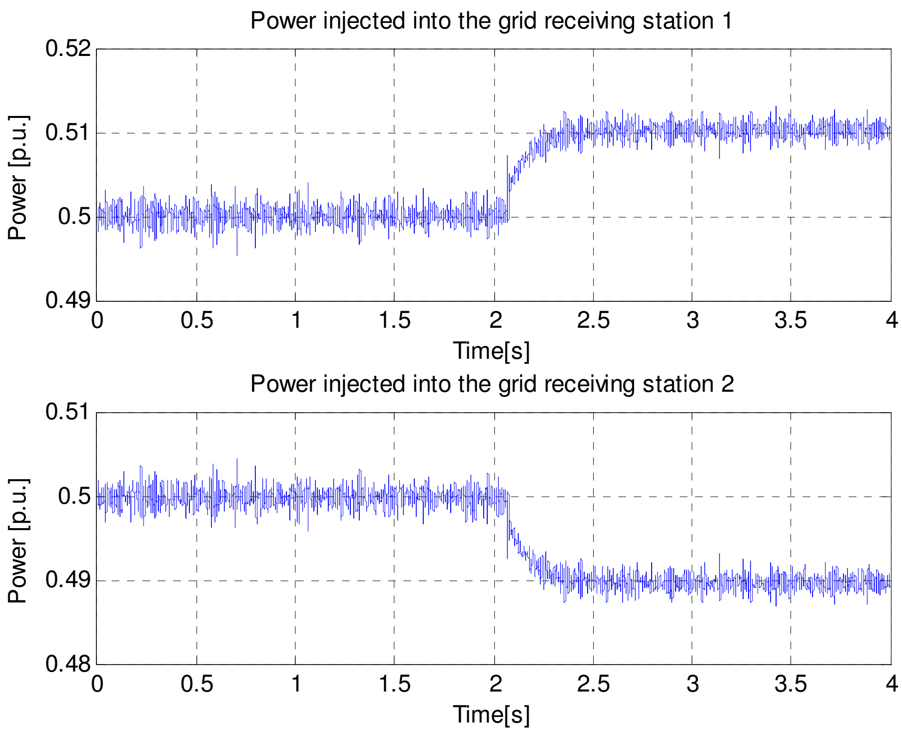

Figure 4-28 Effect of mismatch in line parameters over the AC powers injected into the grid

4.3 Discussions

For the MTDC system to be implemented in real application the concept of multi terminal HVDC layout had first to be simulated and the behavior analyzed. The purpose of the simulations was to test the control structure and check the performance of the components involved in the system.

In the beginning, the MTDC configuration was tested with the intention of validating the system and the goal was to prove that the system functions in normal operation when certain parameters were changed.

First the multi terminal system was examined in case of power steps in the wind power production. In this situation, the system had a unitary sharing factor of active power and all along the simulation the power was divided equally between the converters. Furthermore, the sharing capability was inspected and in this study case the converters in the receiving stations had different DC powers at the input depending in the sharing factor imposed by the system operator.

From the results obtained it was concluded that the converters were injecting the power into the AC grid according to the droop algorithm and the key elements in this matter were the virtual resistances α_1, α_2 and the sharing factor k. The algorithm sets different voltage references for both receiving stations in order to split the power among them. Having the same value of DC voltage at the input of each converter would not decide the amount of power injected into the grid by each converter and in this case the sharing of power is decided by the voltage drop created by the effect of the HVDC cable.

One important element which has to be careful analyzed in the droop technique presented in Equation(3.32) is the value of the virtual resistance. While the sharing factor decides the sharing of DC current, the value of the virtual resistance multiplied by the value of current decides the value of the DC voltage reference.

The criterion to select the value of α_1 should be based mainly on the DC voltage variation which the virtual resistance brings to the system. An increased value of the virtual resistance produces a higher jump in the DC voltage and by considering the safety margins of such system to be around $\pm 10\%$, the level of voltage at the input of the converters should not exceed this value otherwise the converters will trip.

As a conclusion when deciding the value of the virtual resistance, it must be chosen in such a way that it should not produce a big variation during transient condition and also the losses produced should be as small as possible.

The results for this part of validation have showed that the system is stable and the power produced by the offshore wind farm is injected into both grids accordantly with the intention of the system operator.

The second part of this chapter had the objective to investigate the reaction of the system when one of the components has to be shut down. In this situation the main problem is the active power in the system which has to be evacuated or dissipated on a resistance. Having surplus of active power in the system means overvoltage in the DC circuit and eventually when the upper limit is reached, the converters will trip.

The first study case analyzed was when abnormal operation of the offshore station decides that the production has to be stopped and no active power is injected into the DC link. In this way the capacitors are kept charged at the set point of DC voltage by the use of active from the AC side of the receiving station. When the wind farm is reconnected into the system and starts to inject active power, the droop algorithm still keeps the sharing of power accordantly to the system operator request.

The third study case involves the shutdown of one receiving station and the problem of evacuation of active power still remains. The solution is to direct all the power through the other receiving station or to burn it by means of a chopper.

In both situations the system remains stable, without disconnecting and when every part of the system is cleared of faults, the power is still shared.

The last study case analyses the real situation when the parameters of the line have a dynamic behavior and changes in the resistance appear, resulting in differences between the estimated value and the real one. In this case having mismatches between the resistances means introducing errors in the sharing algorithm and the sharing of power is no more controlled by the system operator.

Chapter 5

Experimental work

The goal of Chapter 5 is to test the MTDC system on a laboratory implementation. In the first part, the description of the laboratory setup is realized followed by the validation of the control under different situations. Moreover, the study cases proposed Chapter 4 are also analyzed and the results are compared.

5.1 Setup description

The MTDC system implemented in PSCAD/EMTDC simulation software has been developed on a similar prototype platform in the laboratory. One of the limitations of the HVDC systems is the lack of high power and high voltage equipments as mentioned in Chapter 1, so the system was downscaled. The experimental platform is represented in Figure 5-1.

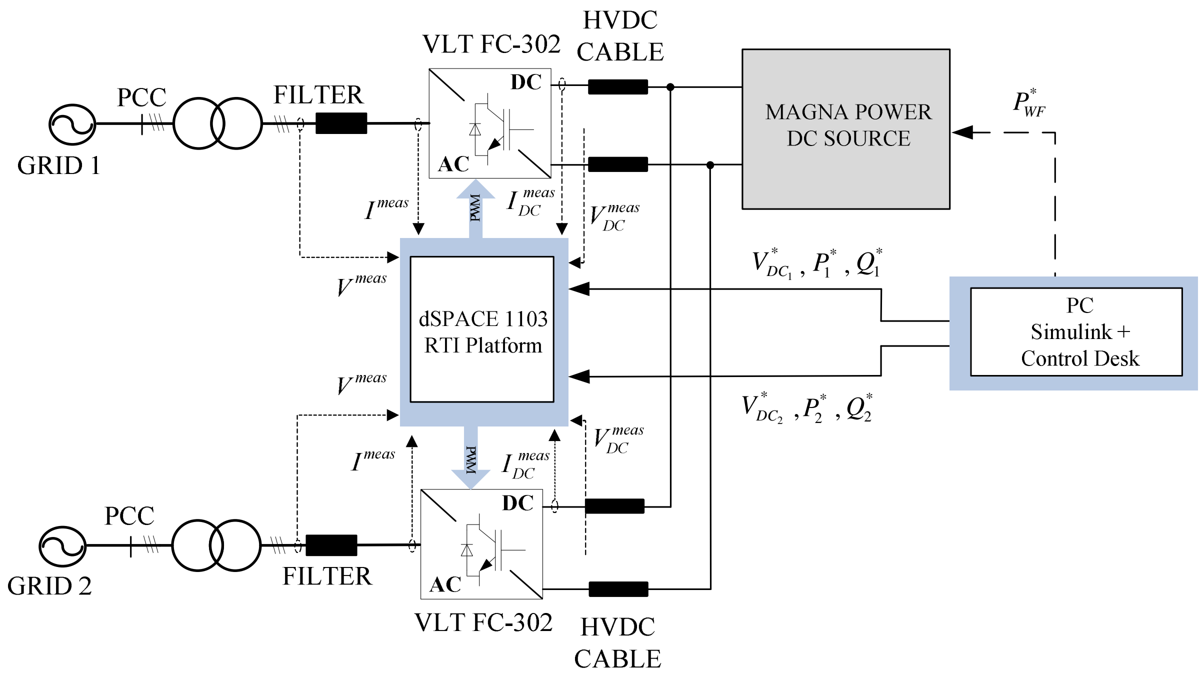

Figure 5-1 Structure of the experimental setup

From the structure of the experimental setup presented in figure above and illustrated in Appendix C, it can be noticed that the FC-302 VLT Danfoss inverters are controlled by a graphical interface from the PC through the dSPACE system and MATLAB/SIMULINK.

The connection between dSPACE which generates the PWM signals and the inverters is realized by the use of optic fiber and by means of the IPC2 interface board. The dSPACE system generates five signals to the IPC2 card: three duty cycle for the inverters switches, one enable signal which decides when the converter is ON or OFF and a reset signal which clears the interface in case the inverters are in abnormal operation like over current and over voltage.

The control structure for the MTDC system requires that the DC and AC values of current and voltage have to be measured and for this purpose LEM sensors are used. After the control is realized, references in active power, reactive power and DC voltage are sent to the inverters in order to realize the MTDC operation.

The WF and the offshore station are replaced by a DC power source which all the time injects power into the DC circuit. If the power source is stopped and no power is injected into the DC link, the MTDC operation is still kept but also the system can function into a point to point HVDC configuration.

In the user interface realized in the Control Desk software, different signals are plotted and different parameters in the control can be modified in order to see the behavior of the entire system.

The specifications for the equipments used in the laboratory can be found in Appendix A.

5.2 Study cases

The goal of the study cases implemented in the laboratory platform was to analyze and observe the active power flow and the response of the control under the same situations as it was tested in the simulation.

5.2.1 DC power variation

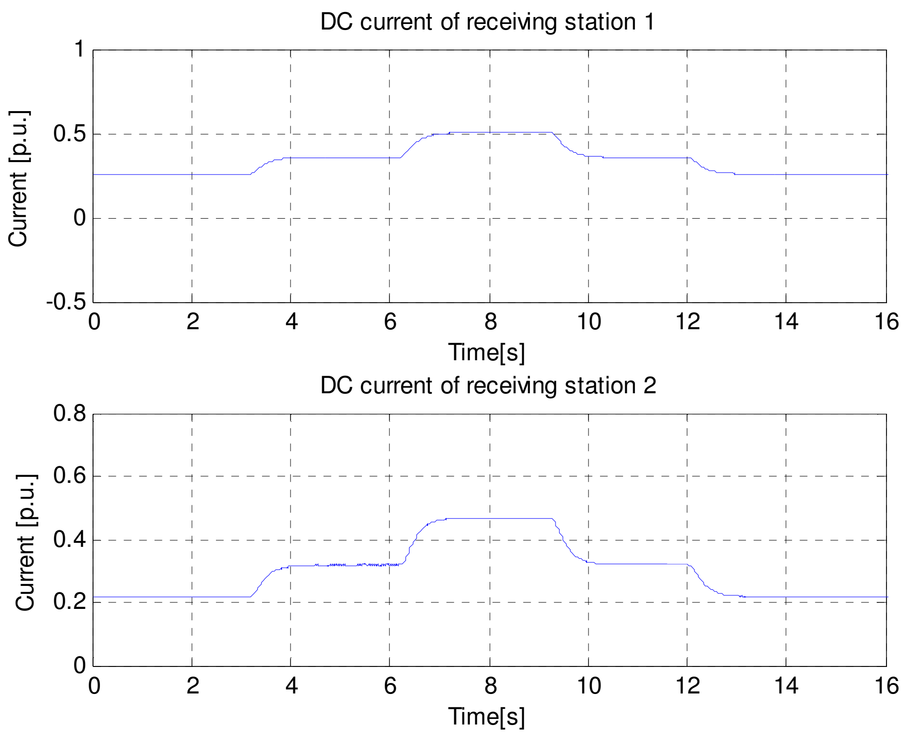

Figure 5-2 DC currents at the input of each receiving station

In the beginning the system was tested during DC power steps. For this study case, the sharing factor was kept unitary only the injected DC power was modified. The results presented in Figure 5-2 shows the DC current distribution and it can be remarked the fact that the sharing is not accordantly with the sharing imposed.

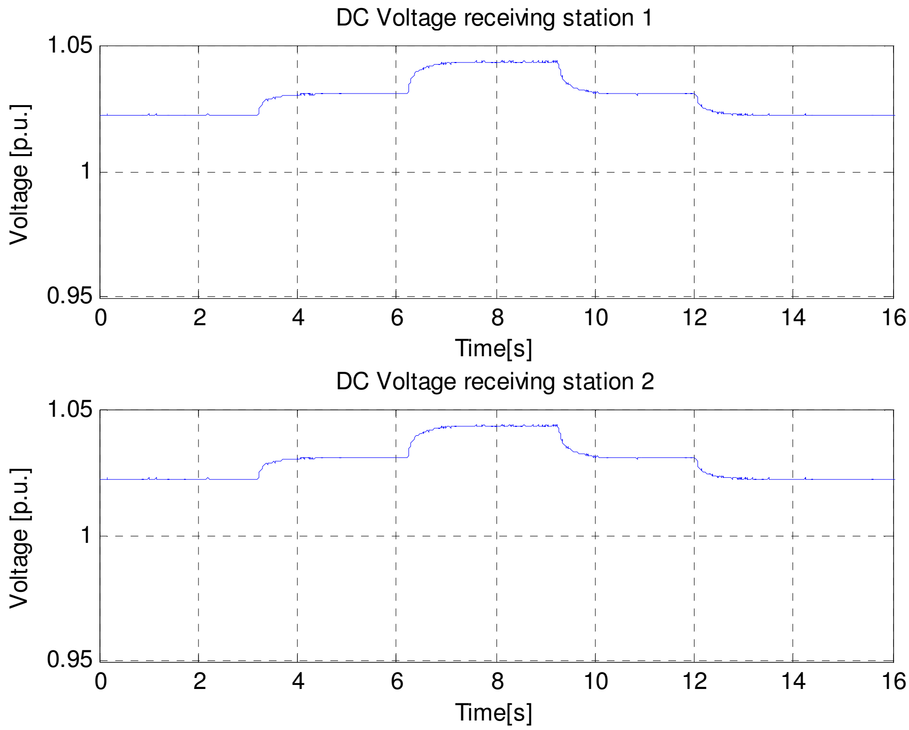

Figure 5-3 DC voltage of each receiving station

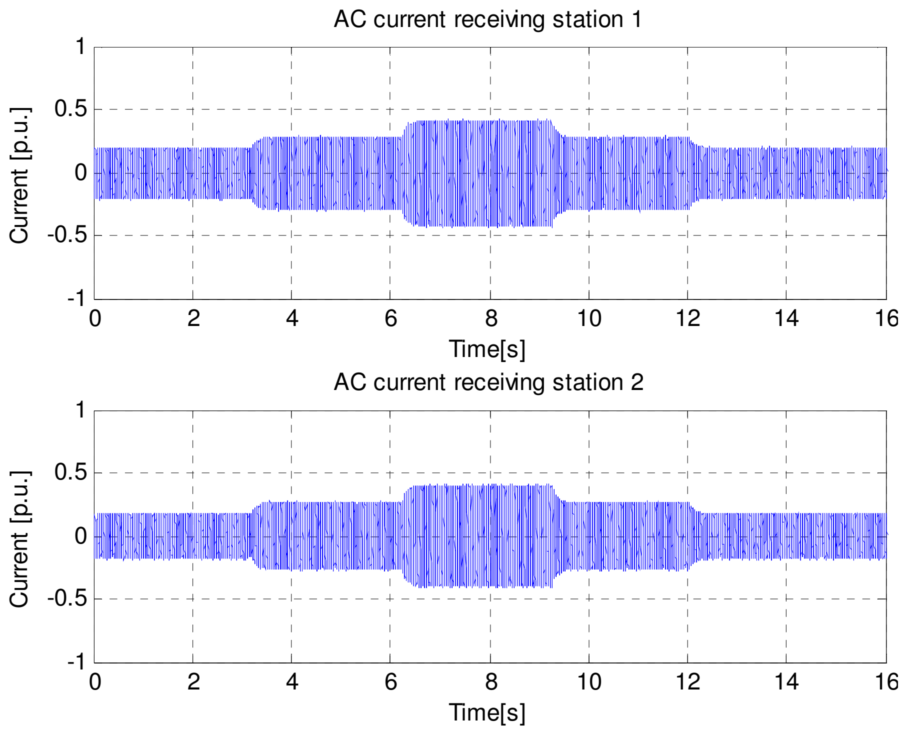

Figure 5-4 AC currents injected into the grid

The explanation for this behavior is that the droop equation is highly dependent on the line parameters and small mismatches between estimated and real value have significant effect in the DC current distribution. The sources of such differences are mainly due to imperfect contacts, load current or heating which can change the value of the line resistance.

Sharing the current through each branch of the MTDC system during DC power variations means modifying the DC voltage reference and this can be observed in Figure 5-3. The voltage increase is proportional with the increase of current and due to the virtual resistance used. This increase in DC voltage should not overcome the limits of $\pm10\%$ otherwise the converters should trip. As is can be seen, during power steps the voltage level is kept at the set point between the stability margins.

The control architecture using the droop algorithm has a direct influence on the ratio between the DC currents. Different values of DC current means also different value of DC power at the REC input and the current injected into the grid as showed in Figure 5-4, changes accordantly.

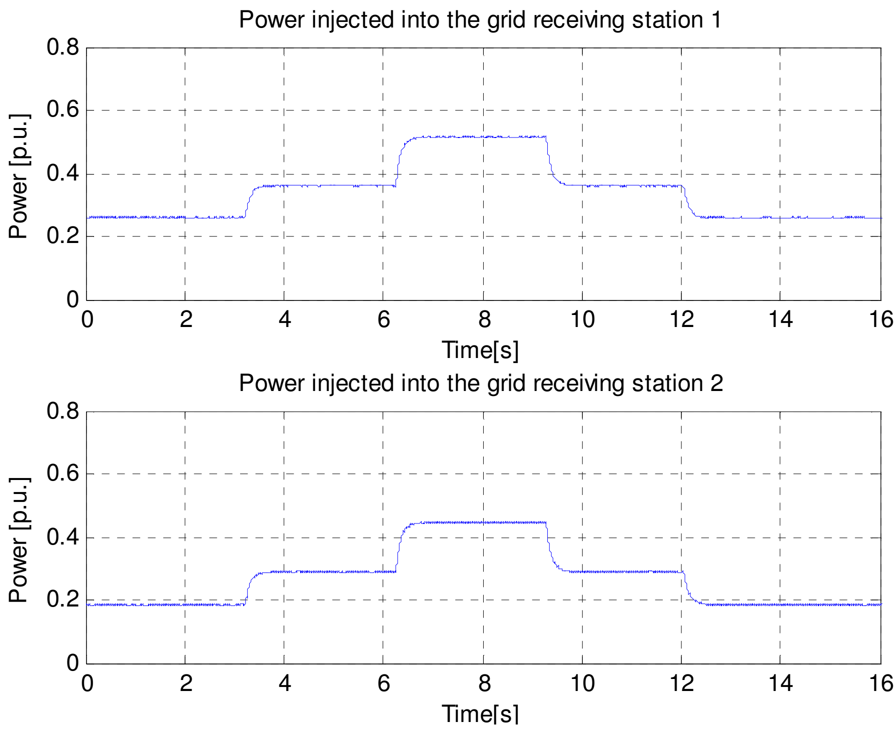

Figure 5-5 AC powers injected into the grid by each receiving station

Steps in wind power production means more current is injected into the DC link. The control architecture used in the MTDC configuration controls the energy stored in the DC capacitors and all the surplus is evacuated into the AC grid as presented in Figure 5-5.

5.2.2 Effect of the sharing factor over the system

The second case considered was to test the sharing capabilities of the MTDC structure. The sharing factor had subunitary values and during this test, the power production was constant.

Different values of the sharing factor for this case impose a higher current through receiving station one as presented in Figure 5-6. The direct influence of the DC current over the DC voltage can also be observed in this case and they are presented in Figure 5-7.

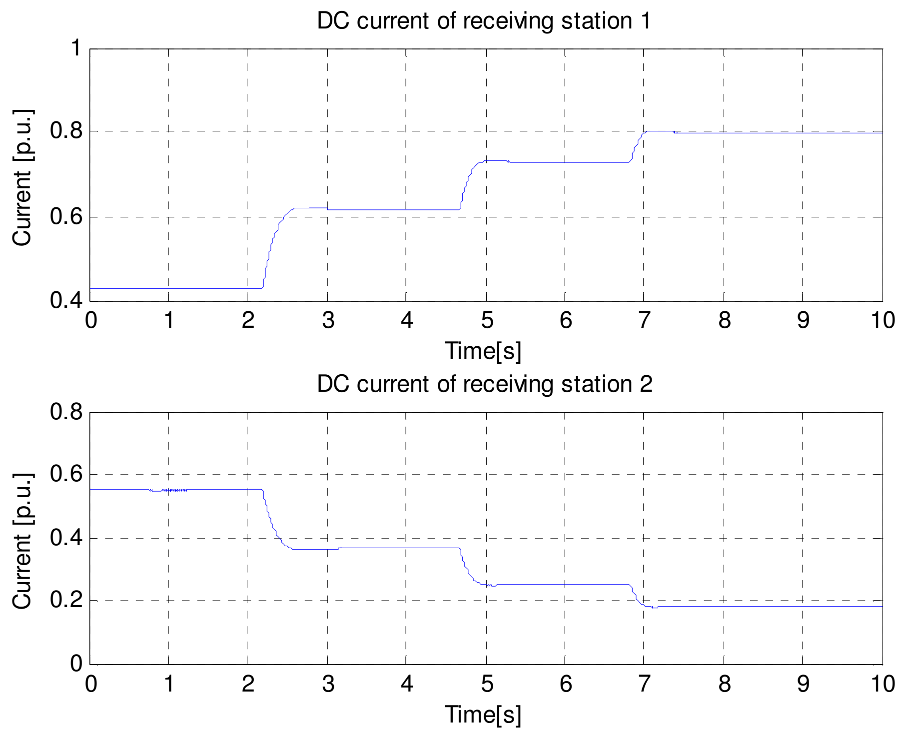

Figure 5-6 DC current distribution (k < 1)

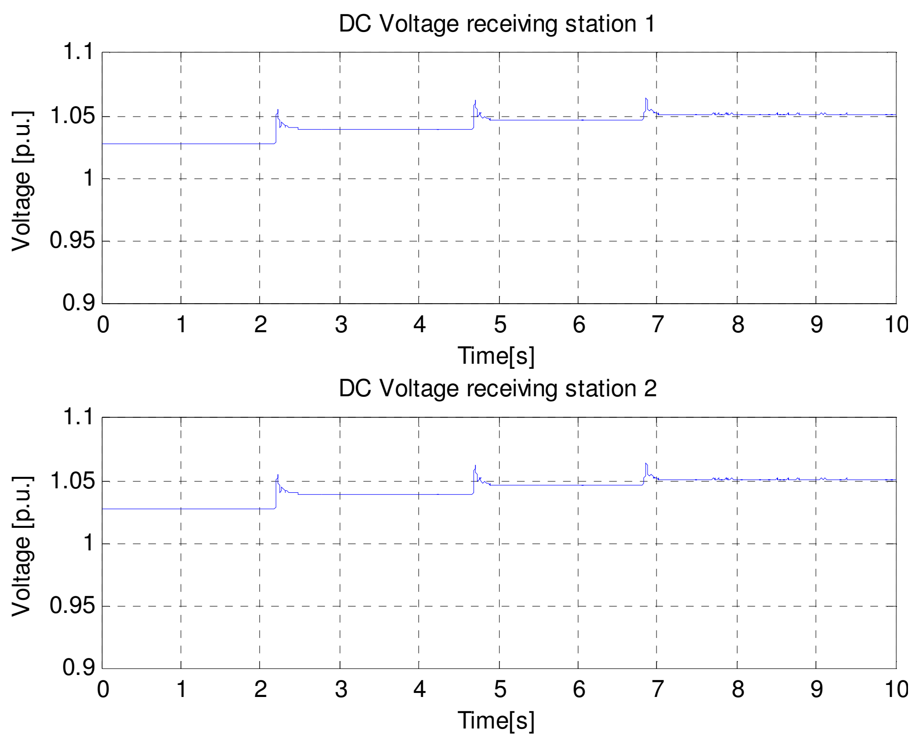

Figure 5-7 DC voltage levels (k < 1)

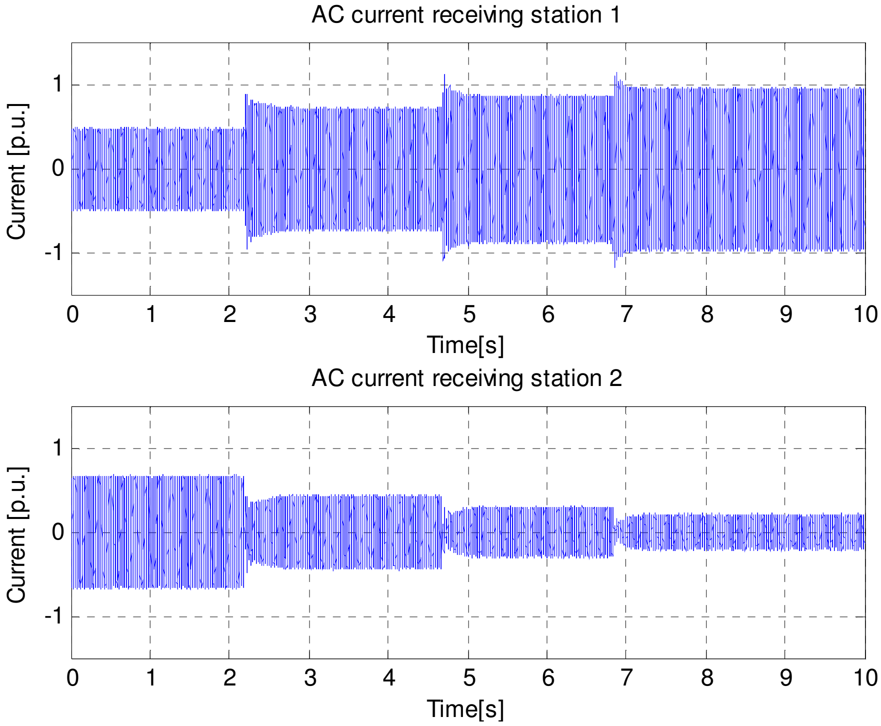

Figure 5-8 AC current injected into the AC grid (k < 1)

As expected, having more DC current through one receiving station means also more current injected into the AC grid (see Figure 5-8) and in consequence also more power is processed by this station (see Figure 5-9) considering the fact that the grid operates in normal conditions.

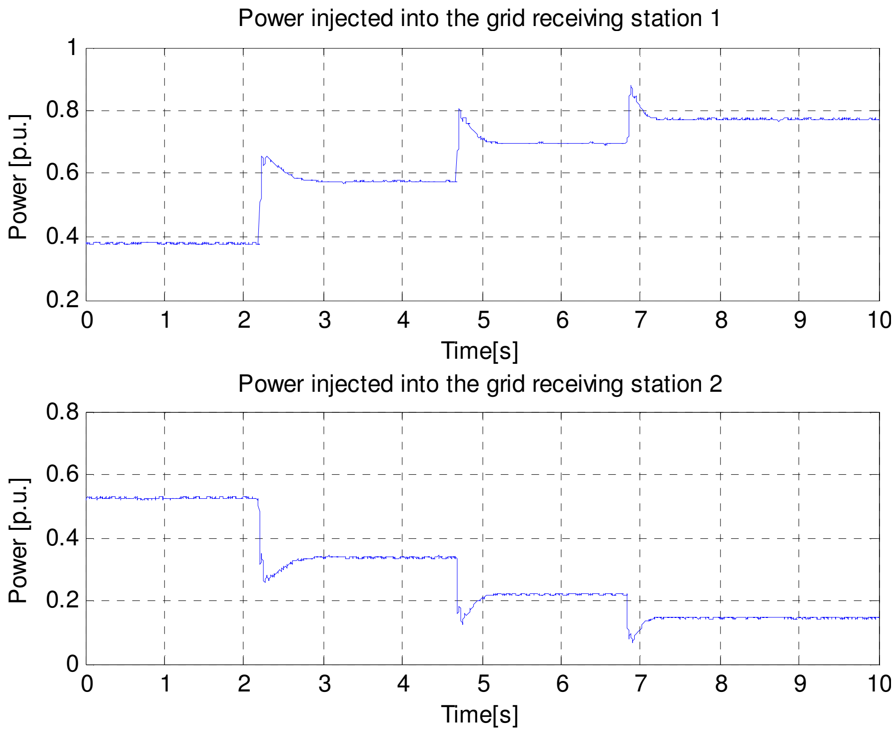

Figure 5-9 AC powers injected into the AC grid (k < 1)

The sharing capabilities of the MTDC system are continued also for the case when the sharing factor k is higher than one. As depicted from the droop equation more current flows through receiving station two (see Figure 5-10). The effect of the sharing factor is also exposed on the DC voltage references which in this case have a descendent character (see Figure 5-11).

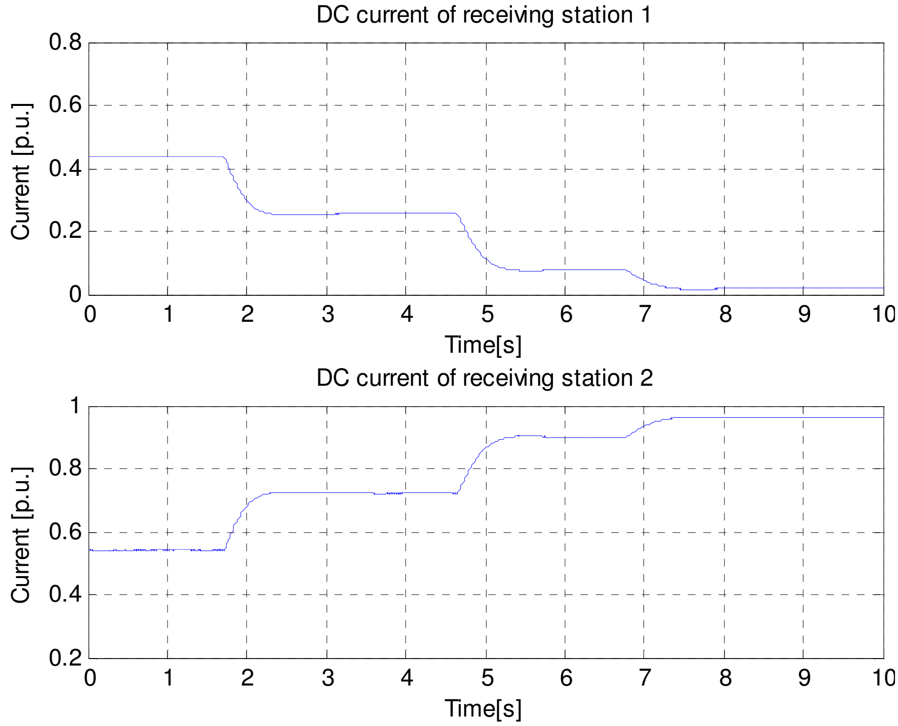

Figure 5-10 DC current distribution (k > 1)

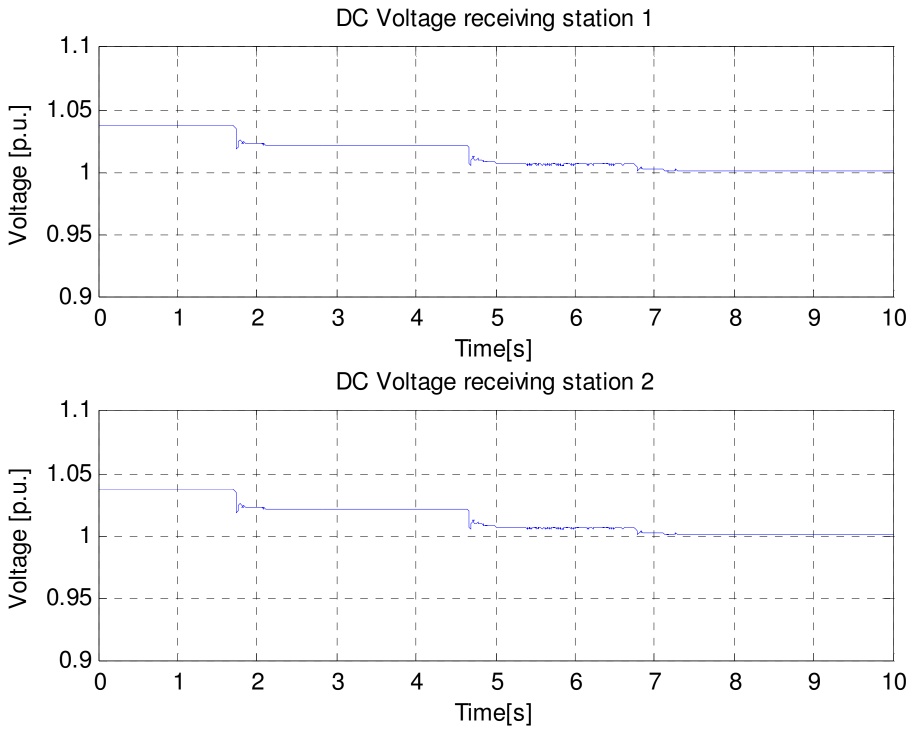

Figure 5-11 DC voltages (k > 1)

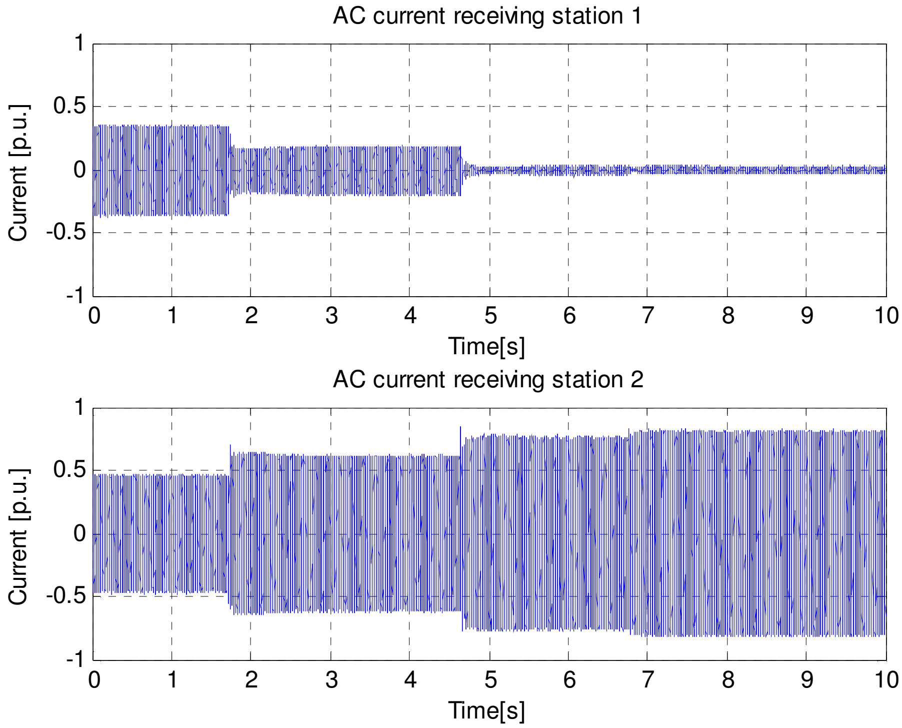

Figure 5-12 AC currents injected into the grid (k > 1)

In the same manner as presented above the amount of AC current injected into the grid (see Figure 5-12) is proportional with the amount of DC current available at the input of the converter and by injecting AC current into the grid means injecting AC power (see Figure 5-13).

As exposed in the previous study case, a common problem occurs and that is the accuracy in power sharing. Even in this case the same situation appears and is created by the changes in the line resistance which has a direct influence in the power sharing.

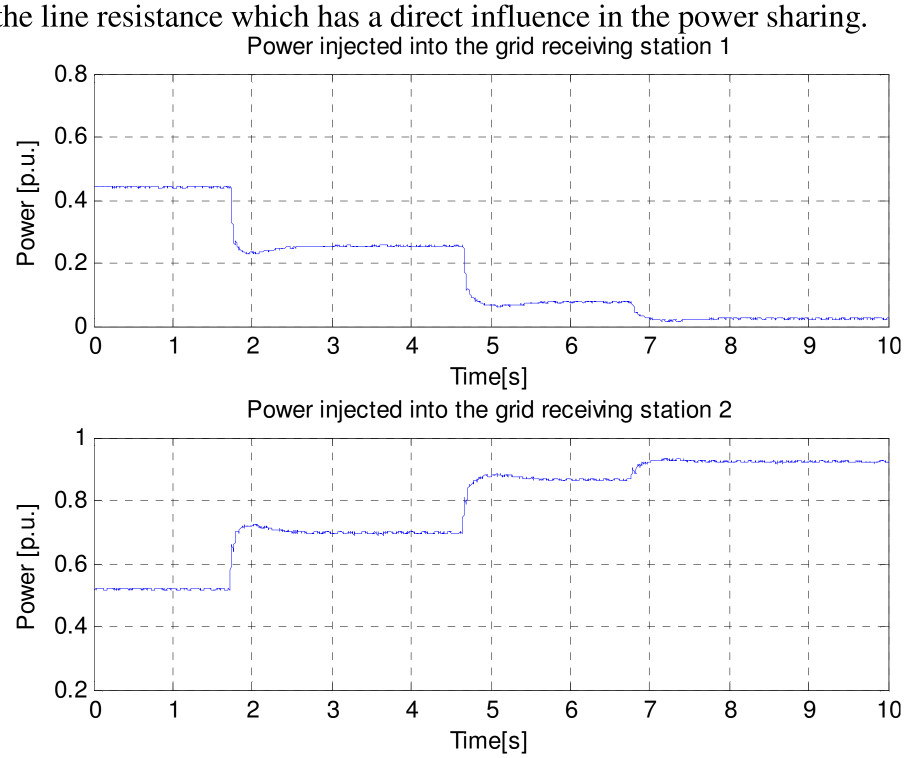

Figure 5-13 AC powers injected into the grid (k > 1)

5.2.3 Effect of virtual impedance in the system

One of the most important study cases in order to validate the control structure is to observe the influence of the virtual resistance in the system.

In the droop equation, in order to share power only the sharing factor k has to be modified and the simulation results in Chapter 4 have proven the only this element decides the power sharing in all situations and for every value of the virtual impedance.

On the real implementation of the system, the resistive nature of the line changes its properties in time and accordantly with the DC current variation.

For this study case different values of virtual impedance were analyzed and the effect on the power sharing was observed.

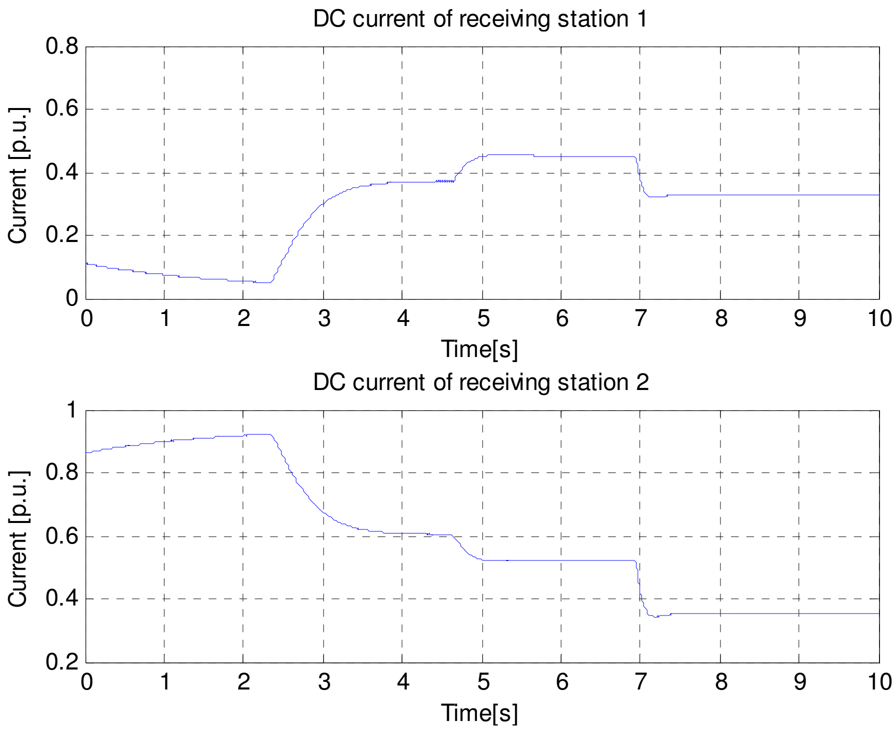

Figure 5-14 DC current distribution during virtual impedance variation

Figure 5-14 shows the current distribution when the virtual impedance is modified form 0.1, 1, 4 and finally 10 ohms and it can be remarked that for the small values, the dynamic behavior of the line characteristics has a predominant effect and the current sharing is severally affected and not accordantly to the sharing imposed. Gradually modifying the impedance to higher values, the effect of the HVDC line is reduced and the power sharing is achieved.

Changes in virtual impedance have a direct impact on the DC voltage reference as presented in Figure 5-15. For small values of the impedance, the voltage rise produced has an insignificant effect over the mismatch in line resistance, while for higher values; the DC voltage level almost reaches the upper limit of stability and has the potential of tripping the inverters.

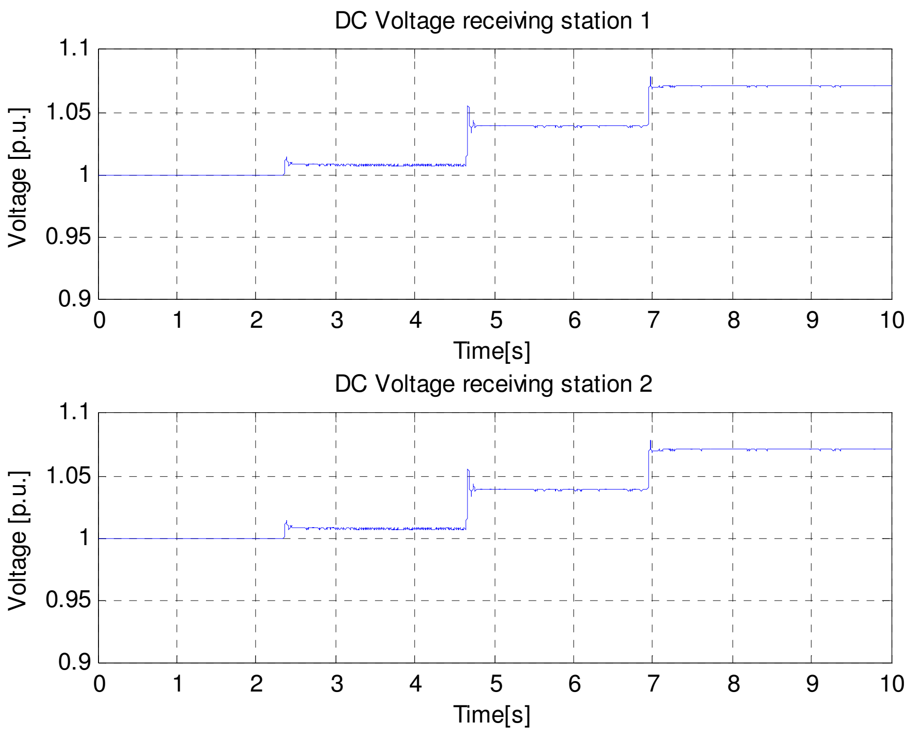

Figure 5-15 DC voltage variation during changes in the virtual impedance

Different DC currents at the input of the receiving station, means also different AC current in the output as exposed in Figure 5-16 and the changes in virtual impedance are transposed into the grid.

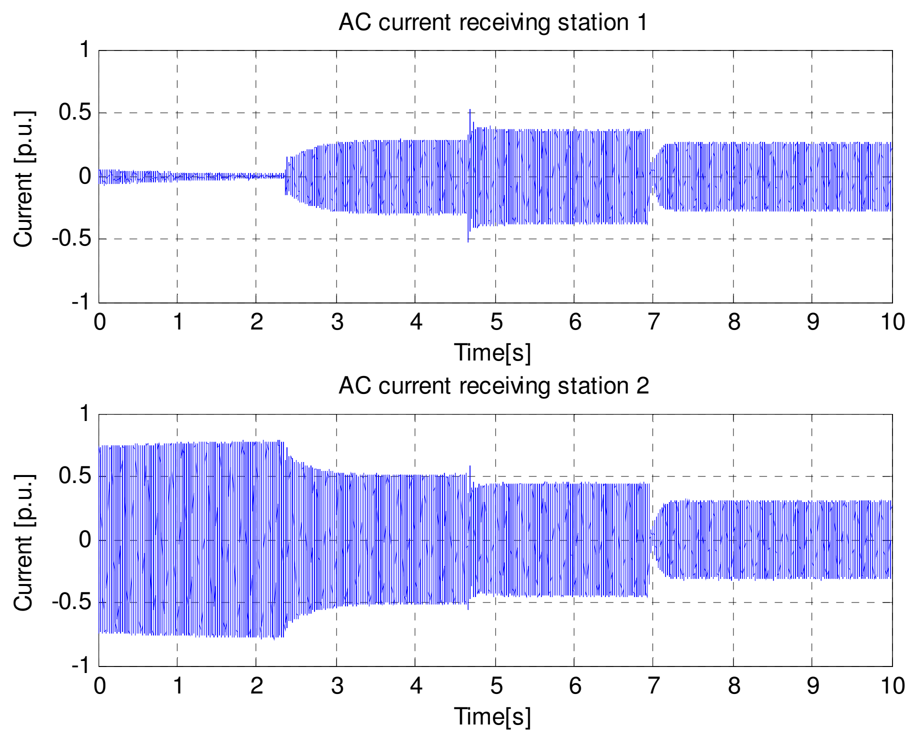

Figure 5-16 AC current distribution during virtual impedance variation

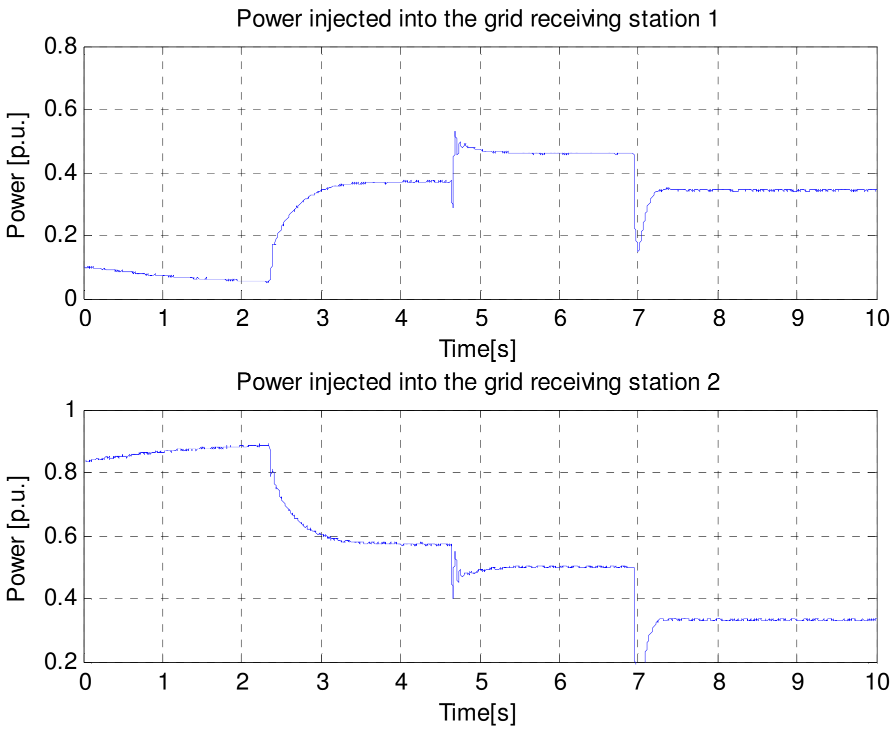

Figure 5-17 AC powers injected into the grid for different virtual impedance

As a consequence of changes in AC current injected into the grid, caused by different values of the virtual impedance which regulated the DC current sharing, the AC power evacuated changes also.

5.2.4 Power production trip

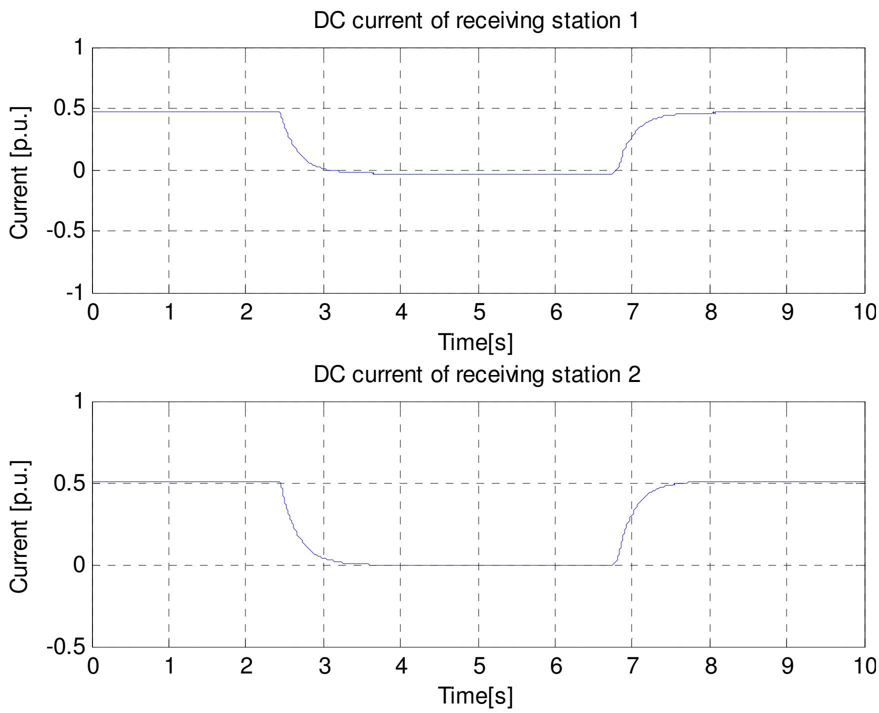

Figure 5-18 DC current during power production trip

This study case was performed with the purpose of testing the MTDC system in a severe situation when the power production was stopped and the converters still had to function. The power was set to a value of 1 pu and the sharing factor was kept constant. Until the production was shut down, the DC current is equally shared as shown in Figure 5-18 and then stopped due to unavailability of DC power in the circuit. Without any DC current in the MTDC branches, the DC voltage reference lowers down to the rated value decided by the system operator as illustrated in Figure 5-19.

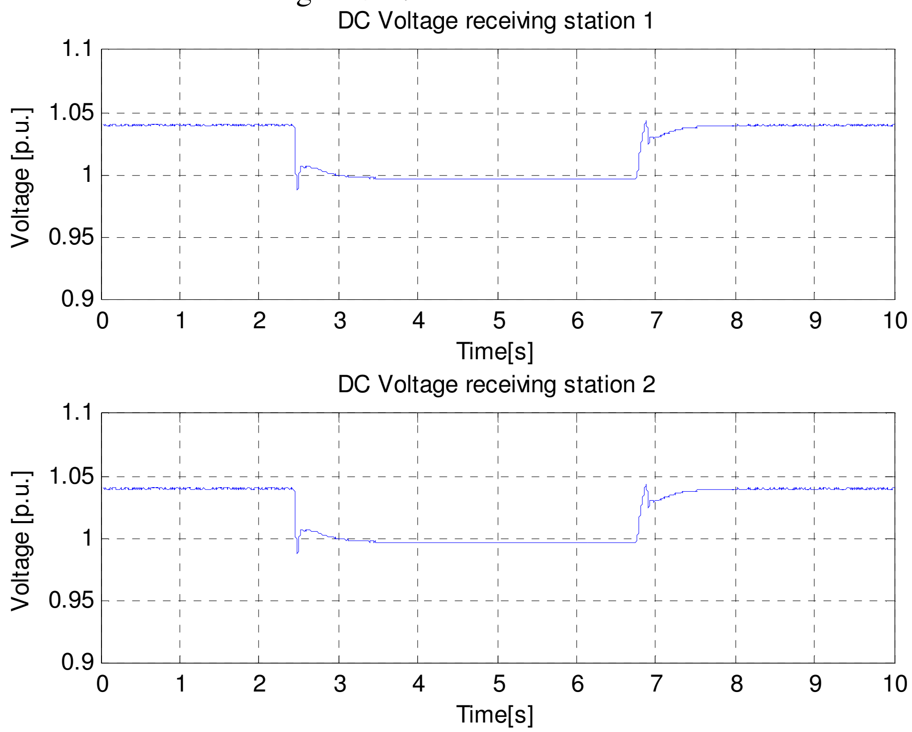

Figure 5-19 DC voltage during power production trip

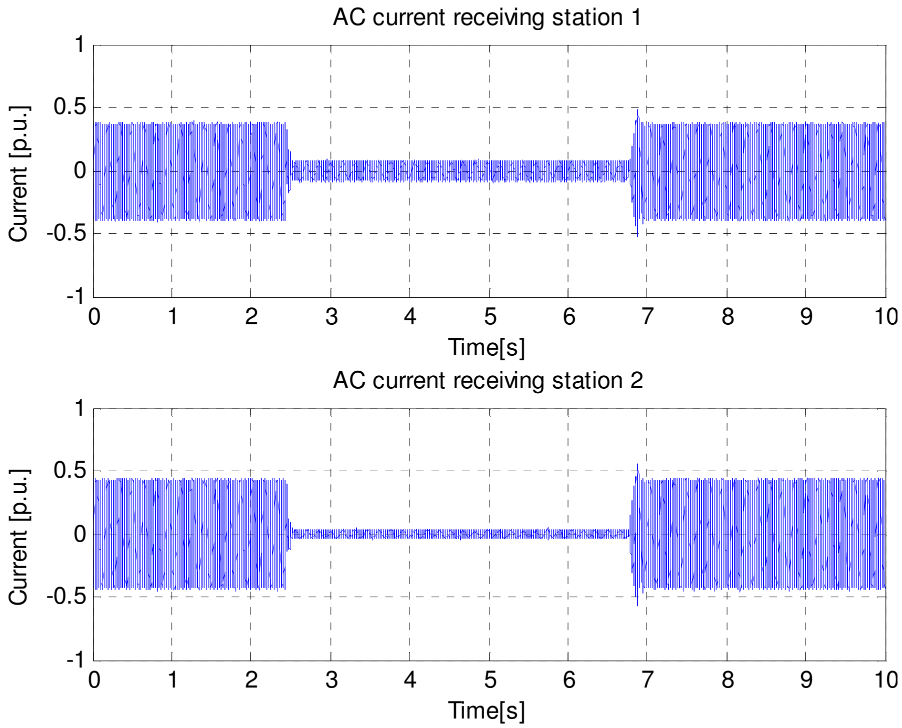

Figure 5-20 AC current during power production trip

During the period without any DC power injection the DC voltage is maintained at the set point using active power from the grid and when the power production recovers, the DC voltage reference is readjusted.

The absence of power on the DC side is also noticed on the AC current, only this time active current is absorbed from the grid to keep the capacitors charged (see Figure 5-20).

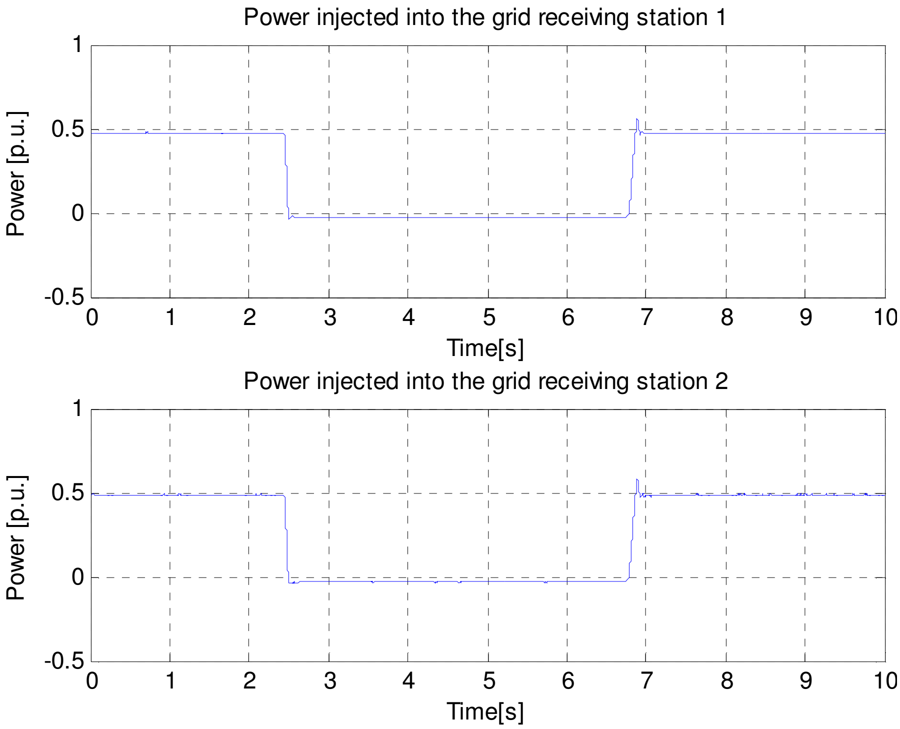

Figure 5-21 AC powers during power production trip

Figure 5-21shows the AC power behavior before and during the trip of the power production in each receiving station. Until the trip, the power is shared equally and when the power production shuts down, no active power is injected and in this situation power is consumed from the grid. This proves once again the bi-directional characteristics which the VSC brings to the system.

5.2.5 Receiving station trip

The system is also tested in case one receiving station has to be shut down and the power has to be processed by the other station.

Figure 5-22 presents the DC current distribution during this transient condition. At the begging, the DC current is imposed by the droop and when one station trips, all the current is then processed by the other station.

This transient condition is noticed also in Figure 5-23, where the DC voltages are presented. In case all the DC current is handled by one receiving station, the voltage reference changes, but doesn't exceeds the security limits of 10%, proving that the system remains stable.

The effect of the trip is also spotted in the AC current distribution (see Figure 5-24) and in the moment when the affected station is reconnected into the system, the sharing is maintained and AC currents are injected into the grid in the same manner the droop controller dictates.

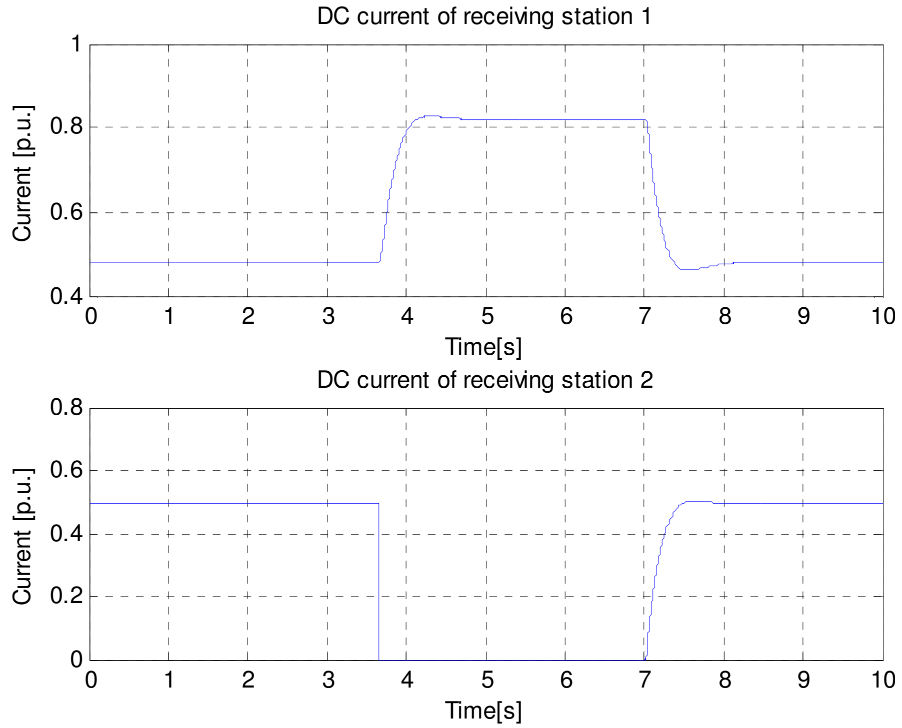

Figure 5-22 DC current during inverter trip

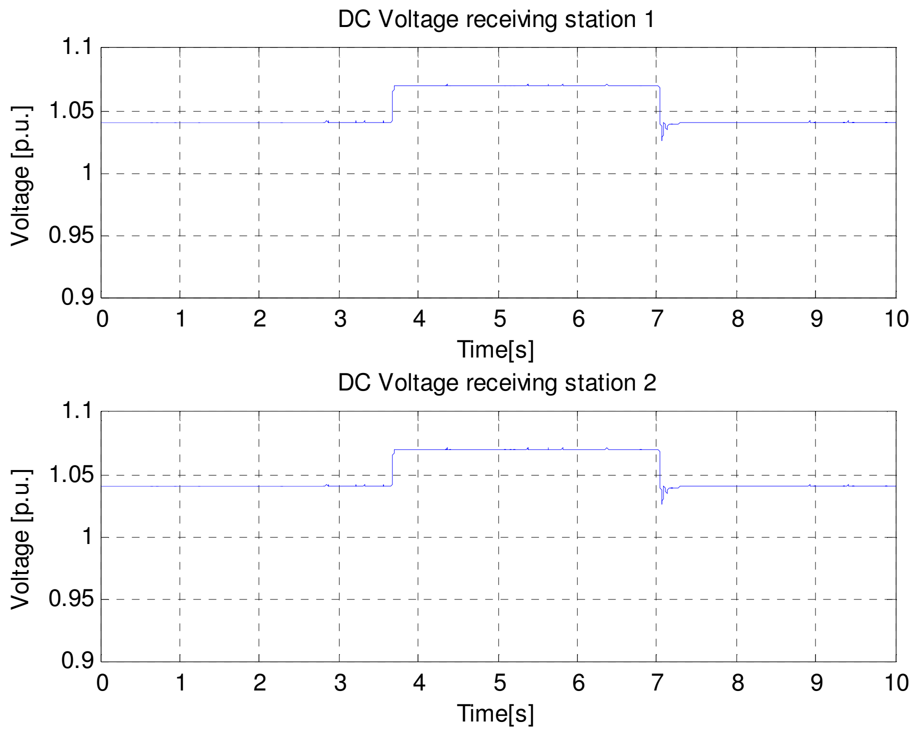

Figure 5-23 DC voltages during inverter trip

Changes in AC currents means changes in AC power delivered into the grid by every receiving station. Both stations are controlling the DC voltage and this means keeping the energy constant in the DC capacitors and the entire surplus evacuated (see Figure 5-25) into the grid.

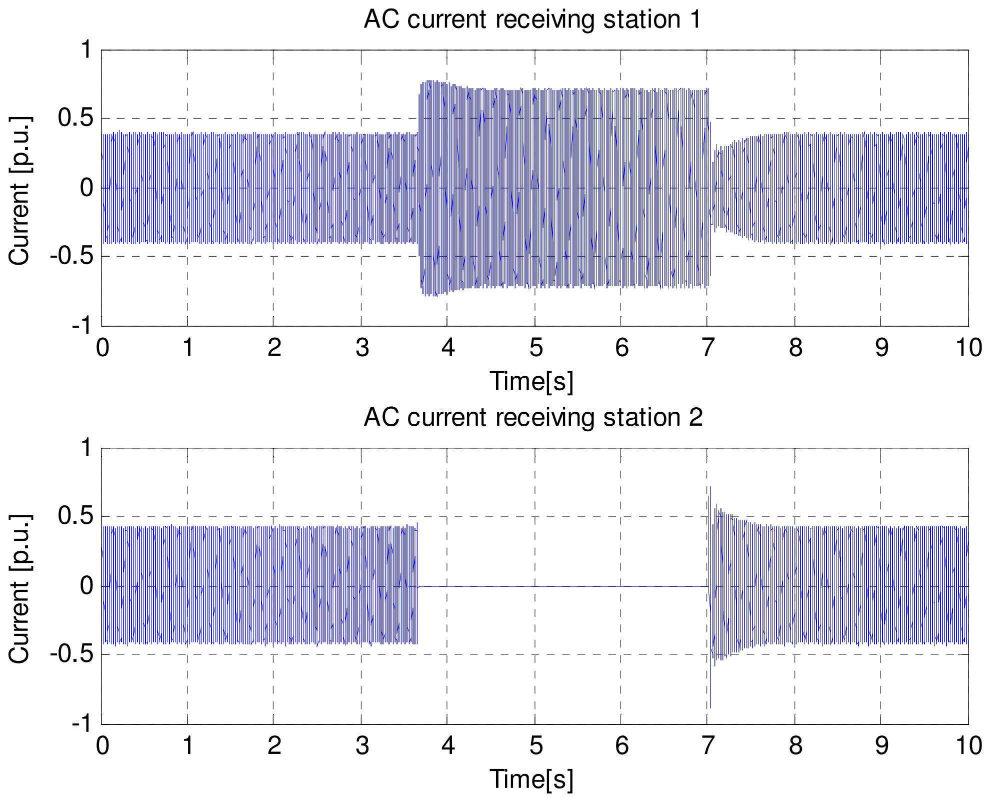

Figure 5-24 AC currents injected into the grid during inverter trip

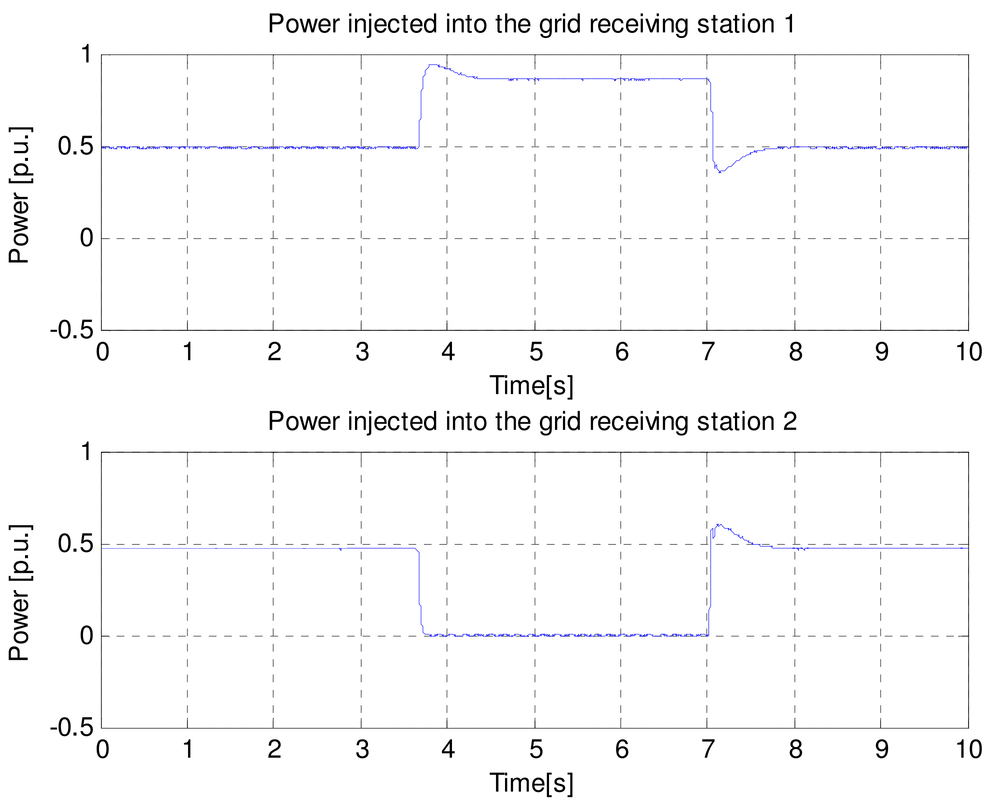

Figure 5-25 AC powers injected into the grid during inverter trip

Chapter 6

Conclusions and future work

6.1 Conclusions

This master thesis evaluates a future concept in power transportation using VSC-based HVDC system in a multi terminal operation. The main objective of the project was to develop a control strategy for grid connected converters in the MTDC system to share the power produced by an offshore WPP. The goal was achieved first, by simulating the system and tests for different conditions were carried out. The second step was to validate the control on a laboratory platform. To fulfill these tasks and to carry out this project, the thesis was divided into several steps and they are summed up as it follows.

In the first chapter a short presentation about the background of wind energy is presented and the main trends point out the increase in size of WT and the offshore installations are preferred over the onshore ones. This evolution caused more distributed power to be produced instead of the conventional power plants and WT started to affect the stability of the grid. Therefore grid codes were imposed by the TSO in order to improve the stability of the system. One solution to meet these requirements is to connect large offshore WF through HVDC systems. HVDC is the preferred method due to its obvious advantages like fewer cables to transfer the same amount of power, reduced losses and requires no compensation equipment to maintain the power transfer. A big improvement for the point to point HVDC connection is the multi terminal connection which brings more flexibility to the system and also new challenges. Adding extra converters into the DC circuit means sharing the active power produced by the WF but also can support the grid with reactive power whenever the TSO requests it.

The purpose of the second chapter was to model the components existing in the MTDC system which connects WFs to the grid. In the beginning a complete description of every part of the MTDC was presented including the offshore station, HVDC cable, DC capacitors, the power converter, the filter, the transformer and the electrical grid, followed by a theoretical description related to mathematical equations.

In the third chapter, the control structure of the MTDC system is explained. Mainly, the control deals with the connection of the VSC into the grid and has to provide secure operation and power quality. For this purpose, the proposed control architecture contains to cascaded loops: an inner loop which controls the current injected into the grid and an outer loop which controls the DC voltage or active power and the reactive power the converter can absorb or inject into the grid. For the inner loop the control is realized in stationary reference frame and PR controllers are used and for the outer loop the control uses PI controllers due to their capabilities of controlling DC values. In both cases the controllers have to meet strict requirements in terms of damping and bandwidth in order for the system to be stable. Even though it seems that the PLL is not used, still it is utilized because it generates the frequency at which the inner controller operates and gives better stability in case of transient condition if a disturbance occurs into the grid. In the last part of the chapter the MTDC operation is emphasized and the sharing of active power is realized by means of two key factors: virtual impedance and sharing factor.

Chapter 4 focuses on the validation of the system and several tests and study cases were performed. First, the system was tested under different steps in active power and constant sharing, than the sharing capabilities were analyzed for different values of sharing factor. One important aspect in the MTDC operation is the value of the virtual impedance which doesn't participate directly in the sharing process but which decides the value of the DC voltage at the input of every converter. The second step in the validation of the system was to test it under abnormal operation and it was demonstrated that the system performed stable without affecting the grid, proving once again the decoupling effect of every HVDC system. In the end of the chapter a more realistic matter was analyzed and that was the case when errors between real and estimated value of the virtual impedance occur reflected on the power sharing. This underlines the idea that small values of virtual impedance can realize the sharing but the dynamic behavior of the line is more visible, while big values of virtual impedance reduces the effect but creates higher voltages on the DC input of each converter.

Chapter 5 describes the experimental work carried out in the laboratory. At the begging the experimental setup is presented with all its components than several tests were developed with the purpose of proving the control structure of the MTDC in a real time application.

6.2 Future work

As always, the possibility for further work remains. The work can be improved considerably in many directions. In the simulation realized in PSCAD a detailed model of the offshore wind farm together with the offshore station control can add a realistic behavior to the system. Another factor which can add realistic behavior is to add to the system a more complex model for the HVDC system in order to study the real phenomenon which takes place in the cables during operation. Also the sharing factor of the MTDC system can be corrected by introducing a master control which calculates the real sharing with the imposed one.

The control of the MTDC system can be realized in rotational reference frame and the results can be compared.

A good test for the MTDC control structure will be to test the system under fault condition and see if the system fulfils the requirements imposed by the TSO.

In the lab a considerably improvement will be the use of a realistic power source which can create the effect of a real wind farm connected to the DC grid.

Bibliography

List of references

[1] S. M. Muyeen*, et al.*, "Low voltage ride through capability enhancement of wind turbine generator system during network disturbance," *Renewable Power Generation, IET,* vol. 3, pp. 65-74, 2009.

[2] http://www.ewea.org/fileadmin/ewea_documents/documents/publications/reports/Pure_Power_Full_Report.pdf.

[3] B. Consult. (March 2011, *BTM Consult: World Market Update 2010 Forecast 2011-2015.Available: www.btm.dk.*

[4] T. Ackermann, *Wind Power in Power Systems* Chichester, West Sussex, England: John Wiley, 2005.

[5] C. Zhe, *Wind turbine system technology - Lecture at AAU*, 2010.

[6] R. Teodorescu, *Grid Converters for Photovoltaic and Wind Power Systems* 2011.

[7] H. L. a. L. S. Petersen, ""Risø Energy Report 6 - Future options for energy technologies," " 2007.

[8] M. Tsili and S. Papathanassiou, "A review of grid code technical requirements for wind farms," *Renewable Power Generation, IET,* vol. 3, pp. 308-332, 2009.

[9] T. J. Hammons*, et al.*, "Role of HVDC transmission in future energy development," *Power Engineering Review, IEEE,* vol. 20, pp. 10-25, 2000.

[10] "East Coast Transmission Network Technical Feasibility Study," *The UK Crown Estate,* January 2008.

[11] V. K. Sood, "HVDC and FACTS Controllers: Applications of Static Converters in Power Systems (Power Electronics and Power Systems)," 2004.

[12] M. P. Bahrman, "OVERVIEW OF HVDC TRANSMISSION," in *Power Systems Conference and Exposition, 2006. PSCE '06. 2006 IEEE PES*, 2006, pp. 18-23.

[13] N. Flourentzou*, et al.*, "VSC-Based HVDC Power Transmission Systems: An Overview," *Power Electronics, IEEE Transactions on,* vol. 24, pp. 592-602, 2009.

[14] J. Arrillaga, *Flexible Power Transmission The HVDC Options*: John Wiley & Sons Ltd, 2007.

[15] G. S. Daelemans, K. Reza, M. Cole, S. Belmans, "Minimization of steady-state losses in meshed networks using VSC HVDC," *Power & Energy Society General Meeting, 2009. PES '09. IEEE* 2009.

[16] X. Jia*, et al.*, "Grid integration of large offshore wind energy and oil & gas installations using LCC HVDC transmission system," in *Power Electronics Electrical Drives Automation and Motion (SPEEDAM), 2010 International Symposium on*, 2010, pp. 784-791.

[17] K. R. Padiyar and N. Prabhu, "Modelling, control design and analysis of VSC based HVDC transmission systems," in *Power System Technology, 2004. PowerCon 2004. 2004 International Conference on*, 2004, pp. 774-779 Vol.1.

[18] D. Jovcic, "Interconnecting offshore wind farms using multiterminal VSC-based HVDC," in *Power Engineering Society General Meeting, 2006. IEEE*, 2006, p. 7 pp.

[19] C. Hairong*, et al.*, "Control Strategy Research of VSC Based Multiterminal HVDC System," in *Power Systems Conference and Exposition, 2006. PSCE '06. 2006 IEEE PES*, 2006, pp. 1986-1990.

[20] Z. Jiebei and C. Booth, "Future multi-terminal HVDC transmission systems using Voltage source converters," in *Universities Power Engineering Conference (UPEC), 2010 45th International*, 2010, pp. 1-6.

[21] H. K. V. Akhmatov, "An aggregate model of a grid-connected, large-scale, offshore wind farm for power stability investigations - importance of windmill mechanical system," *Electrical Power and Energy System 24,* 2001.

[22] Z. A. O. K.S. Rudion, A. Ruhle, "MaWind - tool for the aggregation of wind farm models," 2008.

[23] B. Craciun, Banceanu C, Vranceanu I, "Control of wind farm with HVDC " *Semester Report,* vol. Aalborg, 2010.

[24] C. S. K, R. Teodorescu, P. Rodriguez, P. C. Kjaer and P. W. Christensen, "Modelling and Simulation of VSC-HVDC Connection for Offshore Wind Power Plants," *PhD Seminar on Detailed Modelling and Validation of Electrical Components and System* 2010.

[25] C. Du, "The control of VSC-HVDC and its use for large industrial power systems," PhD, Departament of Electric Power Engineering, Chalmers University of Technology, Goteborg, Sweden, 2003.

[26] e. a. F. Iov, "Wind Turbine Blockset in Matlab/Simulink," 2004.

[27] S. Wei*, et al.*, "Intelligent optimize design of LCL filter for three-phase voltage-source PWM rectifier," in *Power Electronics and Motion Control Conference, 2009. IPEMC '09. IEEE 6th International*, 2009, pp. 970-974.

[28] S. V. Araujo*, et al.*, "LCL filter design for grid-connected NPC inverters in offshore wind turbines," in *Power Electronics, 2007. ICPE '07. 7th Internatonal Conference on*, 2007, pp. 1133-1138.

[29] F. Blaabjerg*, et al.*, "Overview of Control and Grid Synchronization for Distributed Power Generation Systems," *Industrial Electronics, IEEE Transactions on,* vol. 53, pp. 1398-1409, 2006.

[30] M. Ciobotaru, "Reliable Grid Condition Detection and Control of Single-Phase Distributed Power Generation Systems," 2009.

[31] A. Constantin, "Advanced Modelling and Control of Wind Power Systems " *Master Thesis,* vol. Aalborg University, 2009.

[32] E. H. W. Hirofumi Akagi, Mauricio Aredes, "Instantaneous power teory and aplications to power conditining," ed. New Jersey: John Wiley&Sons, 2007.

[33] X. Lie*, et al.*, "Multi-terminal DC transmission systems for connecting large offshore wind farms," in *Power and Energy Society General Meeting - Conversion and Delivery of Electrical Energy in the 21st Century, 2008 IEEE*, 2008, pp. 1-7.

[34] R. da Silva*, et al.*, "Power delivery in multiterminal VSC-HVDC transmission system for offshore wind power applications," in *Innovative Smart Grid Technologies Conference Europe (ISGT Europe), 2010 IEEE PES*, 2010, pp. 1-8.

Appendix A

Laboratory Setup Parameters

Transformer	
Rated power $[S]$	$10\,[kVA]$
Rated voltage $[V]$	$400\ [V]$
Rated current $[I]$	$14.4\ [A]$
Short circuit impedance $[U_z]$	$3\,[\%]$
Connection: DYn11	
Filter Parameters	
Rated power $[P]$	$15\ [kW]$
Rated voltage $[V]$	$500\ [V]$
Rated current $[I]$	$38\ [A]$
Filter inductance $[L_f]$	$1.6\ [mH]$
Filter capacitance $[C_f]$	$10\ [\mu F]$
Inverter Parameters	
Rated power $[P]$	$15\ [kW]$
Supply voltage $[V]$	380 - $500\ [V]$
Power factor $[\cos\varphi]$	>0.98
DC Source	
Rated power $[P]$	$50\ [kW]$
Max. DC voltage $[V]$	$1100\ [V]$
Max. DC current $[I]$	$50\ [A]$
DC link parameters	
Resistance HVDC line 1 $[R]$	$0.2\ [\Omega]$
Resistance HVDC line 2 $[R]$	$0.15\,[\Omega]$
Current Transducer Parameters	
Primary nominal RMS current $[I_{PN}]$	$50\ [A]$
Primary current measuring range $[I_P]$	0-$70\ [A]$
Conversion ration $[K_N]$	1:1000
Supply voltage $[V_C]$	$\pm 12...15\ [V]$
Voltage Transducer Parameters	
Primary nominal RMS current $[I_{PN}]$	$10\ [mA]$
Primary current measuring range $[I_P]$	$0...\pm 14\ [mA]$
Conversion ration $[K_N]$	2500:1000
Supply voltage $[V_C]$	$\pm 12...15\ [V]$

Appendix B

The content on the CD is sorted into different folders as shown below:

- Project
  - Word Version
  - Pdf Version
- Simulation Files
  - .mat_files
  - PSCAD simualtion files
- Laboratory Files
  - MTDC dSPACE files
  - .mat_files
- System and Software Documentation

Appendix C

Laboratory setup of the MTDC system